

# **FIELD-EFFECT LIMITS AND DESIGN PARAMETERS FOR HYBRID HVDC / HVAC TRANSMISSION LINE CORRIDORS**

ANDREW WILLIAMSON

A dissertation submitted in partial fulfilment of the degree of Master of Science in Electrical Engineering (Power and Energy Systems), to the School of Electrical, Electronic and Computer Engineering, University of KwaZulu-Natal, Durban, South Africa.

Supervisors: Prof. Innocent Davidson  
Mr Antony Britten Pr.Eng.



## DECLARATION 1 - PLAGIARISM

I, Andrew Robert Faure Williamson, declare that:

1. The research reported in this thesis, except where otherwise indicated, is my original research.
2. This thesis has not been submitted for any degree or examination at any other university.
3. This thesis does not contain other persons' data, pictures, graphs or other information, unless specifically acknowledged as being sourced from other persons.
4. This thesis does not contain other persons' writing, unless specifically acknowledged as being sourced from other researchers. Where other written sources have been quoted, then:
  - (a) Their words have been re-written but the general information attributed to them has been referenced
  - (b) Where their exact words have been used, then their writing has been placed in italics and inside quotation marks, and referenced.
5. This thesis does not contain text, graphics or tables copied and pasted from the Internet, unless specifically acknowledged, and the source being detailed in the thesis and in the References sections.

.....

A.R.F. Williamson                      Date

As the candidate's Supervisors, we agree/do not agree to the submission of this thesis.

.....

A.C. Britten                      Date                      I.E. Davidson                      Date



## DECLARATION 2 - PUBLICATIONS

No publications, in preparation, submitted, in press or published, form part of and/or include research presented in this thesis.

.....

Andrew Williamson

Date



## ABSTRACT

New generation centres and servitude constraints in Southern Africa have promoted interest in the possibility of dc and ac lines in close proximity to each other, and even sharing structures. Certain interactions of HVDC and HVAC transmission circuits have been analysed by other authors, but this has mainly focused on conversion of existing double-circuit transmission lines to hybrid lines, and has mostly been in European contexts. The dissertation reviews this prior work, and extends it to a Southern African context. First a framework is developed to describe engineering considerations for ac and dc lines in terms of power transfer capability, air insulation, corona-related phenomena, electric and magnetic fields, and behaviour under fault conditions. A study system amenable to analysis is developed, consisting of two hybrid dc/ac transmission corridors, each with a 1000 MW ac line and a 3000 MW dc bipole. The ac current flowing in the pole conductors due to coupling is estimated, and found to be an issue requiring mitigation. Line transposition is adequate mitigation during normal operation, but 50 Hz blocking filters or special converter controls are needed under fault conditions. A parametric study of conductor surface gradients for the study system was carried out; some calculated dc values seemed misaligned with service experience, possibly due to ionic current flow and space charge. Using the corona saturation method, ion density, ion current and electric field at ground level are estimated. Corona-related phenomena are investigated using empirical equations from the literature and the calculated conductor surface gradients. Behaviour under hybrid dc/ac energisation is not fundamentally different to corona behaviour under pure ac or dc energisation. For ac, sound pressure levels were calculated for each phase, but for dc only the positive pole was considered, because the contribution from the negative pole is negligible. Radio interference for both ac and dc is calculated using empirical expressions. Optimal voltage and conductor sizes are investigated using generalised cost models developed by Cigré. It is found that the study system could be optimised better. Feasible improvements to the system, limits on some field-effect related parameters appropriate to Southern African conditions are suggested. These consist of different conductor bundles, and a reduction in the power transfer to 800 MW for the ac circuits and 2000 MW for the dc circuits. Based on the analysis, it is concluded that there is scope for hybrid dc/ac corridors in the region, and the theoretical basis for doing this is exemplified.



## ACKNOWLEDGEMENTS

Although my name appears on the cover of this dissertation, several people have made important contributions towards it.

Foremost are my supervisors Mr Antony Britten and Prof. Innocent Davidson, who have helped immensely with relevant (and often hard-to-obtain) literature, insightful advice, and pragmatic guidance throughout the research and document preparation process.

I have been helped by many members of the University administrative staff, but none more than Mrs Fiona Higginson. I never anticipated the logistical challenges of part-time, long-distance study, but she has gotten me over difficult hurdles (many of my own making) more times than I can remember. This dissertation, and indeed the coursework that preceded it, would simply not have happened without her patient assistance and repeated intervention.

Last, but certainly not least, I want to thank my wife, Cathy du Plessis, and my family for the support and encouragement they have provided. I would not have finished this dissertation without them.



## CONTENTS

<b>List of Figures</b>		<b>xiii</b>
<b>List of Tables</b>		<b>xv</b>
<b>1 Introduction</b>		<b>1</b>
1.1 The benefit of hybrid lines . . . . .		1
1.2 Southern African environmental conditions . . . . .		2
1.3 Research objectives . . . . .		3
<b>2 Literature survey</b>		<b>5</b>
2.1 Planning issues . . . . .		5
2.2 Field experience and experimental data . . . . .		6
2.3 Theoretical design issues . . . . .		6
2.4 Audible noise . . . . .		7
2.5 Radio interference . . . . .		7
2.6 Space charge and ionic currents . . . . .		7
2.7 Ripple on dc current . . . . .		8
2.8 Issues related to faults . . . . .		9
2.9 Dissertation scope . . . . .		9
<b>3 Analysis framework</b>		<b>11</b>
3.1 Engineering of ac lines . . . . .		11
3.1.1 Line parameters . . . . .		11
3.1.2 Power transfer limits . . . . .		13
3.1.3 Corona . . . . .		14
3.1.4 Calculation of conductor surface gradients . . . . .		16
3.1.5 Audible noise . . . . .		16
3.1.6 Radio interference . . . . .		17
3.1.7 Electric and magnetic fields . . . . .		17
3.2 Engineering of dc lines . . . . .		17
3.2.1 Brief history of HVDC . . . . .		18
3.2.2 HVDC scheme configurations . . . . .		19
3.2.3 Power transfer limits . . . . .		21

3.2.4	Corona, audible noise and radio interference . . . . .	21
3.2.5	Electric and magnetic fields . . . . .	22
3.2.6	Space charge and ion currents . . . . .	22
3.3	Interactions between ac and dc circuits . . . . .	23
3.3.1	Induced ac voltages on the dc line . . . . .	23
3.3.2	Converter interference due to ac faults . . . . .	24
3.3.3	DC currents in the ac line due to ion migration . . . . .	24
3.3.4	Secondary arc effects on the dc line . . . . .	24
3.4	Summary . . . . .	25
<b>4</b>	<b>Study system</b>	<b>27</b>
4.1	System design . . . . .	27
4.1.1	Transmission distance . . . . .	28
4.1.2	Power transfer capacity . . . . .	28
4.1.3	AC system equivalent . . . . .	29
4.1.4	Conductor selection . . . . .	30
4.2	AC line . . . . .	31
4.2.1	Air insulation . . . . .	31
4.2.2	Insulator selection . . . . .	34
4.2.3	Phase conductor arrangement . . . . .	36
4.2.4	Shield wire placement . . . . .	38
4.2.5	Transmission line geometry . . . . .	40
4.2.6	Line parameters . . . . .	40
4.2.7	Power transfer capacity . . . . .	44
4.3	DC line . . . . .	46
4.3.1	Air insulation . . . . .	46
4.3.2	Insulator selection . . . . .	46
4.3.3	Pole spacing . . . . .	47
4.3.4	Shield wire placement . . . . .	47
4.3.5	Line parameters . . . . .	48
4.3.6	Transmission line geometry . . . . .	51
4.3.7	Power transfer capability . . . . .	51
4.4	Spacing of ac and dc lines . . . . .	52
4.5	Summary . . . . .	53
<b>5</b>	<b>Analysis of the study system</b>	<b>55</b>
5.1	Voltage and conductor optimisation . . . . .	55
5.2	Induced ac currents in pole conductors . . . . .	58
5.3	Conductor surface gradient . . . . .	61
5.3.1	Base case analysis of study system . . . . .	61

5.3.2	Phase conductor bundle parameters . . . . .	64
5.3.3	Pole conductor bundle parameters . . . . .	65
5.3.4	Separation parameters . . . . .	65
5.4	Audible noise . . . . .	69
5.5	Radio interference . . . . .	70
5.6	Space charge and ion currents . . . . .	72
5.6.1	Corona-free condition . . . . .	73
5.6.2	Saturated-corona condition . . . . .	73
5.6.3	Degree of corona saturation . . . . .	76
5.6.4	Space charge and ion current at ground level . . . . .	77
5.6.5	Ion currents injected into phase conductors . . . . .	78
5.7	Summary . . . . .	79
<b>6</b>	<b>Conclusions</b>	<b>81</b>
6.1	Key questions . . . . .	81
6.2	Servitude usage . . . . .	82
6.3	AC ripple in pole currents . . . . .	82
6.4	Audible noise . . . . .	83
6.5	Radio Interference . . . . .	83
6.6	Space charge and ion currents . . . . .	83
6.7	Analytical tools . . . . .	84
6.8	Possible design improvements . . . . .	85
6.9	Design criteria and field-effect limits . . . . .	86
<b>7</b>	<b>Possibilities for further investigation</b>	<b>89</b>
7.1	Long-term space charge and ion current measurements . . . . .	89
7.2	Experimental study to characterise the radio interference excitation function for dc lines . . . . .	89
7.3	Converter operation in the presence of distortion . . . . .	89
7.4	Line cost study . . . . .	90
	<b>References</b>	<b>91</b>
	<b>Appendices</b>	<b>97</b>
	<b>Appendix A Results from EPRI TL Workstation 3.0</b>	<b>97</b>
	<b>Appendix B Hand calculation results</b>	<b>113</b>



## LIST OF FIGURES

3.1	Double-circuit 220 kV ac lines from GECOL-2 project . . . . .	12
3.2	Monopole from Cahora Bassa HVDC scheme . . . . .	18
3.3	Types of HVDC Links . . . . .	20
3.4	Effect of power, voltage and distance on HVDC costs . . . . .	21
4.1	Single line diagram of the study system . . . . .	28
4.2	Configurations for gap factor calculations . . . . .	33
4.3	Dependence of exponent $m$ on the coordination switching impulse with- stand voltage . . . . .	34
4.4	Drawing of standard insulator profile . . . . .	35
5.1	Typical cost contours and trajectory through turning points . . . . .	56
5.2	Effect of varying phase conductor bundle parameters . . . . .	66
5.3	Effect of varying pole conductor bundle parameters . . . . .	67
5.4	Effect of varying separation parameters . . . . .	68
5.5	Lateral profiles of electric field . . . . .	74
5.6	Corona-free and saturated-corona electric field . . . . .	75
5.7	Saturated-corona space charge density . . . . .	76



## LIST OF TABLES

2.1	Voltages of hybrid systems discussed in literature . . . . .	6
4.1	Conductor parameters (from ASTM B 232/B 232M-99) . . . . .	31
4.2	Glass cap and pin insulator parameters (from IEC 60305:1995) . . . . .	36
4.3	AC transmission line conductor data of the study system . . . . .	40
4.4	DC transmission line conductor data for the study system . . . . .	51
5.1	Calculated pricing coefficients for ac and dc lines . . . . .	57
5.2	Calculated maximum conductor surface gradients . . . . .	65
5.3	Calculated audible noise levels for hybrid dc/ac line . . . . .	70
5.4	Calculated radio interference from hybrid dc/ac line . . . . .	71
5.5	Direct current injected into phase conductors (from [18]) . . . . .	79
6.1	Calculated servitude power density . . . . .	82
6.2	Key design limits for hybrid 400 kV ac/500 kV dc line . . . . .	87



## LIST OF SYMBOLS

$\alpha$	Coefficient of thermal expansion [ $/^{\circ}\text{C}$ ]
$\delta$	Relative air density
$\gamma$	Propagation constant of a transmission line [ $/\text{km}$ ]
$\mu$	Ion mobility [ $\text{m}^2/\text{s}/\text{V}$ ]
$\mu_0$	Permeability of free space [ $\text{H}/\text{m}$ ]
$\nu$	Wave propagation velocity for a transmission line [ $\text{m}/\text{s}$ ]
$\phi$	Phase angle difference between the ends of a transmission line [ $^{\circ}$ ]
$\rho_c$	Conductor material resistivity [ $\Omega\text{m}$ ]
$\rho_g$	Earth resistivity [ $\Omega\text{m}$ ]
$\theta$	Hyperbolic angle
$\epsilon_0$	Permittivity of free space [ $\text{F}/\text{m}$ ]
$A$	Conductor cross-section of a transmission line [ $\text{mm}^2$ ]
$a, b, c, d$	Coefficients for estimating life-cycle cost of a transmission line
$C'$	Specific capacitance [ $\text{F}/\text{m}$ ]
$C'_m$	Mutual-capacitance [ $\text{F}/\text{m}$ ]
$C'_s$	Self-capacitance [ $\text{F}/\text{m}$ ]
$C_c$	Estimated total capital cost of a transmission line
$C_l$	Estimated capitalised cost of losses of a transmission line
$C_{lc}$	Estimated life-cycle cost of a transmission line
$D$	Window gap [ $\text{m}$ ]
$D1$	Gap to crossarm [ $\text{m}$ ]

$D_2$	Gap to tower body [m]
$D_i$	Radial distance from $i$ th bundle to the measuring point [m]
$D_{ij'}$	Distance between the $i$ th bundle and the image of the $j$ th bundle [m]
$d_{ij}$	Distance between the $i$ th and $j$ th bundles [m]
$E$	Electric field at a point [V/m]
$E_e$	Electrostatically calculated electric field [V/m]
$E_i$	Maximum conductor surface gradient for the $i$ th bundle [kV/cm]
$E_s$	Electric field under saturated corona conditions [V/m]
$E_v$	Conductor surface gradient for inception of visible corona [kV/cm]
$E_{ave}$	Average conductor surface gradient in a bundle [kV/cm]
$E_{max}$	Maximum conductor surface gradient in a bundle [kV/cm]
$ESCR$	Effective short-circuit ratio
$f$	Frequency of the power system (normally 50 or 60) [Hz]
$G'$	Specific conductance [S/m]
$G_0$	Reference gradient for calculating degree of corona saturation [kV/cm]
$GMR_i$	Geometric mean radius of the $i$ th bundle [cm]
$H$	Altitude [m amsl]
$h_a$	Attachment height of a conductor [m]
$h_i$	Height above ground of the $i$ th bundle [m]
$h_m$	Midspan height of a conductor [m]
$H_t$	Height above ground of conductor [m]
$h_{eq}$	Equivalent height above ground of a conductor [m]
$I$	Lightning stroke current [kA]
$I_0$	Offset in phase current [A]
$I_c$	Critical lightning stroke current [kA]
$I_R$	Current at the receiving end of an ac transmission line [A]

$I_{50}$	Nominal phase current [A]
$I_{sc}$	Short-circuit current of the ac system at the converter bus of an HVDC link [kA]
$J_i$	Ion current density [A/m <sup>2</sup> ]
$J_{+s}, J_{-s}$	Ion current density for positive and negative ions under saturated corona conditions [A/m <sup>2</sup> ]
$K$	Gap factor
$K_a$	Altitude correction factor
$K_c$	Exponent for calculating degree of corona saturation
$k_l$	Loss capitalisation factor for a transmission line
$l$	Length [m]
$L'$	Specific inductance [H/m]
$L'_m$	Mutual-inductance [H/m]
$L'_s$	Self-inductance [H/m]
$l_L$	Length of a transmission line [m]
$l_{span}$	Span length [m]
$m$	Exponent for altitude correction factor
$m_v$	Surface roughness factor
$N_i$	Ion density [ions/cm <sup>3</sup> ]
$n_i$	Number of individual conductors in the $i$ th bundle
$N_{is}$	Space charge density under saturated corona conditions [ions/cm <sup>3</sup> ]
$P_i$	Audible noise sound pressure level from $i$ th bundle [dBA above 20 $\mu$ Pa]
$P_L$	Power transmitted on a transmission line [MW]
$P_d$	Transmitted power on an HVDC link [MW]
$P_{tot}$	Total sound pressure level from multiple bundles [dBA above 20 $\mu$ Pa]
$Q_c$	Reactive power generation at the converter bus of an HVDC link [Mvar]
$r$	Conductor radius [cm]
$R'$	Specific resistance [ $\Omega$ /m]

$r_c$	Attractive radius of a shield-wire or phase conductor [m]
$r_g$	Attractive radius of the ground [m]
$R_i$	Radius of the $i$ th bundle [cm]
$r_i$	Individual conductor radius in the $i$ th bundle [cm]
$R_L$	Resistance of transmission line [ $\Omega$ ]
$r_{ei}$	Equivalent conductor radius of $i$ th bundle [cm]
$RI_i$	Radio interference from $i$ th bundle [dB]
$RI_{tot}$	Total radio interference [dB]
$S$	Depth of structure [m]
$S_c$	Degree of corona saturation
$s_i$	Spacing between individual conductors in $i$ th bundle [cm]
$s_{min}$	Minimum conductor-to-conductor air gap [m]
$s_{ph}$	Phase spacing [m]
$S_{sc}$	Short-circuit power of the ac system at the converter bus of an HVDC link [MVA]
$SCR$	Short-circuit ratio
$T$	Temperature [ $^{\circ}\text{C}$ ]
$t_g$	Skin depth [m]
$U^+$	Maximum positive conductor voltage in conductor-to-conductor gap [kV]
$u^-$	Maximum negative conductor voltage in conductor-to-conductor gap [kV]
$U_n$	Nominal ac voltage of a transmission line [kV]
$U_{50rp}$	Critical flashover voltage (CFO) of rod-plane gap [kV]
$U_{50}$	Insulation strength of air gap [kV]
$V$	Potential at a point [V]
$V_R$	Voltage at the receiving end of an ac transmission line [kV]
$V_S$	Voltage at the sending end of an ac transmission line [kV]
$x$	Length of air gap [m]

$X_L$	Reactance of line [ $\Omega$ ]
$y$	Shunt admittance of a transmission line [S/km]
$z$	Series impedance of a transmission line [ $\Omega$ /km]
$Z_c$	Surge impedance of a transmission line [ $\Omega$ ]



## CHAPTER 1

## INTRODUCTION

In Southern Africa, the development of new generation centres combined with constraints on overhead transmission line servitudes, has promoted interest in the possibility of HVDC and HVAC lines in close proximity to each other, and perhaps even sharing transmission line towers. Certain interactions of HVDC and HVAC transmission circuits, such as induced over-voltages, lightning performance, corona, and secondary arc effects, have been analyzed by other authors. By-an-large, these analyses have focused on conversion of existing double-circuit transmission lines to hybrid transmission lines, and have mostly been in European contexts, so critical review and extension of this work in a Southern African context is needed.

### 1.1 The benefit of hybrid lines

Utility engineers are often faced with divergent requirements of delivering additional energy to customers on one hand, without increasing the amount of land used for transmission line servitudes on the other. Much innovative work has been done by engineers to achieve this; methods that have been suggested include [1; 2; 3]:

- Rebuilding lines in the same servitude with a larger conductor.
- Re-insulating the lines for a higher voltage.
- Rebuilding lines in the same servitude as a double circuit.
- Adding shunt and series compensation to the lines.
- Converting the lines to dc in the same servitude.
- Combining ac and dc lines in the same servitude or on the same structure.

The last method suggested is quite appealing. However, there is strong electrical coupling between the ac and dc circuits, due to their close proximity to each other. Developing an understanding of phenomena arising from this coupling, and translating these into engineering design limits, is an important step in deciding whether hybrid dc/ac transmission lines are a practical option in Southern African conditions.

## 1.2 Southern African environmental conditions

Coastal conditions in Southern Africa are similar to sub-tropical conditions in many other parts of the world, but inland conditions are somewhat different. The unique combination of inland environmental factors which are particularly relevant to the design of overhead transmission lines in Southern Africa include [4]:

- High altitudes, with 1800 m above mean sea level being specified routinely for equipment.
- High lightning ground flash density and high average stroke currents.
- Very dry winter months, with a high incidence of bush-fires.
- Strong sunshine, resulting in high solar insolation and ultra-violet radiation levels.
- Considerable populations of large birds, which can cause insulator pollution and flash-overs.
- A high incidence of sandy soils with relatively high earth resistivity.

**Altitude** has an impact on the insulation strength of air, and hence on the size of the air gaps required to provide adequate insulation. Altitude also impacts the ampacity of conductors, because lower air density at altitude reduces convective cooling. Where conductors are selected by deterministic calculation methods, this is not of concern though, because the combination of worst-case assumptions in deterministic methods gives large design margins.

**Lightning** is one of the coordinating stresses for the design of air gaps. In order to adequately deal with high lightning incidence combined with high stroke currents, a higher lightning impulse withstand voltage is required. Combined with the impact of altitude, this results in air gaps which are significantly longer than in many other parts of the world. Air gap dimensions directly affect the cost of transmission line towers and insulators, so design margins are relatively small.

**Dry winters** result in an accumulation of dust and other air-borne pollutants on insulators. When wetted by first rains, this often results in insulator failures, and it is common for transmission line performance to be poor at the start of the rainy season. The use of polymeric insulators can help to deal with this problem.

**Bush fires** underneath a transmission line weaken the air insulation, and can result in phase-to-phase or phase-to-ground flash-overs. This is especially the case when the bush is very dry, and ambient temperatures are high, resulting in hot fires that produce a lot of carbon particles. In some parts of Southern Africa, sugar cane growing under transmission lines is burned prior to harvesting, and this is a reasonably well-documented cause of poor line performance.

**Strong sunshine** affects the longevity of polymeric insulators, and increases radiative heat transfer to conductors, thereby reducing their ampacity. The long-term effects of ultra-violet radiation on polymeric insulators is being studied, but the expected useful life of polymeric insulators is still uncertain.

**Large birds** perch and roost on transmission line towers, because the towers are frequently high points of the terrain. If insulators are below these perches, then pollution of the insulators by bird-droppings is common. When some species of birds fly away from towers, they eject a "streamer" which can cause flash-overs. Their large wingspans can also cause phase-to-phase flash-overs.

**Poor soil** conditions affect the structural design of foundations for transmission line towers, but also have an impact on the electrical design. Poor soil tends to have high resistivity, which increases the footing resistance of the towers, resulting in higher ground potential rise following lightning strokes, that can cause back-flash-overs.

### 1.3 Research objectives

The research explores the impact of field-effect limits on the design of parallel-circuit hybrid HVDC/HVAC overhead transmission lines, with the objective of increasing power density in overhead transmission line servitudes, while simultaneously conserving land allocated to servitudes. The aims are to produce guidelines to help utility planners assess possible improvements in servitude utilisation and power density by using hybrid HVDC/HVAC transmission lines, to provide utility engineers with an exemplified framework for designing hybrid lines, and hopefully to lay the groundwork for possible future work on the subject of hybrid lines. The approach taken is a critical review of existing literature, particularly from Cigré, combined with calculations and mathematical analysis to yield practically useable results. No field work or laboratory work is envisaged.

Based on a preliminary literature survey, aspects included in the framework will certainly include:

- the roles of conductor clearance and height above ground,
- ac- and dc-voltage effects,
- coupling of phase and pole conductors to overhead ground-wires,
- modulation of the surface gradient on the pole conductors by the ac voltage,
- the effect of the ac field on ion generation,
- capacitive coupling under fault conditions,
- secondary arc effects on the dc line and converter interference due to ac faults,

- audible and radio noise,
- corona losses,
- shielding of telephone interference by the ac line, and
- the possible effects of fire.

The key questions addressed are:

- What ac current flows in the dc line (through coupling), and what effects could this have?
- What dc current flows in the ac line (through ion flow), and what effects could this have?
- How do the length and separation of the ac and dc lines affect these interactions?
- How do these factors influence the technical feasibility of hybrid lines in specific applications?

## CHAPTER 2

## LITERATURE SURVEY

The subjects of hybrid dc/ac transmission lines and parallel operation of ac and dc transmission links have been investigated since the late 1980's, and interest in these subjects continues. Publication rates seem to have increased in the last decade or so, indicating that the subject is relevant to present challenges of extending and reinforcing transmission grids. Nevertheless, at the time of writing, there are apparently no commercially operating hybrid dc/ac transmission lines.

## 2.1 Planning issues

Difficulty obtaining new corridors is often quoted [5; 6; 7; 8; 9; 10] as one of the main reason for contemplating ac and dc lines in the same corridor, or on the same tower. Prudent integration of high-voltage dc transmission (HVDC) allows the power density in a particular corridor to be increased substantially, which obviates the need to obtain new corridors. Power density is higher with HVDC, because dc lines can operate close to the thermal limit. For dc lines, angle- and voltage-stability margins do not apply. Maintaining stability margins and balancing reactive power results in ac lines operating substantially below the thermal limit for most of the time.

Corridor acquisition challenges are not the only justification for greater use of HVDC, and hence hybrid dc/ac lines, in modern transmission networks. Lotfjou et al. [9] has shown that in some circumstances, even a relatively short HVDC link can be financially and economically more attractive than an ac line of similar capacity. This is because some technical characteristics of HVDC become valuable where grid codes become stringent, which is happening world-wide, and especially in Europe and North America. Especially desirable characteristics are the ability of line-commutated converter (LCC) and voltage-source converter (VSC) HVDC to precisely control the power transmitted, and the ability of VSC-HVDC to independently control reactive power.

The bulk of papers deal with so-called "hybrid lines" where the pole and phase conductors share a common structure, as opposed to "hybrid corridors", where ac and dc lines are adjacent and run parallel for a considerable distance. Furthermore, the bulk of literature on hybrid lines focuses on conversion of existing multi-circuit ac lines to

**Table 2.1:** Voltages of hybrid systems discussed in literature

Authors	Date	AC voltage (kV)	DC voltage (kV)
Chartier et al [15]	1981	500	500
Ramesh et al [6]	1988	220	200
Woodford [1]	1993	230	250
Ulleryd, Ye and Moreau [11]	1998	735	450
Kizilcay, Agdemir and Lösing [10]	2009	400	500
Lundkvist, Gutman and Weimers [3]	2009	380	450
Straumann and Franck [2]	2011	400	500
Lee and Shin [14]	2012	154	80
Petino, Fuchs, Schnettler [8]	2014	400	400
Sander et al [13]	2014	380	400

hybrid lines. This is relevant to European paradigms, where multi-circuit ac lines are a common feature, but less so to the African context. Development of a hybrid line from first principles is not discussed in the literature, although the considerations relevant to conversion would be applicable. Only two papers from North America [5; 11] deal with hybrid corridors, which is probably more relevant to the African context.

## 2.2 Field experience and experimental data

Few papers deal with operational issues, field experience or experimental results, probably because there are very few installations or test facilities. Interactions between ac and dc links sharing with common terminal networks have been discussed [12] from the perspective of stability of the interconnected power systems. Field measurements have only been reported from the Quebec-New England multi-terminal HVDC system [11] and a test line in Europe [13]. Other test lines have been proposed [6; 14], but at the time of writing had not been built. Regarding experiments, only investigation of electric field strength on a reduced scale model [7] and laboratory testing of dc insulators [13] had been done at the time of writing.

## 2.3 Theoretical design issues

Most papers deal with theoretical design issues, in particular coupling effects. These effects are dependent on the magnitudes of the ac and dc voltages. Table 2.1 shows that by-an-large, authors have investigated extra- and ultra-high voltages, supporting an observation that the focus of current work is on transmission system improvements. The lower voltages in table 2.1 are related to test lines[6; 14].

The design issues that are thoroughly covered in the literature are induced overvolt-

ages [16], coupling (both capacitive and inductive) [1; 5; 10; 11; 17], and environmental effects [2; 3; 7; 13; 14]. Calculations, electromagnetic simulations and measurements have all been used, and all authors concluded that interactions between ac and dc lines on the same tower or corridor do not present an insurmountable obstacle, but are significant enough to warrant study.

## **2.4 Audible noise**

Definitely audible noise is the most common topic in the published literature. For hybrid lines and corridors, audible noise due to dc corona is likely to cause complaints, because for dc, corona and audible noise are highest in fair weather, whilst for ac they are highest in foul weather [2]. The polarity of dc lines also plays a significant role, because corona from positive conductors is higher than from negative conductors. Audible noise from the dc poles is, therefore, an important defining criterion for pole conductor bundle configuration design. The ac phase conductors also generate noise in rainy weather, which can be a defining criterion for the phase conductor bundle design too. In the literature, calculation methods supported by experimental data are not plentiful, but there seems to be consensus that the corona behaviour under hybrid dc/ac energisation is not fundamentally different to corona behaviour under pure ac or dc energisation [2]. This means that data and calculation techniques for pure ac and dc lines can be used for hybrid dc/ac lines too.

## **2.5 Radio interference**

Radio interference is possibly the most difficult corona-related phenomenon to calculate, even for single-circuit ac transmission lines, let alone hybrid dc/ac transmission lines. In principle, radio interference can be tackled analytically or empirically. An analytical approach requires that the radio interference excitation function is known, and to date excitation functions have only been measured for single-circuit lines. For multi-circuit lines and for hybrid dc/ac lines, an empirical treatment is really the only option [15]. The approach suggested by Chartier et al. [15] is to calculate the radio interference from each phase- and pole-conductor separately, and to combine the contributions assuming that the line to ground propagation mode is the main contributor to radio interference at a point. The method is relatively simple, and seems to be valid for multi-circuit ac lines and for hybrid dc/ac lines.

## **2.6 Space charge and ionic currents**

The mechanism for formation of space charge and ionic current flow is well-described qualitatively [18; 19; 20] but little is written about practical and accessible calculation

methods. In "The Transmission Line Reference Book HVDC to  $\pm 600$  kV" a calculation method developed by Harrington and Kelley [21] which was used in a computer program at Bonneville Power Administration (BPA) is described. The method relies on Deutch's assumption, which is that space charge changes only the magnitude of the electric field; not the direction. This is not true in general, but experiments have demonstrated that the error resulting from this assumption is small, and the same assumption is used in the more sophisticated numerical methods developed by other authors [18; 22]. In a later EPRI publication "HVDC Transmission Line Reference Book", Johnson and Zaffanella [19] proposes an empirical technique called the degree of corona saturation, which is intuitive and simple, but the method benchmarked poorly against the BPA software in a comparison done by Cigre [20]. The method is also criticized by other corona experts [22] as being contrary to corona physics and requiring too many arbitrarily chosen empirical coefficients. Nevertheless, the method shows qualitative correlation to measurements [19; 23] and despite criticizing the method, [20] uses the method for preliminary engineering.

Recently there have been some publications of more sophisticated numerical methods for calculating space charge and ionic current flow by solving partial differential equations and two-point boundary value problems. All the methods seem similar to that of Maruvada [22], but computer programs using these methods are not freely available and the algorithms are described vaguely. This is regrettable, because this is a particularly important phenomenon for dc lines, and it is expected to have an effect for hybrid dc/ac lines as well. It could be that in extremely hot and dry conditions, the impact of the space charge on the insulation below the dc line, and between the ac and dc lines, may be of similar importance to corona-related phenomena such as audible noise.

## 2.7 Ripple on dc current

With ac and dc lines running parallel and close to each other, an ac ripple on the dc current due primarily to inductive coupling is identified by many authors, both from a theoretical basis [1; 5; 10; 17] and measurements [6; 11]. This ripple causes problems with the operation of the converters and saturation of the converter transformers. Under normal operating conditions, transposition of the ac line, the dc line or both lines reduces the ripple to a level that is not problematic. Larsen et al. [17] estimates this level to be in the region of 0.1% of the converter rated current. Under ac fault conditions, the ripple is much larger, with Woodford [1] suggesting that 10% to 15% can be expected, even with transposition. This can be eliminated with a fundamental frequency blocking filter, and it seems that such a blocking filter would probably be required for a hybrid dc/ac transmission line. An alternative of applying special converter firing controls to eliminate much of the ripple is mentioned [1; 16], but not explored.

## 2.8 Issues related to faults

Line faults are normally cleared by the operation of circuit breakers for ac, and control actions to reduce the primary arc current to zero in the case of dc. Automatic reclosing is applied on most ac lines, and automatic restarting of the converters is applied on almost all dc lines. For high-voltage ac lines where the majority of faults are single line-to-ground, single-pole tripping and autoreclosing is often done. The issue of capacitive coupling to the faulted phase from the healthy phases driving a secondary arc current is well-known in ac, and the technique of applying a neutral-connected shunt reactor to assist in commutating the secondary arc current is routine. For pole-to-ground faults where ac and dc lines are in close proximity, capacitive coupling will also drive a secondary arc current, which will not be affected by the ac neutral reactor. This is identified by Ramesh et al. [6] and studied in some detail, using the Electromagnetic Transients for Direct Current (EMTDC) software, by Woodford [1]. Except for the obvious need to increase the "dead time" from fault detection to converter restart, no generally applicable results emerge from this study.

Ramesh et al. [6] also identifies ac phase conductor to dc pole conductor faults as particularly difficult to deal with, because conventional protection cannot reliably identify the fault, nor can conventional approaches clear the fault. Petino et al. [8] comes to a similar conclusion, and suggests advanced interaction between dc controls and ac protection. Using a slightly different approach, Woodford [1] presumes that the fault can be identified, and explores the behaviour of the secondary arc currents only. In the course of his study he identifies that the ac and dc ground connections need to be separated to limit injection of dc into the ac fault current, which could threaten successful interruption of the fault current by the ac circuit breakers.

## 2.9 Dissertation scope

Considering the current interest in hybrid dc/ac transmission lines, and based on results and discussions from the surveyed literature, this dissertation focuses on:

- Insulation of dc and ac lines, especially considering altitude.
- Voltage and conductor optimisation, in the context of prevailing economic parameters.
- Field effects with dc/ac energisation, considering altitude.
- Applicability of existing calculation methods to dc/ac energisation.
- Opportunities for future field measurements and experimental work.



## CHAPTER 3

## ANALYSIS FRAMEWORK

In order to analyse hybrid dc/ac transmission lines, an understanding of the engineering of the ac and dc lines, and of interactions between the ac and dc circuits is needed. Since both ac and dc power transmission are complex electro-magnetic systems, the range of possible interactions is vast. Therefore, the analysis framework has been limited to those interactions which have the largest effect on the environmental and technical performance of the lines, and which will have the most significant impact on engineering design of the hybrid dc/ac line.

### 3.1 Engineering of ac lines

Typical ac transmission lines are shown in figure 3.1. The design of ac transmission lines consists of electrical, mechanical, structural, and civil engineering of many sub-systems and components. From the perspective of this thesis, the main interest is the electrical engineering, and specifically the electrical performance characteristics of an ac overhead transmission line.

- Power transfer capability.
- Insulation performance for operating voltages, switching overvoltages, and lightning overvoltages.
- Corona performance, which affects audible noise, radio interference, and corona power losses.
- Electric and magnetic fields at ground level.
- Coupling and interactions during fault conditions.

#### 3.1.1 Line parameters

Four parameters are classically used to characterise a three-phase ac transmission line. This assumes that the three-phase line is symmetrical, which in practice is never the



**Figure 3.1:** Double-circuit 220 kV ac lines from GECOL-2 project [24]

case, but the value of this assumption is that the line can be represented as a single-phase equivalent. This drastically simplifies calculations and improves understanding of the electrical performance of the line, and the errors resulting from this assumption are generally insignificant. For long transmission lines, the phase conductors are also transposed several times along the line route, which results in the complete line being close to symmetrical, even though the individual line segments between transpositions are not. The parameters used in the theory are [25]:

- Inductance  $L'$ , measured in Henries per metre;
- Shunt capacitance  $C'$ , measured in Farads per metre;
- Resistance  $R'$ , measured in Ohms per metre; and
- Shunt conductance  $G'$ , measured in Siemens per metre.

In most cases, the shunt conductance is neglected, because it is generally extremely low [25]. The series resistance at power frequency, while not negligible, is generally

much smaller than the inductive reactance ( $\frac{X}{R} > 10$ ), so it can often be neglected in calculations. Generally this simplifies calculations and aids understanding of the fundamental phenomena. For direct currents and low frequencies, the series resistance must be taken into account, since the inductive reactance is zero or small.

### 3.1.2 Power transfer limits

The power transfer capacity of an ac transmission line can be characterised in several ways. The most commonly-used are described below. Both the "stability limit" and the "voltage limit" can be increased through the use of shunt- and series-compensation. Thus, these limits are not fundamental to the system and the transmission line, which renders them of secondary importance in the analysis and discussion in subsequent chapters. By contrast, the "thermal limit" and the "surge impedance loading" cannot be altered except by changing the selection and placement of the phase conductors and shield-wires. They are thus more important to the discussion on power transfer limits.

**Stability limit.** From the basic power transmission formula in equation (3.1), the maximum power that can be transferred over a transmission line, with the terminals remaining in synchronism, corresponds to a power angle of  $90^\circ$ . In practice, a transmission line cannot be operated at a power angle of  $90^\circ$  since any disturbance would result in the power system becoming unstable [26]. Depending on the characteristics of the system, the maximum angle that can be safely accommodated varies substantially. With flexible ac transmission system (FACTS) devices, angles of up to 65 degrees are possible [26]. For a practical estimate on typical lines, though, the capability curves developed by St Clair [27] translate to an angle of 44 degrees from the generator to the load. Allowing for step-up and step-down transformers at both ends of the line reduces this to around 35 degrees across the line.

$$P_L = \frac{V_S \cdot V_R \cdot \sin \phi}{X_L} \quad (3.1)$$

where  $P_L$  is power transmitted on the line,  $V_S$  is the sending end voltage,  $V_R$  is the receiving end voltage,  $X_L$  is the line inductive reactance, and  $\phi$  is the difference in phase angle between the voltage phasors and the sending and receiving ends (the power angle) [26].

**Voltage limit.** In some circumstances, the power transfer limit is determined by the voltage drop between the sending end and the receiving end. Often, the maximum and minimum voltages at a particular busbar are also governed by regulations or statutes. Generally the receiving end voltage is limited to 90% to 95% of the sending end voltage at full load.

**Thermal limit.** The current flowing in the phase conductors generates resistive losses, which heat up the conductor. Due to thermal expansion, the phase conductors sag more, and the ground clearance at midspan reduces until the minimum allowable

clearance is reached. No further increase in conductor temperature or current can be tolerated, and this limits the power that can be transmitted (unless the voltage is increased, or environmental conditions provide extra cooling to the conductor). Linear thermal expansion is given by [28]:

$$\frac{\Delta l}{l} = \alpha \cdot \Delta T \quad (3.2)$$

where  $\alpha$  is the coefficient of thermal expansion,  $l$  is length, and  $T$  is temperature.

**Surge impedance loading.** Due to the fact that a transmission line has both series inductance and shunt capacitance, the amount of reactive power generated or consumed by the line varies with the current flowing in the line and the applied voltage. At low loads, the line generates a surplus of reactive power, and the voltage on the line increases (the "Ferranti effect"). Conversely, at high loads, the line consumes a surplus of reactive power, and the voltage on the line decreases. At both low and high loads, the variation of voltage with load is high [26].

At a particular load, the reactive power generated and consumed are balanced, and there is no reactive volt drop. This is determined by the characteristic- or surge-impedance of the line, and is in a sense the "natural" loading of the line. Around the surge-impedance loading, the variation of voltage with load is relatively low, which is desirable from a system operation perspective. For a lossless, three-phase, ac transmission line, the surge impedance loading is given by equation (3.3) [25].

$$\begin{aligned} P_L &= 3 \cdot \frac{\left(\frac{V}{\sqrt{3}}\right)^2}{Z_c} \\ &= \frac{V_R^2}{Z_c} \end{aligned} \quad (3.3)$$

where  $U_n$  is the nominal voltage of the transmission line, and  $Z_c$  is the surge impedance of the line.

### 3.1.3 Corona

Audible noise and radio interference, which are described later, are primarily caused by corona discharges [29]. This is a phenomenon where the air around an energised conductor ionises and partially breaks down. It occurs only in a non-uniform electric field, when the conductor surface gradient exceeds a critical value. The magnitude of the operating conductor surface gradient in relation to this critical value (termed the inception gradient) is the primary factor determining the generation of corona [29].

The inception gradient for visible corona on parallel conductors under ac conditions is given by Peek's Formula [29]. The inception gradient is polarity, geometry, and frequency dependent, and equation (3.4) is valid for positive corona from parallel,

cylindrical conductors up to power frequency (50 Hz or 60 Hz). (This equation uses the rms conductor surface gradient; some references use a peak value which will obviously be different by the factor  $\sqrt{2}$ .)

$$E_v = 21.2m_v\delta \left[ 1 + \frac{0.308}{\sqrt{r\delta}} \right] kV/cm \quad (3.4)$$

where  $E_v$  is the conductor surface gradient for inception of visible corona,  $m_v$  is the surface roughness factor,  $\delta$  is relative air density, and  $r$  is the conductor radius.

The conductor surface gradient is dependent on many factors [29]. The most significant factors, which are discussed briefly below, are:

- System voltage;
- Conductor diameter;
- Clearances to other nearby conductors and to earth;
- Number of conductors in a bundle and bundle geometry;
- Surface roughness of the conductors.

**System voltage:** System voltage is normally regarded as fixed, at the maximum system operating voltage. For a particular geometry, the conductor surface gradient is directly proportional to the applied voltage.

**Conductor diameter:** As the diameter of the conductor changes, the conductor surface gradient varies in a complicated way, but in general it varies inversely with the conductor diameter. That is, a larger diameter results in a lower conductor surface gradient, and a smaller diameter results in a higher conductor surface gradient.

It is worth noting that for a defined conductor surface gradient, the audible noise and radio interference increase with increasing conductor diameter, because the rate at which electric field decreases with radial distance, decreases as the conductor becomes larger. This results in longer streamers around a larger conductor [29].

**Clearances:** Larger clearances generally decrease the conductor surface gradients, but the relationships are complex [29]. Clearances are limited by other considerations, such as lightning- and switching-impulse withstand, but they are the parameter over which designers generally have the most control.

**Bundle configuration:** Increasing the number of conductors in the bundle is a commonly-used technique for reducing the conductor surface gradient. The total charge on a conductor bundle is determined by its equivalent diameter and position relative to other conductor bundles. The number of conductors in a bundle has only a small effect on the total charge, so by increasing the number of individual conductors in the bundle, the charge on each individual conductor is reduced, as is the conductor surface gradient [29]. Corona limitation is not the only reason for using bundled

conductors; it also decreases inductance and increases the surge impedance loading [25].

### 3.1.4 Calculation of conductor surface gradients

For geometries involving multiple conductors and/or bundles, the Maxwell Potential Coefficient Method is a sufficiently accurate and relatively simple method for calculating conductor surface voltage gradients [29]. It is amenable to hand calculation, and can easily be coded in spreadsheets or numerical software.

For a system of conductors:

$$[V] = [P] [Q]$$

where  $[V]$  and  $[Q]$  are respectively phasors of the voltage and charge on the bundles, and  $[P]$  is the potential coefficient matrix. The elements of  $[P]$  are given by [29]:

$$P_{ij} = \begin{cases} \frac{1}{2\pi\epsilon_0} \ln \frac{2 \cdot 100 h_i}{GMR_i} & \text{if } i = j \\ \frac{1}{2\pi\epsilon_0} \ln \frac{D_{ij}'}{d_{ij}} & \text{if } i \neq j \end{cases} \quad (3.5)$$

where  $\epsilon_0$  is the permittivity of free space,  $d_{ij}$  is the distance between the  $i$ th and  $j$ th bundles,  $D_{ij}'$  is the distance between the  $i$ th bundle and the image of the  $j$ th bundle,  $h_i$  is the height above ground of the  $i$ th bundle,  $GMR_i$  is the geometric mean radius of the  $i$ th bundle,  $n_i$  is the number of individual conductors in the  $i$ th bundle,  $r_i$  is the individual conductor radius in the  $i$ th bundle, and  $R_i$  is the radius of the  $i$ th bundle.

Since  $[V]$  and  $[P]$  are known,  $[Q]$  is determined by:

$$[Q] = [P]^{-1} [V]$$

This requires solving a system of linear equations, for which there are many efficient and well-known techniques. Having determined  $[Q]$ , the average and maximum electric field on each bundle are calculated from:

$$E_{ave,i} = \frac{|Q_i|}{2\pi\epsilon_0 n_i r_i} \quad (3.6)$$

$$E_{max,i} = E_{ave,i} \left[ 1 + (n_i - 1) \frac{r_i}{R_i} \right] \quad (3.7)$$

where  $E_{ave}$  is the average conductor surface gradient in a bundle, and  $E_{max}$  is the maximum conductor surface gradient in a bundle [29].

### 3.1.5 Audible noise

Audible noise is a significant environmental impacts of a transmission line. It is noise pollution which people find irritating, and it is extremely difficult to reduce or mask

audible noise after a line has been constructed. As a result, it is very important that transmission lines are designed from the outset to limit audible noise to an acceptable level. Design errors in this regard are so expensive to rectify after the fact, as to be virtually impossible. Because audible noise is a corona-related phenomenon, the conductor surface gradients on the phase-conductors and shield-wires have a significant effect, which is reflected in audible noise prediction formulae [30].

### 3.1.6 Radio interference

Radio interference due to corona is broadband up to approximately 30 MHz, and hence it can affect all radio broadcasts in the vicinity. Modern digital broadcasts are less susceptible to interference, because they employ digital encoding to ensure that the desired signal is reliably transmitted even when there is significant interference on the carrier frequency [31]. Nevertheless, signal degradation can take place even with digital broadcasts if interference on the carrier frequency is large enough. Radio interference from transmission lines and substations has been identified as a particular risk to astronomical radio-telescopes, and for example, radio quiet zones have been legislated to protect the Square Kilometre Array in South Africa [32].

### 3.1.7 Electric and magnetic fields

Over the last three decades, a considerable amount of attention has been given to the alleged health effects of fields from ac transmission lines. To date, there has been no conclusive demonstration that these fields cause disease or ill-health, but some epidemiological studies have suggested a possible link between fields and cancer. As a result, there is public pressure on ac line designers to reduce these fields to levels as low as reasonably attainable. The guideline limits set by the International Commission for Non-Ionising Radiation Protection (ICNIRP) are  $5 \text{ kV/m}$  for ac electric fields and  $100 \mu\text{T}$  for ac magnetic fields [33].

## 3.2 Engineering of dc lines

The majority of the electric power transmission and distribution in the world is done using ac transmission lines and cables. Largely, this is due to the invention of the power transformer in the late 19th century, which allowed the voltage at which the power is transported to be changed easily, and thereby allowed the losses incurred to be reduced without increasing the cost and complexity of electrical machinery in factories and homes [34]. Nevertheless, there are circumstances when it is economically or technically preferable to use dc transmission lines and cables for transmission and distribution of electric power.



Figure 3.2: Monopole from Cahora Bassa HVDC scheme [35]

### 3.2.1 Brief history of HVDC

The first power distribution systems utilised dc. However, voltages were low, and this limited the capacity of these systems, and ac almost completely replaced dc during the first half of the 20th century. It was realised that for dc distribution and transmission to be cost effective, high voltages are required, which could not be achieved using dc generators. However, during the 20th century, techniques were developed to convert ac to dc and vice versa using controlled rectifiers built from mercury arc valves, thyristors, and IGBTs. This allowed higher dc voltages, which are needed for cost-effective distribution and transmission, to be generated [34].

In 1951 an experimental system was built in Russia consisting of a 116 kV, 200 km long dc transmission line from Moscow to Kasira. The system transmitted 30 MW. In 1954, Asea commissioned the first commercial HVDC link between Gotland and mainland Sweden using a 100 kV, 96 km long dc cable to transmit 20 MW. This link used mercury-arc valve based, line-commutated converters [36]. Several mercury-arc, line-commutated converter HVDC links were constructed, including the Pacific Intertie in North America and the North-South Island link in New Zealand. At the time, these were the longest overhead line and undersea cable HVDC links [36].

The development of the thyristor promised improved performance of rectifiers and inverters. In 1972, the 320 MW Eel River Scheme was the first thyristor-based, line-

commutated converter HVDC link. It inter-connected New Brunswick and Quebec. Shortly after, the Cahora Bassa Scheme was commissioned in Southern Africa, which connected the hydro-electric power station at Cahora Bassa with the Apollo substation in the Eskom grid. Over time, thyristor-based, line-commutated converters replaced mercury-arc based schemes, and schemes of higher voltages and higher power transmission capability were constructed. For very-high-power transmission over long distances overland, thyristor-based, line-commutated converters are still the technology of choice [36].

Development of insulated-gate bipolar transistors, and voltage-source converters promised further improvements in performance. A test scheme was built in Sweden in 1977 by ABB, linking Hallsjon and Grangesberg in central Sweden. The link transmitted 3 MW over a  $\pm 10$  kV dc line [37]. The first commercial scheme was a commissioning in 1999, linking the city of Visby with wind generation in the southern part of Gotland. It uses 70 km long,  $\pm 80$  kV dc cables, and is able to transmit 50 MW [38]. Initially voltage-source converters suffered from high losses, and were not considered suitable for transfer of large amounts of power, but improvements in converter technology have resulted in the technology rivalling thyristor based, line-commutated converters in terms of capability. For undersea cable connections, voltage-source converters are rapidly becoming the technology of choice.

Both line-commutated and voltage-source converter HVDC are still in active development, with 800 kV, 3000 km line-commutated schemes and multi-terminal voltage-source converter schemes being developed in China and Europe for integration of large-scale hydro-electric and wind-power generation.

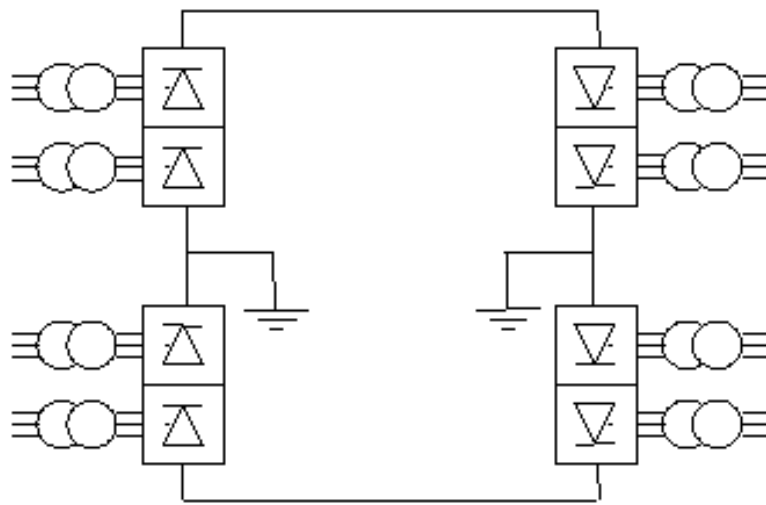
### 3.2.2 HVDC scheme configurations

HVDC schemes can be divided into three categories [39], namely:

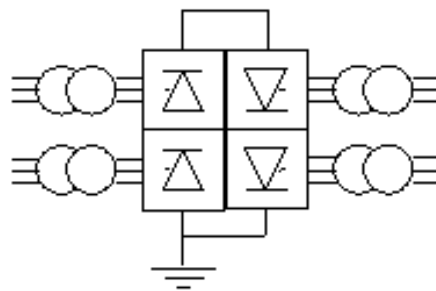
- Point-to-point links, which have a rectifier and inverter, connected by a dc transmission line and/or cable;
- Back-to-back links, which have a rectifier directly connected to an inverter for frequency conversion or asynchronous power transfer; and
- Multi-terminal links, which have several rectifiers and inverters, connected by dc transmission lines and/or cables.

Furthermore, schemes can be configured in three ways [39], namely:

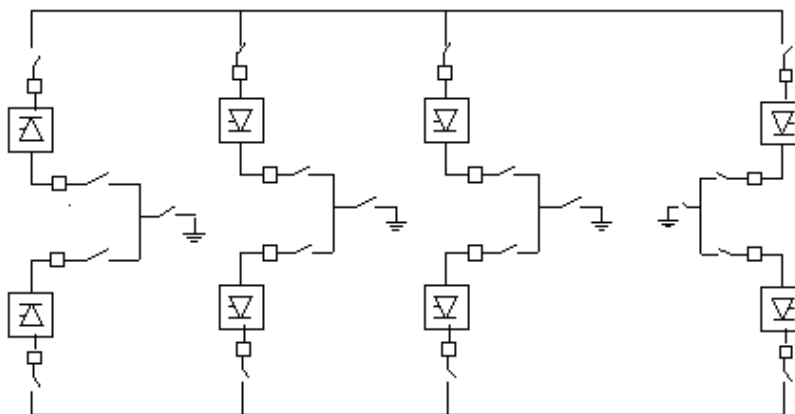
- Monopolar links, which use one pole conductor at high voltage, and another at earth potential (often the second conductor is the earth or sea itself);
- Bipolar links, which use two pole conductors at high voltage, and a third at earth potential (which is usually the earth or sea); and



(a) Point-to-point link



(b) Back-to-back link



(c) Multi-terminal link

**Figure 3.3:** Types of HVDC links [39]

- Homopolar links, which use two pole conductors at high voltage, and omit the conductor at earth potential entirely.

Obviously, only schemes which utilise dc lines are of interest to this thesis. In practise, most such schemes are point-to-point, bipolar links. The link between the rectifier and converter can be either two monopoles, as is done on the Cahora Bassa scheme, or a single bipole, which is the more usual configuration. One pole of the Cahora Bassa scheme is shown in figure 3.2. The majority of dc lines that have been installed in the world operate at  $\pm 500$  kV, but higher voltages do exist [40]. In China, most recent links operate at  $\pm 800$  kV for distances up to 3000 km, and the installed base of  $\pm 800$  kV lines will probably overtake  $\pm 500$  kV within a few decades. Nevertheless, for distances up to approximately 1500 km to 2000 km,  $\pm 500$  kV remains a suitable option [40].

### 3.2.3 Power transfer limits

The power transfer limits for a dc transmission line are determined from the maximum current and voltage that the line and converters can accommodate. The voltages, frequencies and phase angles of the sending and receiving networks do not affect the power transfer limit. Power transfer limits for dc are thus by-an-large economic, rather than technical, limits. [20] has analysed the economic transfer limits for dc lines in some detail, and the results of this analysis are summarised in figure 3.4.

### 3.2.4 Corona, audible noise and radio interference

Audible noise and radio interference are both highly-noticeable corona-related environmental effects of transmission lines. Levels are obviously related to the level of corona, so the inception gradient is a relevant parameter for dc too. Similar to equation (3.4), the inception gradient for visible corona from a positive pole under dc conditions [29, p.

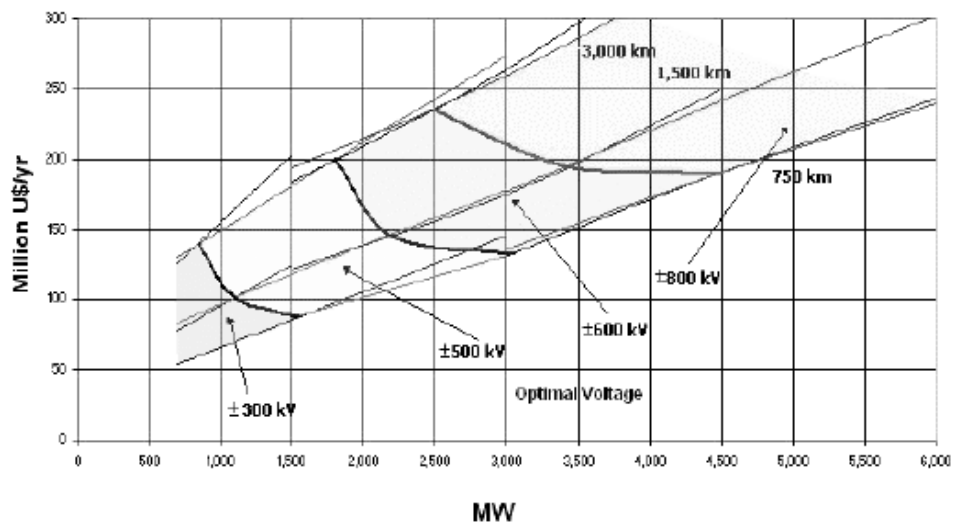


Figure 3.4: Effect of power, voltage and distance on HVDC costs [20]

131] is given by:

$$E_v = 30m_v\delta \left[ 1 + \frac{0.308}{\sqrt{r\delta}} \right] kV/cm \quad (3.8)$$

Unlike ac, where corona is greatest for rainy conditions, corona, audible noise, and radio interference under dc conditions are greatest in fair weather. A further difference between ac and dc is that audible noise emanates from all three phase-conductors under ac conditions, but due to the physics of corona, only the positive pole is a significant contributor to audible noise under dc conditions. The noise from the negative pole is much less than from the positive pole, and due to the method of summing audible noise contributions, it can be safely ignored. For radio interference calculations, the same applies. This means that a lateral profile of audible noise and radio interference for an ac line is centred on the centre phase-conductor, but the profile is centred on the positive pole for a dc line [15].

### 3.2.5 Electric and magnetic fields

Unlike ac, field-enhancing effects due to the corona-generated space charge described above, means that dc electric field is not directly proportional to the applied voltage. The presence of space charge keeps the conductor surface gradient at the corona inception gradient, and enhances the electric field at other points. The maximum enhancement occurs at ground level [20; 22]. Since it would be prohibitively expensive to design a corona-free dc line, practical design criteria must address enhanced electric fields and the ionic current at ground level. Limits of  $25 kV/m$  and  $100 nA/m^2$  have been suggested [20].

DC magnetic fields are not affected by the space charge. A tentative limit for dc magnetic fields has been set [3] as 40 mT, which normally does not affect designs. The earth's magnetic field swamps the magnetic field due to the currents flowing in an HVDC line.

### 3.2.6 Space charge and ion currents

Corona discharge at the surface of a conductor produces positive and negative ions around the conductor. Under ac conditions, ions are attracted back to the conductor in successive half-cycles, and reabsorbed. Under dc conditions, the ions of the opposite polarity are attracted and reabsorbed. The ions of the same polarity are repelled, and eventually reabsorbed by the ground or the other pole. Thus, a space charge of constantly migrating ions is formed in the space between the pole conductors and the ground, and in the space between the two pole conductors. The presence of a space charge in a dc electric field is termed a "space charge field" [20]. The space charge field is described by a set of coupled, non-linear partial differential equations. With appropriate boundary conditions, these equations can be solved numerically, and the space charge density

and ion current can be determined at all points [22]. The space charge and ion current density at ground level are normally the phenomena of particular interest.

Johnson and Zaffanella [19] developed an empirical method for determining ground level space charge density and ion current called the Degree of Corona Saturation Method, which is explained in the EPRI HVDC Transmission Line Reference Book[19]. According to some other experts, the method is based on assumptions which apparently contradict corona physics, needs many arbitrarily selected empirical constants, and so should not be used [22]. To test this, [20] applied Johnson's equations to the Pacific Intertie and compared the results to those from the BPA software. The results do correlate, but apparently not very well, which may support criticism of the method. Nevertheless, a simplification of the method was used for preliminary engineering of dc lines for the Cigre study, suggesting that while not appropriate for detailed analysis, the method does provide useful insights.

### 3.3 Interactions between ac and dc circuits

There are numerous possible interactions between ac and dc lines. Some of the major interactions, which affect the design of hybrid ac-dc lines, include [1]

- Induced ac voltages on the dc line.
- Converter interference due to ac faults.
- DC current in the ac line due to ion migration.
- Secondary arc effects on the dc line

#### 3.3.1 Induced ac voltages on the dc line

At power frequencies, transmission lines which are in close proximity will be electromagnetically coupled, and will, therefore, influence each other. The coupling effects can be modelled by mutual-capacitance and mutual-inductance elements. According to [5] and [11] for short and medium-length transmission lines on separate structures, the capacitive coupling effects can be ignored. Voltage induced longitudinally at power frequency is due mostly to the inductive coupling between the phase conductors of the ac line and the pole conductors of the dc line. The degree of coupling is affected by the separation of the ac and dc lines. Using Fourier series analysis, it can be shown that the power frequency current flowing in the dc line as a result of induced power frequency voltage creates a dc current flowing into the valve-side of the converter transformer [5; 17]. The degree of interference is influenced by the separation of the ac and dc lines, as well as transposition of the ac and dc line.

### 3.3.2 Converter interference due to ac faults

Under fault conditions, the magnitudes of currents in the ac line increase tremendously, so the longitudinally induced ac voltages under fault conditions are significantly larger than under normal conditions. The higher magnitude of the ac currents flowing into the dc side of the converters is more likely to cause converter maloperation, but since the duration of ac faults is typically short, there is a chance that the converters will ride through the fault. If the converters cannot ride through the fault, then converter-control intervention to shut down and restart the converters would be needed. EMTP-type simulations are probably the only way to analyze this interaction in more detail, and the analysis would be relevant to a specific configuration of lines and converters. From literature, it is apparent [1; 11]

A fault in the ac network close to an inverter can disturb the ac voltages required to turn off thyristors, resulting in a so-called "commutation failure" which also needs converter-control intervention. This, however, is an issue for any HVDC inverter [41; 42], and it is unrelated to coupling between ac and dc lines.

### 3.3.3 DC currents in the ac line due to ion migration

Due to the fact that the polarity of dc lines does not reverse every half-cycle of the power frequency, dc lines in corona act as a source of ions. These ions migrate under the influence of the dc electric field, producing a space charge and causing an ionic current between poles and between the poles and earth. In hybrid lines, an ionic current will also flow from the poles to the ac phase conductors, which injects a dc current into them. Calculations of space charge and ionic current, even for pure dc, are difficult, but possible using modern numerical methods and computer programs [15; 18]. Although several computer programs are mentioned in the literature, none seem to be readily available or widely used.

### 3.3.4 Secondary arc effects on the dc line

When a pole-to-ground fault occurs on an HVDC transmission line, the fault is normally detected extremely quickly, and the line current is quickly reduced to zero by protection actions in the converters. This extinguishes the primary arc current, and the line can then be restored to service quickly by the converters after a defined recovery time. Typically this is of the order of 100 ms [1].

For an isolated dc line, this will extinguish the arc current, but for a dc line in close proximity to a parallel ac line, coupling from the ac line will result in a secondary arc current. This secondary arc current will only be extinguished if there is insufficient coupling from the ac line to maintain the arc current. Only the geometry of the hybrid dc/ac line will determine if secondary arc extinction is likely. A similar phenomenon

occurs on ac lines when single-pole auto-reclosing is done, but in the ac case a neutral reactor can be installed to reduce the secondary arc current to a level where extinction is likely. For a dc line, extinction of the secondary arc will normally take longer than extinction of the primary arc, so the recovery time must be extended [1].

For a hybrid dc/ac transmission line (where the ac and dc circuits share one tower), there may also be the possibility of unusual faults, such as pole-to-phase-to-ground. In these fault cases there could be simultaneous operation of ac circuit-breakers and protection actions of the converters, making analysis of the secondary arc currents particularly complicated [1; 8].

### 3.4 Summary

This chapter develops an analysis framework for ac and dc lines. For ac lines, the framework covers power transfer limits, a discussion of corona and related phenomena, electric and magnetic fields. The calculation technique that is used in subsequent chapters to calculate conductor surface gradients is also explained. To place HVDC technology in context, a brief history of dc power transmission is presented. The framework then covers similar material as for ac lines, namely power transfer limits, corona and related phenomena, electric and magnetic fields. Space charge and ion currents which are of particular interest to dc are also discussed. Finally, the chapter outlines the interactions between ac and dc lines in the same corridor which are analysed in subsequent chapters.



## CHAPTER 4

## STUDY SYSTEM

Reasons for contemplating a hybrid ac-dc line or corridor include increasing the power density on the corridor, conserving available servitude space, and accommodating tourist and recreational activities outside of the servitude. A study system has been developed which includes a large installed generation capacity, a substantial distance from the anticipated load centre, where the lines must traverse sensitive areas. Under this combination of circumstances, a high power density in the corridor will minimise adverse environmental impacts of the corridor, while still supporting economic growth in the load centre. A single line diagram of the study system is shown in figure 4.1.

At the time of writing, significant expansion of the Eskom coal-fired, thermal, generating capacity, supported by mines in the Waterberg coalfield is expected. South Africa's Waterberg Coalfield contained approximately forty percent South Africa's confirmed coal resources. Exxaro Resources Limited's 19 million sales tonnes per annum Grootegeluk coal mine supported Eskom's 3,690 MW (net capacity) Matimba power station, and Exxaro had also been contracted to supply a further 14 million tonnes per annum to support Eskom's 4,800 MW Medupi power station, which is still under construction. The raw calorific value of coal in the Waterberg coalfield is in the range of 20 to 24 MJ/kg [43]. Significant load increases were expected in the Witwatersrand load centre due to Gauteng government economic transformation initiatives. These aimed to bring about social transformation, by reducing poverty, through re-industrialisation and modernisation [44]. Overhead transmission lines between the Waterberg coalfield and the Witwatersrand must traverse the sensitive Waterberg ecosystems, which support significant game farming and eco-tourism industries.

#### 4.1 System design

System design is generally the result of extensive system studies. Such studies require accurate data of the existing network, are extremely time-consuming, and are neither instructive nor relevant to this dissertation. This is an empirical study based on selected technical and economic criteria, and not on an accurate model of any real network. Nevertheless, the study system displays some characteristics of the Southern Africa

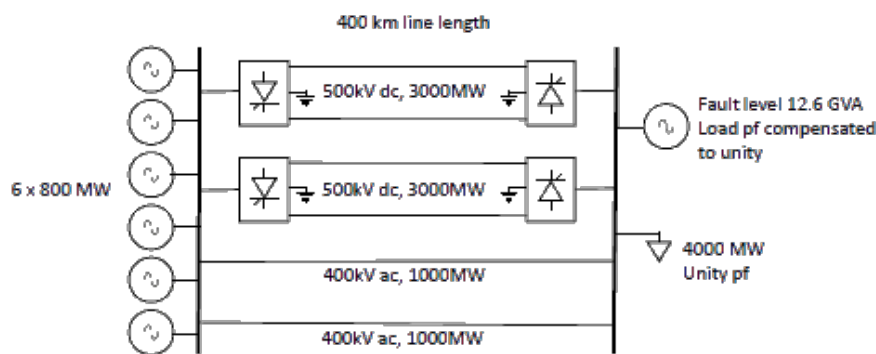


Figure 4.1: Single line diagram of the study system

Power Pool (SAPP) network, which makes the findings relevant to the Southern African context.

#### 4.1.1 Transmission distance

The hybrid line is assumed to be 400 km long. This is the approximate distance from the Waterberg coalfield to the Witwatersrand. Often HVDC transmission is analysed in terms of a "break-even" distance where savings on the transmission line itself offset the cost of the converters, and on this basis 400 km would normally be considered too short for an HVDC link. However, since a dc transmission line has better conductor utilisation, and requires a narrower servitude than an ac transmission line, it may be advantageous to use HVDC to increase the power density in the servitude notwithstanding the higher cost.

#### 4.1.2 Power transfer capacity

It is being assumed that the output capacity of the power station is 4800 MW, made up of six 800 MW generating units. This is the designed net capacity of Medupi power station, and future coal-fired thermal power stations are expected to be of similar magnitude. Loss of a single generating unit results in an output capacity reduction of 800 MW.

It is assumed that the power would be evacuated by means of two hybrid dc/ac transmission lines. The ratings of the individual ac and dc lines, operating at 400 kV and  $\pm 500$  kV respectively, will be 1000 MW and 3000 MW respectively. (These are normal ratings at these voltage levels, based on current materials and state-of-the-art.) This provides 5000 MW of firm capacity (3000 MW dc and 2000 MW ac for loss of a bipole). Loss of a bipole is taken as a single contingency event here, but many planning codes regard it as a double-contingency event, so the study system is robust.

The line design concept for the study system is an three-phase ac line adjacent to a bipolar dc line. A possible variation would be a dc line of two widely-spaced monopoles,

with a three-phase ac line between them. In the former concept, the ac and dc lines can be engineered largely separately, before interactions are investigated, with possible modifications to the initial design. In the latter, the interactions will play a much more significant role in the initial engineering phase, but there may be benefits in terms of line compactness and electric fields. Thus, investigation of the "adjacent bipole" design concept will hopefully provide insights that can be used to develop a "dual adjacent monopole" design concept. In addition to possible technical benefits, the "dual adjacent monopole" design concept will also have better firm capacity, because loss of a bipole will definitely be a double-contingency

### 4.1.3 AC system equivalent

The ac voltages at the rectifier and inverter commutation buses are expected to be 400 kV. The short-circuit ratio (*SCR*) and effective short-circuit ratio (*ESCR*) indicate the relative strength of the ac system, with additional reactive power compensation provided for the converters, at these buses. For operation of the inverter in an HVDC link, without main circuit and control system interventions to improve commutation stability, an *ESCR* of at least 3 is required [41].

$$SCR = \frac{S_{sc}}{P_d} \quad (4.1)$$

$$ESCR = \frac{S_{sc} - Q_c}{P_d} \quad (4.2)$$

where  $S_{sc}$  is the short-circuit power of the ac system at the converter bus,  $I_{sc}$  is the short-circuit current,  $P_d$  is the transmitted power on the HVDC link, and  $Q_c$  is the reactive power generation at the converter bus. For typical operating conditions, the reactive power generation at the converter bus will be of the order of 55% to 80% of the transmitted power on the HVDC link[45].

The study system will not be able to operate in isolation, and will require that the *ESCR* at the inverter station in the load centre is increased. In practice, other generation connected to the load centre is expected to provide sufficient short-circuit power for reliable operation of the inverters.

For a single line, the short-circuit power at the receiving end will be determined by the line reactance and voltage. Specifically, for a 400 kV line, approximately 400 km long, with a positive-sequence inductance of around 1  $\mu\text{H}/\text{m}$ , the short-circuit power at the

receiving end will be approximately:

$$S_{sc} = \frac{U_R^2}{2\pi f l_L L'} \quad (4.3)$$

$$= \frac{(400 \cdot 10^3)^2}{2\pi \cdot 50 \cdot 400 \cdot 10^3 \cdot 1 \cdot 10^{-6}}$$

$$= 1273 \text{ MVA}$$

$$I_{sc} = \frac{1273 \cdot 10^6}{\sqrt{3} \cdot 400 \cdot 10^3} \quad (4.4)$$

$$= 1.84 \text{ kA}$$

where  $U_n$  is the nominal voltage of the ac system,  $f$  is the power frequency,  $l_L$  is the length of the line, and  $L'$  is the inductance per unit length of the line.

This is inadequate for reliable operation of a 3000 MW HVDC bipole. However, it is reasonably assumed that either a synchronous condenser, a static synchronous compensator (STATCOM), or other generation connected to the load centre would increase the short-circuit current of the study system to at least 20 kA. In this case:

$$S_{sc} = \sqrt{3} U_n I_{sc} \quad (4.5)$$

$$= 13850 \text{ MVA}$$

$$P_d = 3000 \text{ MW}$$

$$Q_c = 0.55 \cdot P_d$$

$$= 1650 \text{ Mvar}$$

$$SCR = \frac{13850}{3000}$$

$$= 4.6$$

$$ESCR = \frac{13850 - 1650}{3000}$$

$$= 4.1$$

#### 4.1.4 Conductor selection

The preliminary selection of ac conductor bundle is triple aluminium-conductor, steel-reinforced (ACSR) Tern. This is a low steel-ratio conductor, with a nominal rating of 610 A, and which appears appropriate for a line with a rated current of 1440 A. Low steel-ratio conductors from table 4.1 are suitable for Southern African conditions, where ice-loading is rarely a design consideration. The dc line will have a rated current of 3000 A, and likewise a bundle of low steel-ratio conductors is chosen. In this case, the preliminary selection is quadruple ACSR Bittern. Bittern has a current rating of 802 A. For shield-wires, 19/2.65 galvanised steel wire (or similar optical ground wire (OPGW) conductor) is selected. (19/2.65 means 19 strands each 2.65 mm in diameter.) This has

**Table 4.1:** Conductor parameters (from ASTM B 232/B 232M-99)

Name	Area (mm <sup>2</sup> )			Stranding (mm)		d (cm)	I (A)
	Alum.	Steel	Total	Alum.	Steel		
Chickadee	201.4	11.2	212.6	18/3.77	1/3.77	1.885	403
Pelican	241.7	13.4	255.1	18/4.14	1/4.14	2.070	449
Osprey	282.0	15.7	297.7	18/4.47	1/4.47	2.235	492
Kingbird	322.3	17.4	340.1	18/4.78	1/4.78	2.388	530
Tern	402.8	27.9	430.7	45/3.38	7/2.25	2.702	610
Ruddy	456.1	31.5	487.6	45/3.59	7/3.59	2.873	656
Ortolan	523.7	36.2	559.9	45/3.85	7/3.85	3.081	712
Bluejay	563.9	39.0	602.9	45/4.00	7/4.00	3.196	743
Bunting	604.3	41.6	645.9	45/4.14	7/4.14	3.312	772
Bittern	644.5	44.5	689.0	45/4.27	7/2.85	3.417	802
Dipper	684.8	47.1	731.9	45/4.40	7/4.40	3.516	802
Bobolink	725.2	50.3	775.5	45/4.53	7/4.53	3.624	831
Lapwing	805.8	55.5	861.3	45/4.78	7/4.78	3.816	859
Shield-wire					19/2.65	1.325	

adequate fault-current carrying capabilities and is readily available in Southern Africa (indeed, it is almost a de facto standard for shield-wires on overhead lines).

## 4.2 AC line

Design of a transmission line is an iterative optimisation process. There are a host of design variables, as well as design criteria, so an explicit solution of the optimisation problem is generally not possible. The design of the ac line for the study system is based to a large extent on experience of similar lines in similar applications.

Electrical design of the transmission line deals with four main areas [22]:

- Air insulation
- Insulator selection
- Lightning performance
- Corona performance

### 4.2.1 Air insulation

Air insulation deals with determining the required clearances in air between the phases and earth, and between the different phases. Minimum clearances are determined based on the behaviour of the air gaps under switching surge and power frequency conditions.

Structural design considerations in combination with the minimum clearances are used to determine the overall geometry of the transmission line at the tower and at the midspan.

Minimum electrical clearances based on Eskom practice are 3.2 m phase-to-earth and 4.8 m phase-to-phase. It is required to verify that these clearances provide adequate insulation strength. From IEC 60071-1:1997, a standard switching surge withstand voltage of 1050 kV is appropriate for a 400 kV transmission line, and a lightning surge withstand voltage of 1425 kV. Table A.1, A.2 and A.3 in IEC 60071 do not take altitude correction factors into account. Therefore, the actual withstand values for an air gap of 3.2 m at an altitude of 1800 m are calculated to verify that this gap has enough insulation strength.

The design concept for the tower is a guyed-vee structure, with I insulator strings on the outer phases and V insulator strings on the middle phase. The gap factor for slow-fronted surges for the outer phases is calculated from the formula for gaps to cross-arms, and for the middle phase from the formula for gaps in tower windows. In all practical cases, the gap factor for the tower window case will be less than that for the cross-arm case, and the tower window size, therefore, determines the insulation strength.

The configurations for gap factor calculations are shown in figure 4.2. By iteration, the parameters of the tower geometry are height above ground  $H_t = 19.2$  m, structure depth  $S = 0.5$  m, window gap  $D = 3.5$  m, crossarm gap  $D_1 = 3.5$  m and tower body gap  $D_2 = 4.5$  m. Using these values, the calculated gap factors [46] are:

$$K_{crossarm} = 1.45 + 0.15 \left( \frac{H_t}{D_1} - 6 \right) + 0.25 \left( e^{\frac{-8S}{D_1}} - 0.2 \right) + 0.135 \left( \frac{D_2}{D_1} - 1.5 \right) \quad (4.6)$$

$$= 1.39$$

$$K_{window} = 1.25 + 0.25 \left( \frac{H_t}{D} - 6 \right) + 0.25 \left( e^{\frac{-8S}{D}} - 0.2 \right) \quad (4.7)$$

$$= 1.27$$

The altitude correction factor is calculated from:

$$K_a = e^{m \frac{H}{8150}} \quad (4.8)$$

where  $K_a$  is an altitude correction factor,  $H$  is the altitude (above mean sea level), and  $m$  is an exponent determined from IEC 60071-2. The value of  $m$  is 1.0 for lightning impulse withstand voltages and short-duration power-frequency withstand voltage with clean insulators, and determined from figure 4.3. In particular, for a switching impulse withstand voltage of 1050 kV,  $m$  is 0.4.

Thus, the switching impulse withstand strength of the suggested gap is calculated

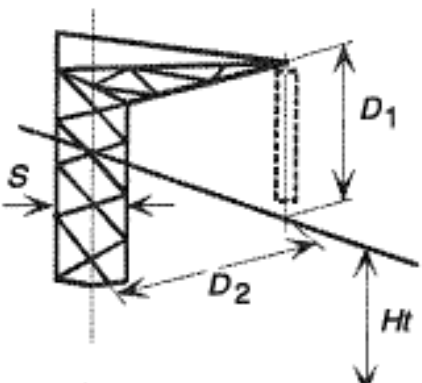
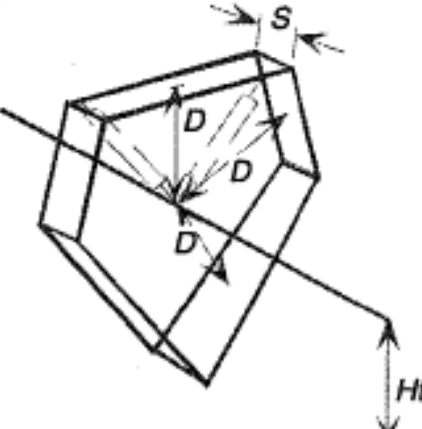
Gap type	Parameters
 <p>Conductor - Crossarm</p>	K
	$D_2 / D_1$
	$Ht / D_1$
	$S / D_1$
 <p>Conductor - Window</p>	K
	$Ht / D$
	$S / D$

Figure 4.2: Configurations for gap factor calculations [46]

as:

$$\begin{aligned}
 K_a &= 1.09 \\
 U_{50rp} &= \frac{1080 \ln(0.46x + 1)}{K_a} \quad (4.9) \\
 &= \frac{1080 \ln(0.46 \cdot 3.5 + 1)}{1.09}
 \end{aligned}$$

$$= 895 \text{ kV}$$

$$\begin{aligned}
 U_{50} &= K_{window} U_{50rp} \quad (4.10) \\
 &= 1138 \text{ kV}
 \end{aligned}$$

Similarly, the lightning impulse withstand strength of the suggested gap is calcu-

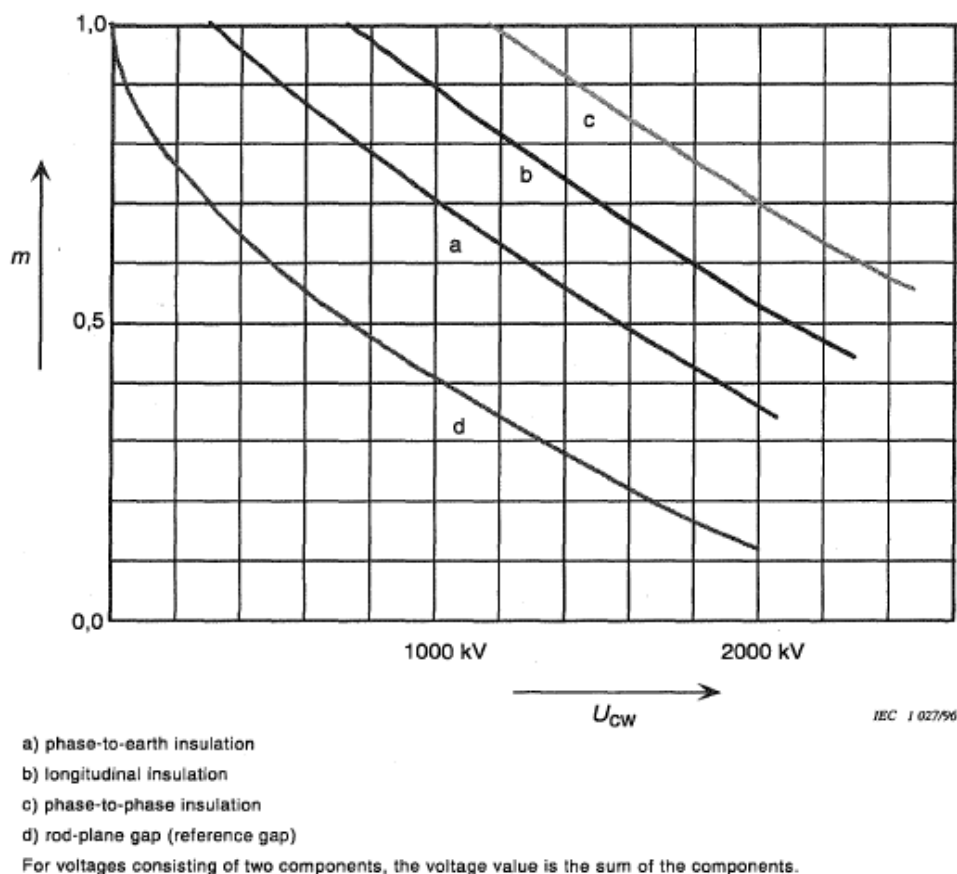


**Figure 4.3:** Dependence of exponent  $m$  on the coordination switching impulse withstand voltage (from figure 9 in IEC 60071-2:1997)

lated.

$$\begin{aligned}
 K_a &= 1.25 \\
 U_{50rp} &= \frac{530x}{K_a} \\
 &= \frac{530 \cdot 3.5}{1.25} \\
 &= 1360 \text{ kV}
 \end{aligned}
 \tag{4.11}$$

$$\begin{aligned}
 U_{50} &= (0.74 + 0.26K_{window}) U_{50rp} \\
 &= 1456 \text{ kV}
 \end{aligned}
 \tag{4.12}$$

## 4.2.2 Insulator selection

Insulator strings are selected to provide adequate clearance between conductor and structure, adequate insulation strength of the insulator string itself, and creepage distance suitable for the prevailing pollution environment. Traditionally glass disc insulator strings have been used for transmission lines. These have the advantages that:

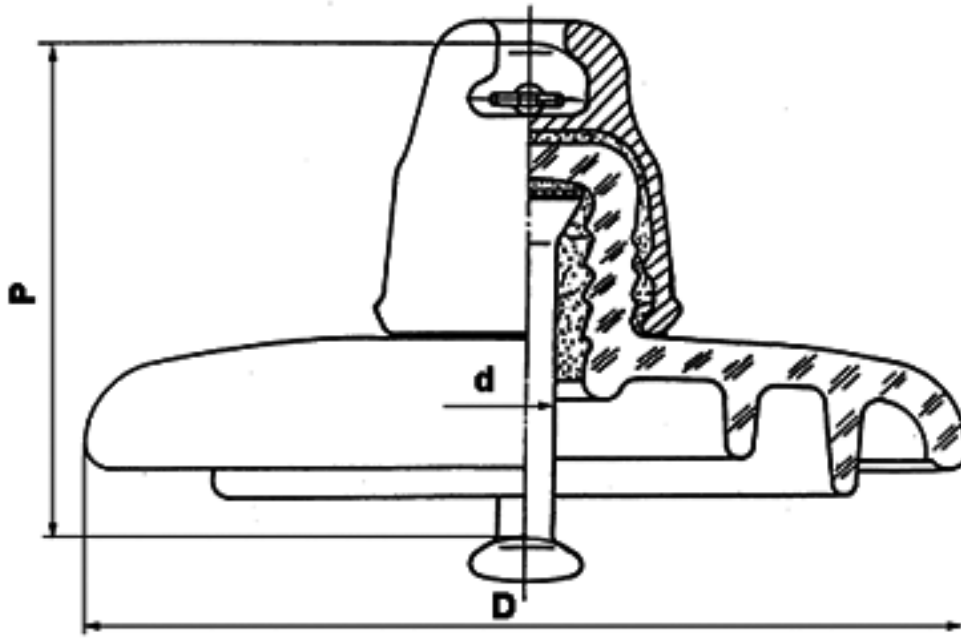


Figure 4.4: Drawing of standard insulator profile [47]

- Glass disc insulators have proven to have a very long service life.
- The properties of insulator strings can easily be changed by varying the number of discs.
- Failed glass disc insulators are easy to locate [47].

In some regions, porcelain disc insulators are used. However, these are prone to puncture, resulting in shattering due to power frequency fault currents, which breaks the string and drops the line. Glass disc insulators are not prone to puncture. Thus, the likelihood of a glass disc insulator string breaking is much lower than for a porcelain disc insulator string.

Glass disc insulator strings are heavy, though, and their performance in heavily polluted environments is sometimes poor. Furthermore, since glass disc insulators require metal fittings for assembly in strings, only a portion of the total length provides insulation, and insulator strings must be longer than composite, long-rod insulators with similar insulation strength. This becomes a more significant factor as the voltage increases. Therefore, increasing use is made of composite, long-rod insulators, especially at high voltages, notwithstanding issues around longevity, flexibility, and maintainability.

Details of individual glass insulator discs are manufacturer-dependent, but the main electrical and dimensional characteristics have been standardised in IEC 60305:1995, which allows a high degree of interchangeability, even between different manufacturers.

**Table 4.2:** Glass cap and pin insulator parameters (from IEC 60305:1995)

IEC60305 designation	U120BP	U120B	U70BL	U70B
Mechanical failing load (kN)	120	120	70	70
Diameter (D) (mm)	255	255	255	255
Spacing (P) (mm)	146	146	146	140
Pin size (d) (mm)	16	16	16	16
Creepage (mm)	450	320	320	320
STW (dry) (kV)	70	70	70	70
STW (wet) (kV)	40	40	40	40
BIL (kV)	100	100	100	100

The standard insulator profile (from the website of a Russian manufacturer) is shown in figure 4.4, and the parameters for two commonly used types of toughened glass cap and pin insulators are given in table 4.2 [47].

For the study system, the I-strings need a length of at least 3.5 m. With a connecting length of 146 mm, this allows 23 glass insulator discs (plus mounting hardware), which provides creepage distance between 7,360 mm (for U70BL and U120B) and 10,350 mm (for U120BP). These equate to a unified specific creepage distance of between 30 mm/kV and 43 mm/kV. (Using the older measure of specific creepage based on phase-to-phase voltage, this is between 18 mm/kV and 25 mm/kV.) This is adequate for the pollution environments that are likely to be encountered inland, which is the assumed location of the study system. The V-strings are longer, but the full length does not need to be taken up with glass insulator discs; steel extension straps can be used for part of the connecting length.

### 4.2.3 Phase conductor arrangement

Phase conductor arrangement deals with phase-to-phase spacing and phase-to-earth clearance, as well as the electrical characteristics of the conductors themselves.

There must be adequate phase-to-phase clearance at midspan, taking asynchronous swinging of the conductors due to wind into account. An empirical relationship calculates the minimum phase-to-phase clearance at the tower from the minimum phase-to-phase clearance at midspan and the span length, for a catenary constant of 1800, and maximum span of 400 m [28].

$$s_{ph} = 0.005 \cdot l_{span} + s_{min} \quad (4.13)$$

For a span of 400 m, equation (4.13) gives the minimum phase spacing at the tower as 6.8 m.

The size of the phase conductors must be taken into account when determining the

phase spacing, especially when bundled conductors are used. The bundle diameter can be calculated from the number of conductors and the conductor spacing.

$$2R_i = \frac{s_i}{\sin \frac{\pi}{n_i}} \quad (4.14)$$

where  $s_i$  is the spacing between individual conductors in the  $i$ th bundle. In this case, the spacing is 45 cm and the number of conductors is 3, so the bundle diameter is 52 cm. Adding this to the phase-to-phase clearance, we get approximately 7 m as the minimum phase spacing.

The geometry must also provide adequate phase-to-ground clearance at the tower. The minimum phase-to-earth clearance at the tower is 3.2 m. If swing-out due to wind is neglected, then the minimum phase spacing will be

$$x = 2 \cdot 3.2 + 0.52 + \text{structure width}$$

which also gives a figure in the region of 7 m. Taking wind into account, there should be an increase in the spacing for those conductors which will be affected by swing-out. Under wind conditions with a return period of 1 to 2 years, the swing-out angle is typically in the range of  $15^\circ$  to  $25^\circ$  [28]. At the higher end of this range, with an insulator length of 3.2 m, this adds approximately 1.5 m to the spacing. For the study system, a conservative phase spacing of 9.9 m is selected.

Attachment height at the tower is determined by midspan height and the conductor sag. The minimum ground clearance gives the height of the conductors at midspan. For this case, it is 8.1 m. The sag can be calculated with a first-order approximation derived from the catenary equation [48].

The Taylor expansion for the hyperbolic cosine function is [49]:

$$\cosh \theta = \sum_{i=1}^{\infty} \frac{\theta^{2i}}{(2i)!} \quad (4.15)$$

Applying the expansion in equation (4.15) to the catenary equation, at the midpoint:

$$\theta = \frac{l_{span}}{2} \quad (4.16)$$

$$\therefore y = C \left( 1 + \frac{l_{span}^2}{8 \cdot C^2} + \frac{l_{span}^4}{384 \cdot C^4} + \dots \right) \quad (4.17)$$

where  $C$  is the catenary constant. Since  $C$  is typically of the order of 4 to 5 times larger than  $l_{span}$ , only the first and second terms are considered. The height at the origin is  $C$ , so the sag is approximated by:

$$sag = \frac{l_{span}^2}{8 \cdot C} \quad (4.18)$$

Applying equation (4.18) for a span of 400 m and  $C$  of 1800 gives a sag of 11.1 m, and, therefore, an attachment height of 19.2 m.

#### 4.2.4 Shield wire placement

In Southern Africa the incidence of lightning is high, and can have a significant effect on the performance of transmission lines. Preventing, or at least substantially reducing, the incidence of lightning related flashovers is an important aspect of transmission line design. This is the primary function of the shield-wires. In addition, the shield-wires provide a path for earth fault currents, and must be selected accordingly.

For structures such as transmission lines which are lower than 100 m high, the most common lightning strikes are negative, downward strokes. That is, the cloud is negatively charged, and the leader progresses from the cloud to the structure. In this scenario, a suitably placed shield wire will intercept the stroke before it reaches the phase- or pole-conductor, and conduct it to ground. This is termed "effectively shielded". If the shield wire does not intercept the stroke and it reaches the phase- or pole-conductor, it is termed a "shielding failure". These normally occur when the lightning stroke current is relatively low. The *electrogeometric model* explains this behaviour.

The electro-geometric model is based on the concept of attractive radius. As a leader progresses, it's path is influenced by the earth and earthed structures in it's vicinity. If the leader approaches to within the attractive radius of the earth or an earthed structure, it will jump to the earth or the earthed structure, otherwise it will progress quasi-randomly. Several functions have been proposed by various authors to relate the attractive radius  $r_c$  to either the stroke charge or peak current [21]. Most are of the form:

$$r_c = a \cdot I^b \quad (4.19)$$

where  $a$  and  $b$  are empirical constants. Perhaps the most widely applied is IEEE 1992 [28], which defines two quantities  $r_c$  the attractive radius of a shield wire or phase conductor, and  $r_g$  the attractive distance of the ground.

$$r_c = 10 \cdot I^{0.65} \quad (4.20)$$

$$r_g = \beta \cdot r_c \quad (4.21)$$

$$\beta = 0.36 + 0.17 \ln(43 - H_t) \quad \text{if } H_t > 40 \text{ then use } H_t = 40 \quad (4.22)$$

Low stroke currents may result in a shielding failure, but shielding failures do not necessarily result in flashovers, because insulator strings and air gaps have a withstand level that must be exceeded before a flashover will occur. The critical stroke current  $I_c$  is the current which will cause a flashover. For complete shielding, it is required that for this critical stroke current, there should be no unprotected arc when the electrogeometric

model is applied [28].

It should be noted that critical stroke current depends on surge impedance, which in turn depends on geometry. Thus, the position of the shield-wires to obtain complete shielding cannot be determined explicitly. For the study system, it is shown below by calculation that the shield wire coordinates (8.1 m;24.2 m), which resulted in a surge impedance of  $263.1\Omega$ , provide complete shielding.

For the assumed line geometry, the surge impedance is calculated as  $Z_c = 263.1\Omega$ . The flashover gradient for negative lightning impulses, without altitude correction, is 650 kV/m. Thus, the critical stroke current is:

$$\begin{aligned} I_c &= \frac{2 \cdot D \cdot 650}{K_a \cdot Z_c} \\ &= \frac{2 \cdot 3.2 \cdot 650}{1.25 \cdot 263.1} \\ &= 13.0 \text{ kA} \end{aligned} \quad (4.23)$$

For the calculated critical stroke current, the attractive radius for shield-wires and phase conductors is:

$$\begin{aligned} r_c &= 11 \cdot 13.0^{0.65} \\ &= 49.7 \text{ m} \end{aligned}$$

The attractive distance for the earth itself is:

$$\begin{aligned} r_g &= 0.36 + 0.17 \ln(43 - 19.2) \cdot 49.7 \\ &= 0.36 + 0.90 \cdot 49.7 \\ &= 44.7 \text{ m} \end{aligned}$$

And through trigonometry, the minimum x-coordinate of a shield wire providing complete shielding is:

$$\begin{aligned} x &= 9.9 + \sqrt{49.7^2 - (44.7 - 19.2)^2} - \sqrt{49.7^2 - (44.7 - 24.2)^2} \\ &= 7.3 \text{ m} \end{aligned}$$

which is less than the actual x-coordinate of 8.1 m, so complete shielding is provided.

It is normal to require that the shield wire sag is 80% of the phase conductor sag (which is 11.1 m from equation (4.18)). The shield wire sag is thus 8.9 m, and since the shield wire attachment height is 24.2 m, the midspan height is 15.3 m.

**Table 4.3:** AC transmission line conductor data of the study system

	Conductor data				
	C1	C2	C3	G1	G2
Conductor number	C1	C2	C3	G1	G2
Conductor type	3 x Tern			19/2.65 steel	
Conductor diameter (cm)	2.703			1.325	
Bundle spacing (cm)	45			-	
DC resistance at 20° C (ohms/km)	0.05906			2.79617	
Attachment height (m)	19.2	19.2	19.2	24.2	24.2
Midspan height (m)	8.1	8.1	8.1	15.3	15.3
Equivalent height (m)	11.8	11.8	11.8	18.3	18.3
Horizontal distance (m)	-9.9	0.0	9.9	-8.1	8.1

#### 4.2.5 Transmission line geometry

The height above ground, phase-spacing, shield wire placement, phase conductor bundle configuration, and shield wire parameters, all affect the conductor surface gradient on the conductors and shield-wires. This determines the level of corona discharges from the transmission line, and in turn audible noise, radio noise, corona loss, and conductor aging. For this analysis, the equivalent height above the ground plane is required for all the conductors and shield-wires, which is calculated as [50]:

$$h_{eq} = \frac{h_a + 2 \cdot h_m}{3} \quad (4.24)$$

The geometry and conductor data for the ac transmission line in the study system is summarized in table 4.3

#### 4.2.6 Line parameters

The line parameters are calculated from the transmission line geometry. These are used for a host of calculations and simulation studies during the design of the power system.

For capacitance calculations, the actual conductor diameters are used, because charge accumulates on the surface of the conductors.

For the shield-wires [29]

$$\begin{aligned} r_{ei} &= r_i \\ &= \frac{1.325}{2} \\ &= 0.663 \text{ cm} \end{aligned}$$

For the phase conductor bundle, with three individual conductors at 45 cm spacing:

[29]

$$\begin{aligned}
 r_{ei} &= \sqrt[n_i]{n_i \cdot r_i \cdot R_i^{n_i-1}} \\
 &= \sqrt[3]{3 \cdot \frac{2.702}{2} \cdot \left[ \frac{45}{\sin \frac{\pi}{3}} \right]^2} \\
 &= 14.0 \text{ cm}
 \end{aligned}$$

Using equivalent heights calculated by equation (4.24), the  $[P]$  matrix is calculated from the line geometry. Image conductors are assumed to reflect in the surface of the earth.

$$[P] = 10^9 \cdot \begin{bmatrix} 92.230 & 17.085 & 7.9525 & 26.973 & 10.894 \\ 17.085 & 92.230 & 17.085 & 19.799 & 19.779 \\ 7.9525 & 17.085 & 92.230 & 10.894 & 26.973 \\ 26.973 & 19.799 & 10.894 & 154.95 & 16.254 \\ 10.894 & 19.799 & 26.973 & 16.254 & 154.95 \end{bmatrix}$$

The  $[P]$  matrix is 5x5 in this case, and it is partitioned into 3x3, 2x3, 3x2 and 2x2 matrices for the purpose of eliminating the shield-wires by Kron reduction [48]. The resulting 3x3 matrix  $[P']$  will represent an equivalent three-phase system having no shield-wires and the same modal capacitances.

$$\begin{aligned}
 [P] &= \begin{bmatrix} P_{cc} & P_{cs} \\ P_{sc} & P_{ss} \end{bmatrix} \\
 [P'] &= [P_{cc}] - [P_{cs}] [P_{ss}]^{-1} [P_{sc}] \\
 &= 10^9 \cdot \begin{bmatrix} 87.110 & 12.710 & 4.6967 \\ 12.710 & 87.660 & 12.710 \\ 4.6967 & 12.710 & 87.110 \end{bmatrix}
 \end{aligned}$$

The capacitance matrix is calculated from  $[P']$ :

$$\begin{aligned}
 [C'] &= [P']^{-1} \\
 &= 10^{-12} \begin{bmatrix} 11.741 & -1.6453 & -0.3929 \\ -1.6453 & 11.885 & -1.6453 \\ -0.3929 & -1.6453 & 11.741 \end{bmatrix} \text{ F/m}
 \end{aligned}$$

This is for an untransposed segment of the transmission line. Since the transmission line will be transposed, the self-capacitances will be equal, as will the mutual-capacitances. Self-capacitances  $C'_s$  are calculated as the arithmetic mean of the diagonal

terms, and mutual-capacitances  $C'_m$  as the arithmetic mean of the off-diagonal terms.

$$\begin{aligned} C'_s &= \frac{C'_{11} + C'_{22} + C'_{33}}{3} \\ &= 11.79 \cdot 10^{-12} \text{ F/m} \\ C'_m &= \frac{C'_{12} + C'_{13} + C'_{21} + C'_{23} + C'_{31} + C'_{32}}{6} \\ &= -1.22 \cdot 10^{-12} \text{ F/m} \end{aligned}$$

The sequence components are easily calculated from the self- and mutual-capacitances [50].

$$\begin{aligned} C'_0 &= C'_s + 2 \cdot C'_m \\ &= 9.33 \cdot 10^{-12} \text{ F/m} \end{aligned} \quad (4.25)$$

$$\begin{aligned} C'_1 = C'_2 &= C'_s - C'_m \\ &= 13.0 \cdot 10^{-12} \text{ F/m} \end{aligned} \quad (4.26)$$

For inductance calculations, the equivalent conductor diameters are used, because current flows throughout the conductors.

For the shield-wires [29]

$$\begin{aligned} r_{ei} &= r_i \cdot e^{-\frac{1}{4}} \\ &= \frac{1.325}{2} \cdot e^{-\frac{1}{4}} \\ &= 0.516 \text{ cm} \end{aligned}$$

For the phase conductor bundle, with three individual conductors at 45 cm spacing [29]

$$\begin{aligned} r_{ei} &= \sqrt[n_i]{n_i \cdot r_i \cdot e^{-\frac{1}{4}} \cdot R_i^{n_i-1}} \\ &= \sqrt[3]{3 \cdot \frac{2.703}{2} \cdot e^{-\frac{1}{4}} \cdot \left[ \frac{45}{\sin \frac{\pi}{3}} \right]^2} \\ &= 12.9 \text{ cm} \end{aligned}$$

Unlike capacitance calculations, the earth is not assumed to be a perfect conductor for inductance calculations. Image conductors are all placed at the skin depth calculated

from the earth resistivity  $\rho$  and frequency  $f$  [50].

$$\begin{aligned}
 \rho_g &= 300 \, \Omega\text{m} \\
 t_g &= \sqrt{\frac{\rho}{2\pi \cdot \mu_0 \cdot f}} \\
 &= 871.7 \, \text{m}
 \end{aligned} \tag{4.27}$$

$$[L] = 10^{-6} \begin{bmatrix} 1.7669 & 0.8983 & 0.7597 & 0.9756 & 0.7666 \\ 0.8983 & 1.7669 & 0.8983 & 0.8889 & 0.8889 \\ 0.7597 & 0.8983 & 1.7669 & 0.7666 & 0.9756 \\ 0.9770 & 0.8904 & 0.7680 & 2.4116 & 0.8013 \\ 0.7680 & 0.8904 & 0.9770 & 0.8013 & 2.4116 \end{bmatrix}$$

The  $[L]$  matrix is 5x5 in this case, and it is partitioned into 3x3, 2x3, 3x2 and 2x2 matrices for the purpose of eliminating the shield-wires by Kron reduction [48]. The resulting 3x3 matrix  $[L']$  will represent an equivalent three-phase system having no shield-wires and the same modal inductances.

$$\begin{aligned}
 [L] &= \begin{bmatrix} L_{cc} & L_{cs} \\ L_{sc} & L_{ss} \end{bmatrix} \\
 [L'] &= [L_{cc}] - [L_{cs}] [L_{ss}]^{-1} [L_{sc}] \\
 &= 10^{-6} \begin{bmatrix} 1.2802 & 0.4155 & 0.3002 \\ 0.4155 & 1.2742 & 0.4155 \\ 0.3002 & 0.4155 & 1.2802 \end{bmatrix} \text{ H/m}
 \end{aligned}$$

This is for an untransposed segment of the transmission line. Since the transmission line will be transposed, the self-inductances will be equal, as will the mutual-inductances. Self-inductances  $L'_s$  are calculated as the arithmetic mean of the diagonal terms, and mutual-inductances  $L'_m$  as the arithmetic mean of the off-diagonal terms.

$$\begin{aligned}
 L_s &= \frac{L'_{11} + L'_{22} + L'_{33}}{3} \\
 &= 1.2782 \cdot 10^{-6} \text{ H/m} \\
 L_m &= \frac{L'_{12} + L'_{13} + L'_{21} + L'_{23} + L'_{31} + L'_{32}}{6} \\
 &= 0.3770 \cdot 10^{-6} \text{ H/m}
 \end{aligned}$$

The sequence components are easily calculated from the self- and mutual-inductances.

$$\begin{aligned} L'_0 &= L'_s + 2 \cdot L'_m \\ &= 2.032 \cdot 10^{-6} \text{ H/m} \\ L'_1 &= L'_2 = L'_s - L'_m \\ &= 0.9012 \cdot 10^{-6} \text{ H/m} \end{aligned}$$

The sequence propagation parameters for the line are thus:

$$\begin{aligned} v_0 &= \frac{1}{\sqrt{L'_0 \cdot C_0}} \\ &= 2.296 \cdot 10^8 \text{ m/s} \\ Z_{c0} &= \sqrt{\frac{L'_0}{C_0}} \\ &= 466.6 \Omega \\ v_1 &= v_2 = \frac{1}{\sqrt{L'_1 \cdot C_1}} \\ &= 2.9198 \cdot 10^8 \text{ m/s} \\ Z_{c1} &= Z_{c2} = \sqrt{\frac{L'_1}{C_1}} \\ &= 263.1 \Omega \end{aligned}$$

#### 4.2.7 Power transfer capacity

The surge-impedance loading of a line with triple ACSR Tern phase conductors is:

$$\begin{aligned} P_l &= \frac{(400 \text{ kV})^2}{Z_{c1}} \\ &= 608 \text{ MW} \end{aligned}$$

The ampacity of ACSR Tern conductor is 610 A, so the thermal limit of the line is:

$$\begin{aligned} P_l &= \sqrt{3} \cdot 400 \text{ kV} \cdot 3 \cdot 610 \text{ A} \\ &= 1268 \text{ MVA} \end{aligned}$$

Even at a power factor of 0.8 (which is poor for a load system with reactive power compensation) this is higher than the figure of 1000 MW suggested in the basic system design.

In practice, a line of 400 km long is most likely to be angle limited to about 35° [27]. To determine the angle limit, it is necessary to calculate the ABCD parameters of the

transmission line from the inductance and capacitance. The series impedance and shunt admittance, propagation constant, and characteristic impedance are calculated: [25]

$$\begin{aligned}
 z &= j2\pi \cdot 50 \cdot 1000 \cdot L_1 \\
 &= j0.2831 \Omega/\text{km} \\
 y &= j2\pi \cdot 50 \cdot 1000 \cdot C_1 \\
 &= j4.0893 \cdot 10^{-6} \text{ S/km} \\
 \gamma &= \sqrt{z \cdot y} \\
 &= j0.0011 \\
 Z_c &= \sqrt{\frac{z}{y}} \\
 &= 263.1 \Omega \text{ as before.}
 \end{aligned}$$

For a 400 km line, the ABCD parameters in matrix form are [25]

$$\begin{aligned}
 ABCD &= \begin{bmatrix} \cosh \gamma \cdot 400 & z_c \cdot \sinh \gamma \cdot 400 \\ \frac{1}{z_c} \cdot \sinh \gamma \cdot 400 & \cosh \gamma \cdot 400 \end{bmatrix} \\
 &= \begin{bmatrix} 0.9088 & j109.78 \\ j0.0016 & 0.9088 \end{bmatrix}
 \end{aligned}$$

The angle limit will be reached if a current flows in the transmission line which produces a phase shift of  $35^\circ$ . Assuming that the receiving network is at the nominal voltage and unity power factor, the magnitude of this current will be:

$$\begin{aligned}
 I_R &= \left| \tan(\phi) \cdot \frac{\frac{V_R}{\sqrt{3}} \cdot \cosh(\gamma \cdot l)}{Z_c \cdot \sinh(\gamma \cdot l)} \right| \\
 &= \left| 0.700 \cdot \frac{230.9 \cdot 0.9088}{j109.78} \right| \\
 &= 1.339 \text{ kA}
 \end{aligned} \tag{4.28}$$

Thus, the power transmitted down the line will be:

$$\begin{aligned}
 P_L &= \sqrt{3} \cdot V_R \cdot I_R \\
 &= \sqrt{3} \cdot 400 \cdot 1.339 \\
 &= 927 \text{ MW}
 \end{aligned} \tag{4.29}$$

This is slightly low, but compares well with the desired capacity of 1000 MW. To increase the angle limit, the inductive reactance of the line must be reduced, which can be done by increasing the GMR of the phase conductor bundle. This will also increase the surge impedance loading of the line, and reduce the reactive power compensation

requirements of the line.

### 4.3 DC line

Similar to the ac transmission line, the design of the dc transmission line is a complex optimisation of many parameters. Arguably the dc design is slightly simpler, because only resistance plays a major role in determining the rating, so there is no need to consider the distributed inductance and capacitance of the line in the basic design. Nevertheless, these will be important when interactions between ac and dc lines are investigated, so they are calculated.

#### 4.3.1 Air insulation

The minimum phase-to-earth clearance for the dc line in the study system is chosen to be 2.3 m. This provides adequate performance under normal operation, and for surges caused by line faults.

According to Pigini et al. [51], under dc conditions, for gaps of practical HVDC lines, the flashover voltage is approximately proportional to the length of the gap. In both dry and wet conditions, the voltage gradient observed in tests was approximately 500 kV/m, and therefore it is suggested that 400 kV/m is an appropriately conservative voltage gradient to use for the design of air gaps in HVDC lines. Applying the cross-arm gap factor from equation (4.6), and the altitude correction factor from equation (4.8), steady-state insulation strength is calculated to be 822 kV, which is clearly adequate.

The defining insulation stress for an HVDC line is normally the surge caused by a line fault, followed by converter blocking and restarting [13]. This produces a switching surge in the region of 1.7 times the normal operating voltage. Using equation (4.9), and the appropriate crossarm gap factor from equation (4.6) and altitude correction from (4.8), the switching surge insulation strength is calculated to be 855 kV, which exceeds the stress of 850 kV.

#### 4.3.2 Insulator selection

Pollution performance is usually the defining consideration for the length of a dc insulator. For a composite insulator with equivalent salt deposit density (ESDD) of 0.06 mg/cm<sup>2</sup>, at 500 kV, [13] calculates that the required insulator length will be 4.8 m.

I-strings are used for the pole conductors, so the swing-out under maximum conditions will be in the range of 50° to 60° [28]. The reduction in clearance due to swing-out will be approximately 4.2 m. Thus, a pole-to-tower clearance of 6.5 m is required.

### 4.3.3 Pole spacing

To calculate air clearances, slow-fronted overvoltages are mainly of interest, and on dc lines they are mainly caused by overvoltages due to an earth fault. For lines of the length under consideration, overvoltages of 1.5 to 1.7 p.u. must be considered.

The insulation strength of a long-span, conductor-to-conductor gap is given in Hutzler et al. [46] as:

$$(U^+ + u^-) = \frac{640 \cdot x^{0.4} (1 - 0.25 \frac{x}{H_t})}{K_a \cdot (1 - \alpha (0.14 + 0.54 \frac{x}{H_t}))} \quad (4.30)$$

$$\alpha = \frac{u^-}{U^+ + u^-} \quad (4.31)$$

With a surge on the positive pole, and normal operating voltage on the negative pole:

$$\begin{aligned} U^+ &= 500 \cdot 1.7 \\ &= 850 \text{ kV} \\ u^- &= 500 \text{ kV} \\ (U^+ + u^-) &= 1250 \text{ kV} \\ \alpha &= 0.4 \end{aligned}$$

By solving equation (4.30) for  $x$ , the minimum pole-to-pole clearance is found to be:

$$s_{min} = 6.3 \text{ m}$$

Applying equation (4.13), the minimum pole spacing is found to be 8.3 m. However, the pole-to-tower clearance already gives a pole spacing of at least 14 m which is used in the study system.

### 4.3.4 Shield wire placement

Assuming that the lightning conditions for an ac and a dc line adjacent to each other, the shield-wires for the dc line are placed using the same principles and calculations as for the ac line. For the study system, it is shown below that the shield wire coordinates (0 m; 29 m) provide complete shielding.

For the assumed line geometry, the surge impedance is calculated as  $Z_c = 250, 1 \Omega$ . The flashover gradient for negative lightning impulses, without altitude correction, is

650 kV/m. Because the insulator length is 4,8 m, the critical stroke current is:

$$\begin{aligned} I_c &= \frac{2 \cdot D1 \cdot 650}{K_a \cdot Z_c} \\ &= \frac{2 \cdot 4.8 \cdot 650}{1.25 \cdot 246.6} \\ &= 18.9 \text{ kA} \end{aligned}$$

For the calculated critical stroke current, the attractive radius for shield-wires and phase conductors is:

$$\begin{aligned} r_c &= 10 \cdot 18.9^{0.65} \\ &= 67.5 \text{ m} \end{aligned}$$

The attractive distance for the earth itself is:

$$\begin{aligned} r_g &= 0.36 + 0.17 \ln(43 - 18.4) \cdot 66.9 \\ &= 0.36 + 0,90 \cdot 67.5 \\ &= 61.1 \text{ m} \end{aligned}$$

And through trigonometry, the minimum x-coordinate of a shield wire providing complete shielding is:

$$\begin{aligned} x &= 7 + \sqrt{67.5^2 - (61.1 - 18.4)^2} - \sqrt{67.5^2 - (61.1 - 29.0)^2} \\ &= -0.1 \text{ m} \end{aligned}$$

which is less than the actual x-coordinate of 0, so complete shielding is provided.

### 4.3.5 Line parameters

For capacitance calculations, the actual conductor diameters are used, because charge accumulates on the surface of the conductors.

For the shield-wires

$$\begin{aligned} r_{ei} &= r_i \\ &= \frac{1.325}{2} \\ &= 0.6625 \text{ cm} \end{aligned}$$

For the phase conductor bundle, with four individual conductors at 45 cm spacing:

$$\begin{aligned} r_{ei} &= \sqrt[n_i]{n_i \cdot r_I \cdot R_i^{n_i-1}} \\ &= \sqrt[4]{4 \cdot \frac{3.417}{2} \cdot \left[ \frac{45}{\sin \frac{\pi}{4}} \right]^3} \\ &= 21.7 \text{ cm} \end{aligned}$$

Using equivalent heights calculated by equation (4.24), the  $[P]$  matrix is calculated from the line geometry. Image conductors are assumed to reflect in the surface of the earth.

$$[P] = 10^9 \cdot \begin{bmatrix} 82.988 & 11.109 & 16.317 \\ 11.109 & 82.988 & 16.317 \\ 16.317 & 16.317 & 159.13 \end{bmatrix}$$

The  $[P]$  matrix is partitioned and shield-wires are eliminated by Kron reduction [48], resulting in a 2x2 matrix  $[P']$ .

$$[P'] = 10^9 \cdot \begin{bmatrix} 81.315 & 9.4357 \\ 9.4357 & 81.315 \end{bmatrix}$$

The capacitance matrix is calculated from  $[P']$ :

$$\begin{aligned} [C'] &= [P']^{-1} \\ &= 10^{-12} \begin{bmatrix} 12.466 & -1.4465 \\ -1.4465 & 12.466 \end{bmatrix} \text{ F/m} \end{aligned}$$

This matrix is symmetrical, with diagonal elements being the self-capacitance and off-diagonal elements being the mutual-capacitances. The common- and differential-mode capacitances are calculated [52], which are similar in magnitude to the zero- and positive-sequence capacitances of an ac line of comparable dimensions.

$$\begin{aligned} C'_0 &= C'_s + C'_m & (4.32) \\ &= 12.02 \cdot 10^{-12} \text{ F/m} \end{aligned}$$

$$\begin{aligned} C'_1 &= C'_s - C'_m & (4.33) \\ &= 13.91 \cdot 10^{-12} \text{ F/m} \end{aligned}$$

For inductance calculations, the equivalent conductor diameters are used, because current flows throughout the conductors.

For the shield-wires [29]

$$\begin{aligned} r_{ei} &= r_I \cdot e^{-\frac{1}{4}} \\ &= \frac{1.325}{2} \cdot e^{-\frac{1}{4}} \\ &= 0.516 \text{ cm} \end{aligned}$$

For the pole conductor bundle, with four individual conductors at 45 cm spacing [29]

$$\begin{aligned} r_{ei} &= \sqrt[n_i]{n_i \cdot r_I \cdot e^{-\frac{1}{4}} \cdot R_i^{n_i-1}} \\ &= \sqrt[4]{4 \cdot \frac{2.703}{2} \cdot e^{-\frac{1}{4}} \left[ \frac{45}{\sin \frac{\pi}{4}} \right]^3} \\ &= 20.3 \text{ cm} \end{aligned}$$

As for ac line parameter calculations, image conductors are all placed at the skin depth calculated from the earth resistivity  $\rho$  and frequency  $f$ , and the inductance matrix is calculated.

$$[L] = 10^{-6} \begin{bmatrix} 1.6750 & 0.8288 & 0.8282 \\ 0.8288 & 1.6750 & 0.8282 \\ 0.8309 & 0.8309 & 2.4127 \end{bmatrix}$$

The  $[L]$  matrix is partitioned and reduced to a 2x2 matrix, eliminating the shield-wires by Kron reduction [48].

$$[L'] = 10^{-6} \begin{bmatrix} 1.3898 & 0.5436 \\ 0.5436 & 1.3898 \end{bmatrix} \text{ H/m}$$

From the diagonal elements, being the self-inductance, and off-diagonal elements, being mutual-inductance, the common- and differential-mode inductances are calculated [52]. As expected, they are similar in magnitude to the zero- and positive-sequence inductances of an ac line of comparable dimensions.

$$\begin{aligned} L'_0 &= L'_s + L'_m \\ &= 1.3898 \cdot 10^{-6} \text{ H/m} \\ L'_1 &= L'_s - L'_m \\ &= 0.5436 \cdot 10^{-6} \text{ H/m} \end{aligned}$$

**Table 4.4:** DC transmission line conductor data for the study system

	Conductor data		
	C4	C5	G3
Conductor number	C4	C5	G3
Conductor type	4 x Bittern	19/2.65 steel	
Conductor diameter (cm)	3.417	1.325	
Bundle spacing (cm)	45	-	
DC resistance at 20°C (ohms/km)	0.04518	2.79617	
Attachment height (m)	18.4	18.4	29.0
Midspan height (m)	7.2	7.2	20.1
Equivalent height (m)	10.9	10.9	23.1
Horizontal distance (m)	-7.0	7.0	0.0

The modal propagation parameters for the line are thus [25]

$$\begin{aligned} v_0 &= \frac{1}{\sqrt{L_0 \cdot C_0}} \\ &= 2.166 \cdot 10^8 \text{ m/s} \end{aligned} \quad (4.34)$$

$$\begin{aligned} Z_{c0} &= \sqrt{\frac{L_0}{C_0}} \\ &= 418.7 \Omega \end{aligned} \quad (4.35)$$

$$\begin{aligned} v_1 &= \frac{1}{\sqrt{L_1 \cdot C_1}} \\ &= 2.9142 \cdot 10^8 \text{ m/s} \end{aligned} \quad (4.36)$$

$$\begin{aligned} Z_{c1} &= \sqrt{\frac{L_1}{C_1}} \\ &= 246.6 \Omega \end{aligned} \quad (4.37)$$

### 4.3.6 Transmission line geometry

The dc transmission line geometry is a combination of the pole conductor and shield wire configurations, the height above ground, and the spacing of the ac and dc lines. The conductor data for the dc line is given in Table 4.4.

### 4.3.7 Power transfer capability

HVDC lines operate at or close to their thermal limit most of the time. Because of the high speed of the converter controls, and the fact that power transmission is asynchronous, HVDC lines are not limited by the need to maintain angle- and voltage-stability margins [26; 41].

For the study system, a four-conductor ACSR Bittern bundle has been chosen. This gives a current rating of 3200 A, and a thermal limit for the bipole of 3200 MW. This is slightly higher than the figure of 3000 MW that is suggested for the study system. Since the thermal coefficient of resistivity for aluminium is  $0.00429/^{\circ}\text{C}$ , the resistance of the four-conductor ACSR Bittern bundle over 400 km, at  $65^{\circ}\text{C}$  is:

$$\begin{aligned} R_L &= 400 \cdot \frac{0.04518}{4} (1 + 0.00429 (65 - 20)) \\ &= 5.39\Omega/\text{pole} \end{aligned}$$

The volt-drop per pole is:

$$\begin{aligned} V_S - V_R &= I_R \cdot R_L \\ &= 3000 \cdot 5.39 \\ &= 14.9 \text{ kV/pole} \end{aligned}$$

Thus, there will be approximately a 3% volt drop, which is well within the 10% limit that is commonly applied to HVDC links.

#### 4.4 Spacing of ac and dc lines

Since charge-carrier mobility plays an important role in the physics of corona, polarity has an impact on the level of corona generated. Corona from the positive pole will be greater than from the negative pole. Thus, the positive pole of a dc line is the principal source of radio interference and audible noise. Therefore, in the study system, the negative pole is placed towards the outside of the hybrid corridor, since this will place the positive pole further from human habitation [22].

Placing the positive pole closest to the ac line allows for a closer spacing of the ac and dc lines. When determining the insulation strength for pole to phase-conductor gap, a negative switching surge on the phase-conductor results in a higher value for  $\alpha$ , a higher insulation strength, and a lower minimum clearance.

According to [13], the air clearance between a pole conductor and a phase conductor is determined by stress of a switching overvoltage on the phase conductor. Therefore, solving equation (4.30) for  $x$  with:

$$\begin{aligned} U^+ &= 500 \\ u^- &= 1217 \text{ kV} \\ \alpha &= 0.4 \end{aligned}$$

gives the minimum clearance between the ac and dc lines to be 10.0 m. Applying equation (4.13) and allowing for the diameter of the pole- and phase conductor bundles,

the minimum centre-to-centre spacing is found to be 28 m. For the study system, a centre-to-centre spacing of 30 m is used.

#### **4.5 Summary**

The chapter develops the study system that is used for analysis. The system consists of two hybrid corridors, each have a 400 kV ac line and a  $\pm 500$  kV bipolar dc line. This configuration provides a firm transfer capacity of 4000 MW. The engineering of the ac and dc lines covers conductor selection, the geometry of the conductors and shield wires based on air insulation strength, and the separation of the ac and dc lines. The line parameters are calculated for the ac and dc lines, and the power transfer capabilities are determined.



## CHAPTER 5

## ANALYSIS OF THE STUDY SYSTEM

The performance of the study system is analysed from several perspectives, and based on the analysis possible improvements to the study system, as well as general guidelines for the design of a hybrid ac-dc line, are developed. The intention is not to generate an optimal design, but to identify and understand the trade-offs which must be made.

### 5.1 Voltage and conductor optimisation

A perennial question facing line designers is choosing the appropriate voltage and conductor for a particular line. Assumptions are made in the development of the study system, which are analysed in more detail here.

It can be shown for any given type of transmission line, that the capital cost is approximately [20; 28]:

$$C_c = l_L \cdot (a + b \cdot U_n + c \cdot A) \quad (5.1)$$

where  $a$ ,  $b$ , and  $c$  are costing coefficients determined from structured breakdowns of historical material and transmission line prices.

Furthermore, the present value of the capitalised cost of losses of the line is [28]:

$$\begin{aligned} C_l &= k_l \cdot I^2 \cdot R_L \\ &= k_l \cdot \left( \frac{P_L}{U_n} \right)^2 \cdot \frac{\rho_c \cdot l_L}{A} \end{aligned} \quad (5.2)$$

where  $k_l$  is a loss-capitalisation factor determined from the marginal cost of generation, utilisation, amortisation period, and weighted cost of capital rates.

Combining capital and losses, it can be shown that that total life-cycle of the line, per unit length (neglecting operating and maintenance costs which are largely fixed costs) is:

$$C_{lc} = a + b \cdot U_n + c \cdot A + \frac{d}{A \cdot U_n^2} \quad (5.3)$$

$$d = k_l \cdot \rho_c \cdot P^2 \quad (5.4)$$

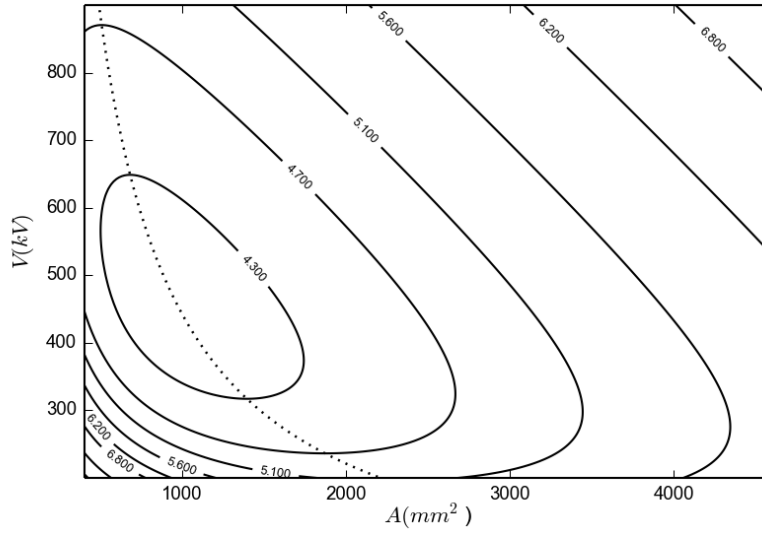


**Figure 5.1:** Typical cost contours and trajectory through turning points

In the plane of  $A$  and  $U_n$ , this equation defines a continuous surface, which can be represented by closed contours at specific values of  $C_{lc}$ . Turning points with respect to  $V$  are either the minimum or maximum cost for a particular value of  $U_m$ . Tracing a trajectory through these turning points leads to the absolute minimum of the surface. This is illustrated in figure 5.1.

Thus, differentiating with respect to  $A$  for an arbitrary value of  $C_{lc}$  identifies this trajectory.

$$\begin{aligned}
 0 &= 0 + b \cdot \frac{dU_n}{dA} + c + d \cdot \left( \frac{-1}{A^2 \cdot U_n^2} + \frac{-2}{A \cdot U_n^3} \cdot \frac{dU_n}{dA} \right) \\
 \frac{dU_n}{dA} &= \frac{c \cdot A^2 \cdot V^3 - d \cdot U_n}{2 \cdot d \cdot A - b \cdot A^2 \cdot U_n^3} \\
 &= 0 \text{ for a turning point} \\
 A \cdot U_n &= \sqrt{\frac{d}{c}} \tag{5.5}
 \end{aligned}$$

The trajectory is a hyperbola on the  $A-U_n$  plane. Substituting for  $A$  into equation (5.3) yields an explicit function for the total life-cycle cost in terms of  $V$  moving along this trajectory.

$$\begin{aligned}
 C_{lc} &= a + b \cdot U_n + c \cdot \sqrt{\frac{d}{c}} \cdot \frac{1}{U_n} + \frac{d}{\sqrt{\frac{d}{c}} \cdot \frac{1}{U_n} \cdot U_n^2} \\
 &= a + b \cdot U_n + 2 \cdot c \sqrt{\frac{d}{c}} \cdot \frac{1}{U_n} \tag{5.6}
 \end{aligned}$$

Differentiating with respect to  $U_n$  allows us to find the minimum along the trajectory,

**Table 5.1:** Calculated pricing coefficients for ac and dc lines

	ac line	dc line
a (R/km)	1 563 900	778 565
b (R/kV/km)	2 837	2 768
c (R/mm <sup>2</sup> /km)	660	460
$P_L$ (MW)	1000	3000
$U_{nopt}$ (kV)	473	589
$A_{opt}$ (mm <sup>2</sup> )	1 430	2 492

and thereby the optimal design voltage and conductor cross-section of the transmission line. It is noteworthy that the optimal voltage and conductor cross-section are independent on the length of the transmission line, because both the estimated capital cost and the estimated operating and maintenance cost are directly proportional to length.

$$\begin{aligned} \frac{dC}{dU_n} &= b - 2 \cdot c \sqrt{\frac{d}{c}} \cdot \frac{1}{U_n^2} \\ &= 0 \text{ for a turning point} \end{aligned}$$

$$U_n = \sqrt{\frac{2 \cdot c}{b}} \cdot \sqrt{\frac{d}{c}} \quad (5.7)$$

$$A = \sqrt{\frac{b}{2 \cdot c}} \cdot \sqrt{\frac{d}{c}} \quad (5.8)$$

There is not much publicly-available costing data for transmission lines, because competition in the market is intense and costing-data is commercially sensitive. Nevertheless, Muftic and Burger [28] presents results of regression analysis on Eskom data ac line data quoted in South African Rand, and Cigre JWG-B2/B4/C1.17 [20] investigated the impact of HVDC line cost on the economics of HVDC projects, quoting results of regression analysis on several hypothetical dc lines in United States Dollars. Applying corrections for exchange rate and commodity price changes results in the price estimating coefficients given in table 5.1. The benchmark rates used are 14.00 ZAR/USD, Steel 0.25 USD/kg, and Aluminium 1.6 USD/kg.

For both ac and dc, optimisation of voltage and conductor is done assuming a marginal cost of generation of 150 R/MWh, a net discount rate of 6%, and an economic life of 25 years, which are considered reasonable economic parameters for the Southern African context. For dc, a power transfer level of 3000 MW and utilisation factor of 90% is used, and for ac 1000 MW and 55%. The optimal voltage and conductor cross-section in table 5.1 suggest that the voltage and power transfer levels selected for the study system are sub-optimal, but the analysis would benefit from coefficients calculated using more recent data. Forcing the calculated optimal voltages to 400 kV and 500 kV for the ac and

dc lines respectively, yields optimum power transfer levels of 792 MW and 2020 MW at conductor cross-sections of 1342 mm<sup>2</sup> and 2968 mm<sup>2</sup>. Interestingly, the ac power transfer level is close to the angle limit, and the dc power transfer level is such that loss of a pole results in a 1000 MW transmission capacity reduction, which is possibly more palatable to system operations than the 1500 MW reduction for the study system.

## 5.2 Induced ac currents in pole conductors

Due to capacitive and inductive coupling effects, an ac current  $I_{50}$  will flow in the pole conductors. By the action of the converters, this ripple current will cause a dc offset in the phase currents on the ac side of the converters. Depending on the phase angle between the ripple and the particular phase, the dc offset will vary. It will be a maximum when the ripple is exactly in-phase or 180° out-of-phase. From converter operation theory, the maximum dc offset in a phase current is [17]:

$$I_0 = \frac{\sqrt{3}}{\pi} \cdot I_1 \quad (5.9)$$

where  $I_1$  is the fundamental frequency current flowing in the ac transmission lines.

Numerical time-domain simulation would probably be a good method of investigating this effect for a particular hybrid dc/ac line and converter configuration, and of determining practical limits. Such simulation studies are outside the scope of this dissertation, but could be included in further work on the topic. However, even if the effects are not simulated, it is useful to estimate the magnitude of the ripple current.

For medium to short lines, such as this study system, the capacitive coupling effects are not significant [5], and only magnetic coupling is considered here. For the system of pole-conductors and phase-conductors, the inductance matrix will be calculated. Since current flows throughout the cross-section of the conductors, the equivalent conductor diameters are used for inductance calculations.

For the shield-wires [29]

$$\begin{aligned} r_{ei} &= r_I \cdot e^{-\frac{1}{4}} \\ &= \frac{1.325}{2} \cdot e^{-\frac{1}{4}} \\ &= 0.516 \text{ cm} \end{aligned}$$

For the phase conductor bundle [29]

$$\begin{aligned} r_{ei} &= \sqrt[n_i]{n_i \cdot r_i \cdot e^{-\frac{1}{4}} \cdot R_i^{n_i-1}} \\ &= \sqrt[3]{3 \cdot \frac{2.703}{2} \cdot e^{-\frac{1}{4}} \cdot \left[ \frac{45}{\sin \frac{\pi}{3}} \right]^2} \\ &= 26.0 \text{ cm} \end{aligned}$$

For the pole conductor bundle

$$\begin{aligned} r_{ei} &= \sqrt[n_i]{n_i \cdot r_i \cdot e^{-\frac{1}{4}} \cdot R_i^{n_i-1}} \\ &= \sqrt[4]{4 \cdot \frac{3.417}{2} \cdot e^{-\frac{1}{4}} \cdot \left[ \frac{45}{\sin \frac{\pi}{4}} \right]^3} \\ &= 31.8 \text{ cm} \end{aligned}$$

The inductance matrix is  $[L]$ , where:

$$L_{ij} = \begin{cases} \frac{\mu_0}{2\pi} \cdot \ln \frac{100D_{ij'}}{GMR_i} & \text{if } i = j \\ \frac{\mu_0}{2\pi} \cdot \ln \frac{D_{ij'}}{d_{ij}} & \text{if } i \neq j \end{cases}$$

The finite conductivity of the earth is taken into account by placing image conductors at the skin depth calculated from the earth resistivity  $\rho_g$  and frequency  $f$ .

$$\rho_g = 300 \Omega\text{m}$$

$$\begin{aligned} t_g &= \sqrt{\frac{\rho}{2\pi \cdot \mu_0 \cdot f}} \\ &= 871.7 \text{ m} \end{aligned}$$

Since  $t_g$  is substantially larger than  $h_i$  and  $d_{ij}$ , the image distances can all be approximated as:

$$\begin{aligned} D_{ij'} &= \sqrt{d_{ij}^2 + (h_i + t_g)^2} \\ &= h_i + \delta \end{aligned}$$

Thus, for the full system of three phase-conductors, two pole-conductors, and three

shield-wires, the inductance matrix is:

$$[L] = 10^{-6} \begin{bmatrix} 1.7173 & 0.8983 & 0.7597 & 0.6582 & 0.5874 & 0.9760 & 0.7666 & 0.6120 \\ 0.8983 & 1.7173 & 0.8983 & 0.7296 & 0.6347 & 0.8891 & 0.8891 & 0.6635 \\ 0.7597 & 0.8983 & 1.7173 & 0.8418 & 0.6969 & 0.7666 & 0.9760 & 0.7294 \\ 0.6580 & 0.7294 & 0.8417 & 1.6750 & 0.8288 & 0.6639 & 0.7947 & 0.8287 \\ 0.5872 & 0.6345 & 0.6967 & 0.8288 & 1.6750 & 0.5952 & 0.6777 & 0.8287 \\ 0.9774 & 0.8906 & 0.7681 & 0.6655 & 0.5941 & 2.4116 & 0.8013 & 0.6288 \\ 0.7681 & 0.8906 & 0.9774 & 0.7963 & 0.6793 & 0.8013 & 2.4116 & 0.7363 \\ 0.6146 & 0.6660 & 0.7319 & 0.8314 & 0.8314 & 0.6299 & 0.7374 & 2.4127 \end{bmatrix}$$

Shield-wires are eliminated by partitioning the matrix and applying Kron reduction[48]:

$$\begin{aligned} [L] &= \begin{bmatrix} L_{cc} & L_{cs} \\ L_{sc} & L_{ss} \end{bmatrix} \\ [L'] &= [L_{cc}] - [L_{cs}] [L_{ss}]^{-1} [L_{sc}] \\ &= 10^{-6} \cdot \begin{bmatrix} 1.2010 & 0.3816 & 0.2584 & 0.2096 & 0.1821 \\ 0.3815 & 1.1857 & 0.3676 & 0.2555 & 0.2071 \\ 0.2584 & 0.3676 & 1.1716 & 0.3511 & 0.2533 \\ 0.2095 & 0.2554 & 0.3511 & 1.2126 & 0.4009 \\ 0.1821 & 0.2071 & 0.2533 & 0.4010 & 1.2747 \end{bmatrix} \text{ H/m} \end{aligned}$$

To calculate the longitudinally induced ac voltages on the pole-conductors, only  $L'[4 \dots 5; 1 \dots 3]$  is relevant. The induced voltages will depend on the currents flowing in the ac line and the length of parallelism. Assuming full-load on the ac line of 1000 MW, the currents on the ac line would be balanced, three-phase currents of 1443 A. The line length is 400 km. Thus, the voltages induced longitudinally in the poles are

$$\begin{aligned} \begin{bmatrix} V'_{p1} \\ V'_{p2} \end{bmatrix} &= 400 \cdot 10^3 \cdot 2\pi \cdot f \cdot 10^{-6} \cdot \begin{bmatrix} 0.2095 & 0.2554 & 0.3511 \\ 0.1821 & 0.2071 & 0.2533 \end{bmatrix} \cdot \begin{bmatrix} I_1 \\ I_2 \\ I_3 \end{bmatrix} \\ &= \begin{bmatrix} 26.33 & 32.10 & 44.12 \\ 22.88 & 26.03 & 31.84 \end{bmatrix} \cdot \begin{bmatrix} 1443 + j0 \\ 722 + j1250 \\ 722 - j1250 \end{bmatrix} \\ &= \begin{bmatrix} 15.03 - j17.00 \\ 7.257 - j8.731 \end{bmatrix} \text{ kV} \end{aligned}$$

These are transformed into common- and differential-mode voltages [52]:

$$\begin{aligned} V_0 &= \frac{1}{2} \cdot (V_{p1} + V_{p2}) \\ &= 22.285 - j25.735 \end{aligned} \tag{5.10}$$

$$\begin{aligned} V_1 &= \frac{1}{2} \cdot (V_{p1} - V_{p2}) \\ &= 7.7712 - j8.2731 \end{aligned} \tag{5.11}$$

The differential mode voltage will cause a circulating ac current through the converters and the poles, which will cause zero sequence currents to flow in the converter transformers [5]. This current can be calculated from the overall differential mode impedance of the two poles, which is the sum of the inductive reactance of the lines and the smoothing reactors installed at each end. A value of 500 mH per pole per converter is assumed for the smoothing reactors.

$$\begin{aligned}
 I_1 &= \frac{V_1}{2\pi \cdot f \cdot L'_1 \cdot L_L} \\
 &= \frac{7.7712 + j8.2731}{2\pi \cdot 50 \cdot (0.846 \cdot 10^{-6} \cdot 400 \cdot 10^3 + 4 \cdot 500 \cdot 10^{-3})} \\
 &= 10.58 - j11.26 \text{ A} \\
 |I_1| &= 15.5 \text{ A}
 \end{aligned}$$

This is in the region of 0.5% of the pole current, which is large enough to create asymmetrical thyristor commutation, introduce non-characteristic harmonics into the ac systems, and cause saturation of converter transformers [2; 17]. Larsen et al. [17] indicates that 0.1% is the threshold above which HVDC system performance will be negatively affected. Transposition of the ac line is probably the most practical method to achieve a five-fold reduction in the ripple current. Substantial increases in the separation distance between ac and dc conductors, or in the size of the smoothing reactors, are impractical.

### 5.3 Conductor surface gradient

The conductor surface gradients for the phase conductors and shield-wires are calculated from the  $[P]$  matrix in equation (3.5) using the relationships in equations (3.6) and (3.7). Parameters of the hybrid dc/ac transmission line are varied to determine which are useful in design development and optimisation. Inspecting the results in figures 5.2, 5.3 and 5.4, only the diameter and number of individual conductors in the pole- and phase-conductors have a significant effect on the conductor surface gradient. From an engineering design perspective, this is a useful result, because it reduces the number of variables that must be considered in the optimisation.

#### 5.3.1 Base case analysis of study system

The conductor surface gradients for the phase conductors, pole conductors, and shield-wires are calculated for the study system. These results are the starting point for parametric studies. The method of potential coefficients described in section 3.1.4 is used.

Geometric mean radii of the phase conductors, pole conductors and shield-wires are

calculated. In this calculation, the actual conductor diameters are used, because charge accumulates on the surface of the conductors.

For the shield-wires

$$\begin{aligned} r_{ei} &= r_i \\ &= \frac{1.325}{2} \\ &= 0.663 \text{ cm} \end{aligned}$$

For the phase conductor bundle, with three individual conductors at 45 cm spacing:

$$\begin{aligned} r_{ei} &= \sqrt[n_i]{n_i \cdot r_i \cdot R_i^{n_i-1}} \\ &= \sqrt[3]{3 \cdot \frac{2.702}{2} \cdot \left[ \frac{45}{\sin \frac{\pi}{3}} \right]^2} \\ &= 14.0 \text{ cm} \end{aligned}$$

For the pole conductor bundle, with four individual conductors at 45 cm spacing:

$$\begin{aligned} r_{ei} &= \sqrt[4]{4 \cdot \frac{3.417}{2} \cdot \left[ \frac{45}{\sin \frac{\pi}{4}} \right]^2} \\ &= 21.7 \text{ cm} \end{aligned}$$

Using equivalent heights calculated by equation (4.24), the  $[P]$  matrix is calculated from the line geometry. Image conductors are assumed to reflect in the surface of the earth. The phase conductors are numbered 1 to 3, the pole conductors, 4 and 5, and the shield-wires, 6 to 8.

$$[P] = 10^9 \cdot \begin{bmatrix} 92.2 & 17.1 & 7.95 & 3.50 & 1.89 & 27.0 & 10.9 & 4.41 \\ 17.1 & 92.2 & 17.1 & 6.12 & 2.87 & 19.7 & 19.8 & 6.50 \\ 7.95 & 17.1 & 92.2 & 12.5 & 4.78 & 10.9 & 27.0 & 10.0 \\ 3.50 & 6.12 & 12.5 & 83.0 & 11.1 & 5.20 & 12.2 & 16.3 \\ 1.89 & 2.87 & 4.78 & 11.1 & 83.0 & 2.91 & 5.76 & 16.3 \\ 27.0 & 19.8 & 10.9 & 5.20 & 2.91 & 155. & 16.2 & 6.85 \\ 10.9 & 19.8 & 27.0 & 12.2 & 5.76 & 16.2 & 155. & 12.2 \\ 4.41 & 6.50 & 10.0 & 16.3 & 16.3 & 6.85 & 12.2 & 159. \end{bmatrix}$$

The  $[P]$  matrix is 8x8 in this case. Since the conductor surface gradient on all phase conductors, pole conductors, and shield-wires is wanted, the system is not reduced. The

capacitance matrix is calculated from  $[P]$ :

$$[C] = [P]^{-1}$$

$$= 10^{-12} \begin{bmatrix} 11.7 & -1.64 & -0.37 & -0.13 & -0.07 & -1.77 & -0.35 & -0.11 \\ -1.64 & 11.9 & -1.59 & -0.31 & -0.10 & -1.00 & -0.98 & -0.17 \\ -0.37 & -1.59 & 11.9 & -1.28 & -0.25 & -0.33 & -1.67 & -0.37 \\ -0.13 & -0.31 & -1.28 & 12.7 & -1.37 & -0.14 & -0.58 & -1.02 \\ -0.07 & -0.10 & -0.25 & -1.37 & 12.5 & -0.08 & -0.19 & -1.10 \\ -1.77 & -1.00 & -0.33 & -0.14 & -0.08 & 6.97 & -0.40 & -0.13 \\ -0.35 & -0.98 & -1.67 & -0.58 & -0.19 & -0.40 & 7.02 & -0.33 \\ -0.11 & -0.17 & -0.37 & -1.02 & -1.10 & -0.13 & -0.33 & 6.57 \end{bmatrix}$$

To calculate the rms ac components of the conductor surface gradients, the voltages on the pole conductors and shield-wires are set to zero. The rms ac voltages are decomposed into sine and cosine functions (with no phase shift), because orthogonal functions can be added termwise, which facilitates matrix multiplication.

$$[V_{ac}] = \frac{400 \cdot 10^3}{\sqrt{3}} \begin{bmatrix} \cos\left(\frac{2\pi}{3}\right) & \sin\left(\frac{2\pi}{3}\right) \\ \cos(0) & \sin(0) \\ \cos\left(-\frac{2\pi}{3}\right) & \sin\left(-\frac{2\pi}{3}\right) \end{bmatrix} \cdot \begin{bmatrix} \cos(\omega t) \\ j \cdot \sin(\omega t) \end{bmatrix}$$

$$= 10^3 \begin{bmatrix} -115.5 & 200.0 \\ 230.9 & 0.000 \\ -115.5 & -200.0 \end{bmatrix} \cdot \begin{bmatrix} \cos(\omega t) \\ j \cdot \sin(\omega t) \end{bmatrix}$$

The rms charge on each conductor due to the rms ac voltages is calculated by multiplying columns 1 to 3:

$$[Q_{ac}] = [C_{1\dots 8,1\dots 3}] \cdot [V_{ac}] = 10^{-6} \begin{bmatrix} -1.6919 & 2.4228 \\ 3.1212 & -0.0088 \\ -1.7021 & -2.4582 \\ 0.0905 & 0.2312 \\ 0.0126 & 0.0374 \\ 0.0113 & -0.2868 \\ 0.0069 & 0.2652 \\ 0.0151 & 0.0510 \end{bmatrix} \cdot \begin{bmatrix} \cos(\omega t) \\ j \cdot \sin(\omega t) \end{bmatrix}$$

The amplitude of the average and maximum conductor surface gradients, due to the ac voltage, on each phase conductor, pole conductor and shield wire are calculated. In this case, only the amplitude of the conductor surface gradient is of interest; the phase shift is irrelevant. For each conductor  $i$ , using equations (3.6) and (3.7):

$$E_{ave_i} = \frac{|Q_{ac_i}|}{2\pi\epsilon_0 n_i r_{cond_i}}$$

$$E_{max_i} = E_{ave_i} \left( 1 + (n_i - 1) \frac{r_{cond_i}}{r_{eq_i}} \right)$$

$$E_{ave} = \begin{bmatrix} 13.1 \\ 13.8 \\ 13.3 \\ 0.65 \\ 0.10 \\ 7.79 \\ 7.20 \\ 1.44 \end{bmatrix} \text{ kV/cm} \quad E_{max} = \begin{bmatrix} 14.5 \\ 15.3 \\ 14.6 \\ 0.76 \\ 0.12 \\ 7.79 \\ 7.20 \\ 1.44 \end{bmatrix} \text{ kV/cm}$$

Similarly, to calculate the dc components of the conductor surface gradients, the voltages on the phase conductors and shield-wires are set to zero.

$$[V_{dc}] = 10^3 \begin{bmatrix} 500 \\ -500 \end{bmatrix}$$

The charge on each conductor due to the ac voltages is calculated:

$$[Q_{dc}] = [C_{1\dots 8,4\dots 5}] \cdot [V_{dc}] = 10^{-6} \begin{bmatrix} -0.03 \\ -0.11 \\ 0.52 \\ 7.06 \\ -6.93 \\ -0.03 \\ -0.19 \\ 0.04 \end{bmatrix}$$

The amplitude of the average and maximum conductor surface gradients, due to the dc voltage, are calculated using equations (3.6) and (3.7).

$$E_{ave} = \begin{bmatrix} -0.14 \\ -0.46 \\ -2.29 \\ 18.6 \\ -18.2 \\ -0.88 \\ -5.28 \\ 1.13 \end{bmatrix} \text{ kV/cm} \quad E_{max} = \begin{bmatrix} -0.15 \\ -0.51 \\ -2.53 \\ 21.6 \\ -21.2 \\ -0.88 \\ -5.28 \\ 1.13 \end{bmatrix} \text{ kV/cm}$$

For comparison, calculations of the conductor surface gradients on phase conductors, pole conductors, and shield-wires were also performed using the program ACDCLINE from the EPRI TL Workstation version 3.0. The results are contained in Appendix A and summarised in table 5.2. The correlation between the results is good, indicating that the Maxwell Potential Coefficient Method is suitable for this calculation.

### 5.3.2 Phase conductor bundle parameters

For the phase conductor bundles, the effect of varying the diameter of individual conductors, the spacing of the conductors, and the number of conductors in the bundle

**Table 5.2:** Calculated maximum conductor surface gradients

Conductor	ACrms	DC	ACrms	DC
	Calculated		EPRI TLW 3.0	
C1	14.47	-0.15	14.52	-0.15
C2	15.28	-0.51	15.34	-0.52
C3	14.65	-2.53	14.69	-2.53
C4	0.76	21.6	0.76	21.52
C5	0.12	-21.2	0.12	21.12
G1	7.79	-0.88	7.77	-0.89
G2	7.20	-5.28	7.18	-5.27
G3	1.44	1.13	1.45	1.13

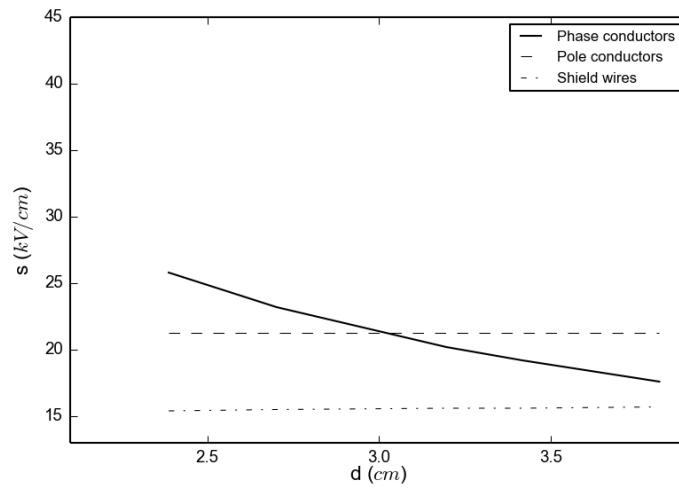
is investigated parametrically. The variation of the conductor surface gradient is plotted, and is shown in figure 5.2. It is apparent that the dominant factors in determining the conductor surface gradient on the phase conductors are the conductor diameter and the number of conductors in the bundle. Unexpectedly, the diameter of the bundle has little effect, and increasing the bundle diameter increases the conductor surface gradient. The gradient on the pole conductors and shield-wires is not affected greatly by the phase conductor configuration.

### 5.3.3 Pole conductor bundle parameters

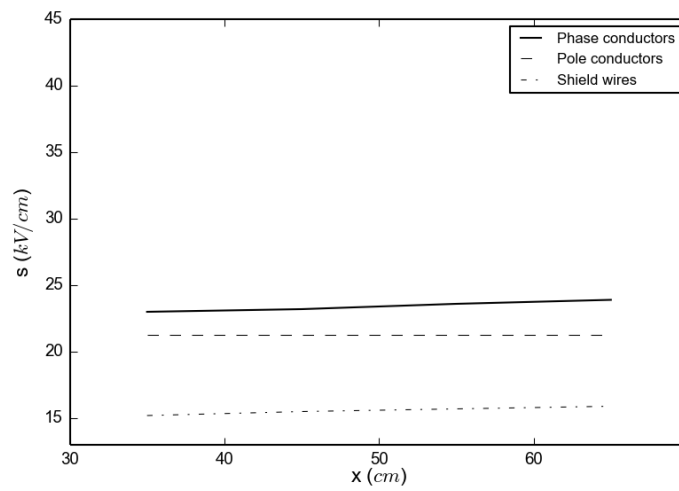
The effect of varying parameters of the pole conductor bundles is investigated similarly to the phase conductor bundles. A similar pattern of results is apparent for the pole conductor bundle from figure 5.3. It is noteworthy that the conductor surface gradient on the pole conductors is above  $20 \text{ kV/cm}$ , in all the figures, which is suggested as a design limit based on theoretical arguments and service experience [53]. This suggests that a bipolar HVDC overhead transmission line operating at 500 kV is likely to be beset with corona-related problems, but yet many such overhead transmission lines are in service with acceptable performance statistics. This is explained by the behaviour of ions in the vicinity of the pole conductors [22] which causes an ionic space charge to surround the pole conductors, and which modifies the conductor surface gradient, as well as the electric field beneath the line. This is discussed and investigated in section 5.6 later.

### 5.3.4 Separation parameters

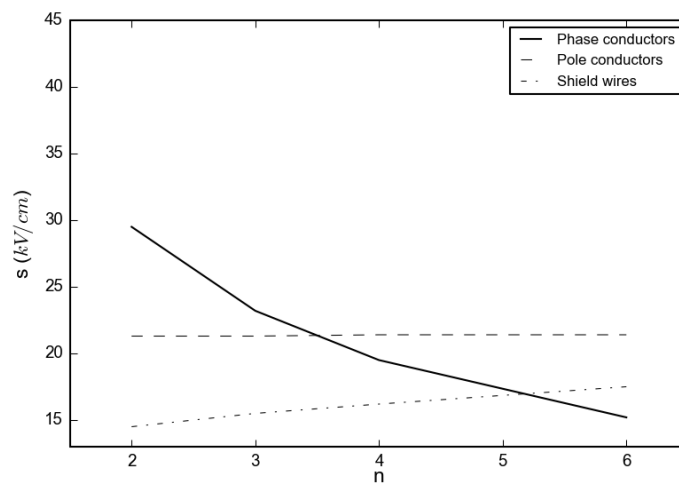
From figure 5.4 it is clear that spacing of the pole- and phase-conductor bundles has only a small effect on the maximum levels of conductor surface gradient. In performing the calculations, an interesting observation is that below 17 m spacing between the pole-



(a) Conductor surface gradient vs Phase conductor diameter

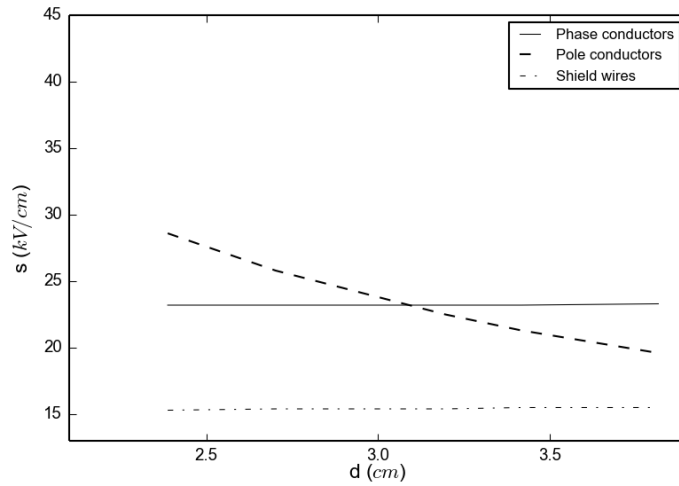


(b) Conductor surface gradient vs Phase bundle size

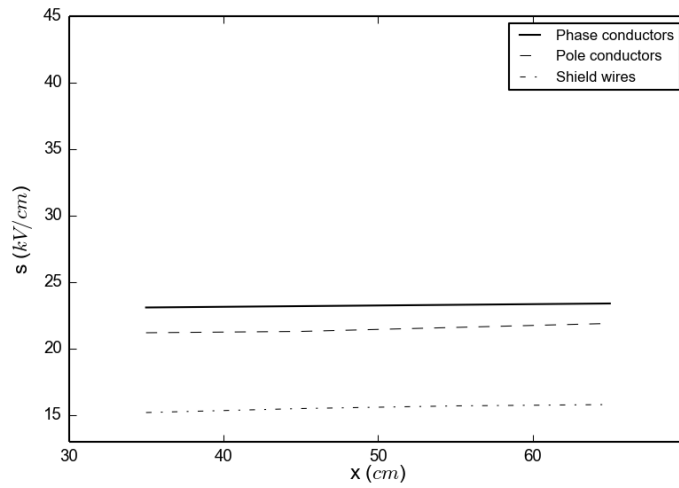


(c) Conductor surface gradient vs Phase bundle number

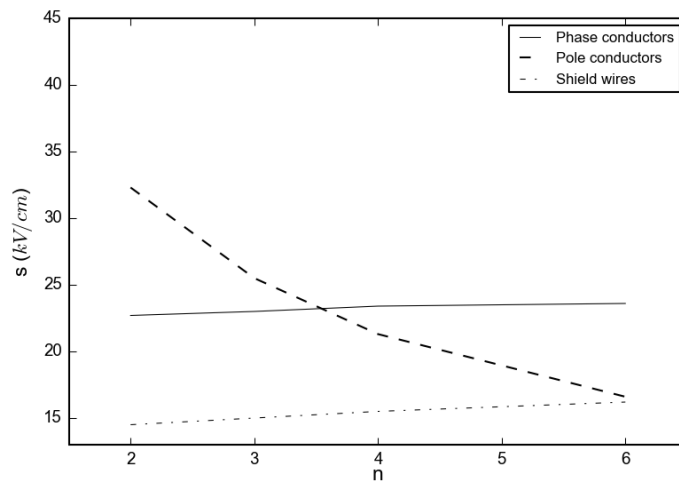
**Figure 5.2:** Effect of varying phase conductor bundle parameters



(a) Conductor surface gradient vs Pole conductor diameter

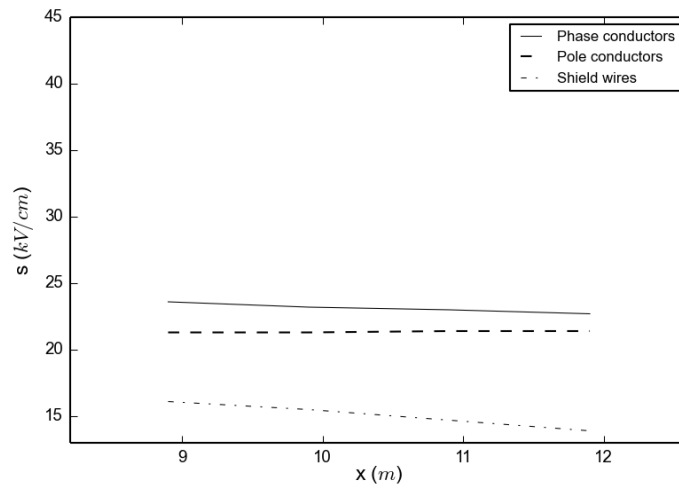


(b) Conductor surface gradient vs Pole bundle size

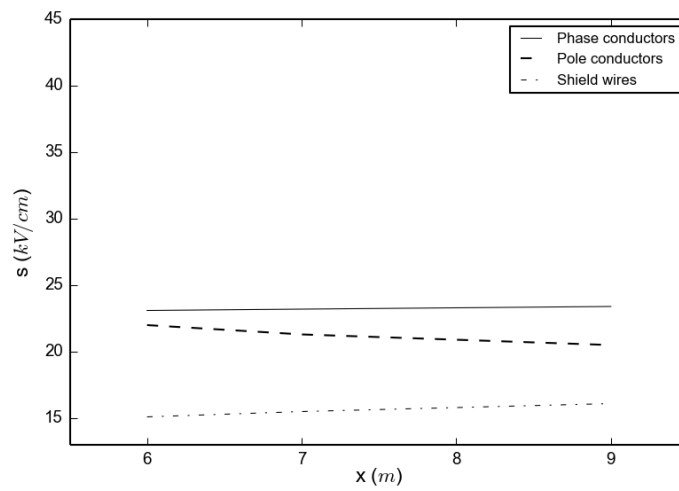


(c) Conductor surface gradient vs Pole bundle number

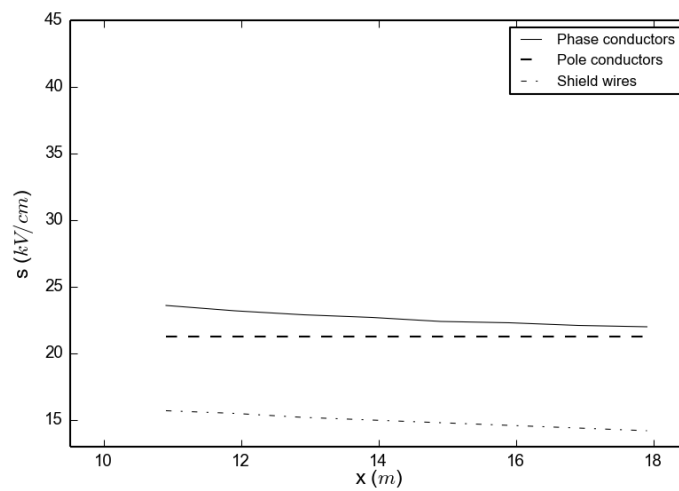
**Figure 5.3:** Effect of varying pole conductor bundle parameters



(a) Conductor surface gradient vs Phase spacing



(b) Conductor surface gradient vs Pole spacing



(c) Conductor surface gradient vs Separation

**Figure 5.4:** Effect of varying separation parameters

and outer phase-conductor, the maximum gradient is on the outer phase-conductor, while above 17 m spacing, it is on the centre-phase conductor.

#### 5.4 Audible noise

For ac audible noise, the sound pressure level in dBA per phase is calculated using the BPA method from the EPRI ac transmission line reference book [30]. Alternative calculation procedures are documented in this book, but the BPA method is selected because it has formulae with a similar form for both ac and dc, and takes altitude into consideration. The BPA formulae differ depending on the number of individual conductors in the pole- and phase-conductor bundles.

For  $n < 3$

$$P_i = 55\log(2r_i) + 120\log(E_i) - 115.4 - 11.4\log(D_i) + \frac{H}{300} \quad (5.12)$$

For  $n \geq 3$

$$P_i = 26.4\log(n_i) + 55\log(2r_i) + 120\log(E_i) - 128.4 - 11.4\log(D_i) + \frac{H}{300} \quad (5.13)$$

where  $P_i$  is the audible noise sound pressure level from  $i$ th bundle,  $E_i$  is the maximum conductor surface gradient for the  $i$ th bundle, and  $D_i$  is the radial distance from the  $i$ th bundle to the measuring point.

The individual phase contributions are then combined to determine the overall level for the line.

$$P_{tot} = 10\log \sum_{i=1}^3 10^{\frac{P_i}{10}} \quad (5.14)$$

where  $P_{tot}$  is the total sound pressure level from multiple bundles.

For dc audible noise, the sound pressure level in dBA is calculated for the positive pole only, because the impact of the audible noise contribution from the negative pole is negligible [2]. For consistency, the BPA formula for dc audible noise [20; 22] is used, which has a similar form to the BPA formula for ac audible noise.

For  $n < 3$

$$P_{tot} = 40\log(2r_i) + 86\log(E_i) - 93.4 - 11.4\log(D_i) + \frac{H}{300} \quad (5.15)$$

For  $n \geq 3$

$$P_{tot} = 25.6\log(n_i) + 40\log(2r_i) + 86\log(E_i) - 100.62 - 11.4\log(D_i) + \frac{H}{300} \quad (5.16)$$

The effect of environmental conditions on ac and dc audible noise is different. Under ac conditions, audible noise is highest under rain conditions, while for dc conditions,

**Table 5.3:** Calculated audible noise levels for hybrid dc/ac line

Configuration	Position (m)	-48	-27	-12	0	12	27	48
a b c p n	Rainy (dBA)	47.5	50.7	51.0	52.3	53.3	51.1	47.7
	Fair (dBA)	39.7	42.0	44.4	47.1	48.0	44.6	41.3
a b c n p	Rainy (dBA)	47.5	50.7	50.9	52.3	53.2	51.2	47.8
	Fair (dBA)	38.7	40.4	42.1	44.0	46.6	47.8	43.3

audible noise is highest under fair weather conditions [2; 22]. Maximum fair weather audible noise from the dc line is obtained by adding from 3.5 dB [22] to 5 dB [20] to the value calculated from equations (5.15) and (5.16). The mean audible noise from the dc line under rain conditions is calculated by subtracting 6 dB [20; 22]. Maximum audible noise under rain conditions from the ac line is the value calculated by adding 3.5 dB to the average value calculated from equations (5.12) and (5.13) [20]. The audible noise in fair weather from an ac line designed to have acceptable performance under rain conditions will normally not be appreciable [30], but if a value is needed, the customary approach seems to be subtraction of a fixed dB from the audible noise under rain conditions. "Eskom High Altitude" experimental results in Britten et al. [30] suggest that a value of 10.5 dB to 15.5 dB may be appropriate, while Chartier [31] suggests a figure of 25 dB combined with an altitude correction of 1 dB per 300 m. These two approaches do not give significantly different results, but the Chartier [31] approach is used for consistency. Table 5.3 gives the calculation results for lateral distances from the mid-line of the ac and dc lines, at ground level. "Configuration" indicates the relative positions of the phase conductors a, b, c, and the positive and negative poles p and n. (Calculation results are in Appendix B.)

Straumann and Franck [2] suggests that a fair weather limit of (40 ... 50) dBA and a rainy conditions limit of (50 ... 60) dBA are reasonable. These limits can be met a short distance away from the hybrid dc/ac line on both sides, with rainy conditions being the more challenging constraint. In the study system, it is proposed to place the positive pole towards the middle of the hybrid dc/ac line for insulation and audible noise reasons, and the calculation results indicate that audible noise levels are indeed reduced slightly by placing the positive pole towards the inside. This also aligns with measurements by BPA which have shown that positive corona from ac conductors is enhanced by proximity to a negative dc conductor [15], but contradicts Lundkvist et al. [3].

## 5.5 Radio interference

In principle, investigation of radio interference from transmission lines can be done analytically and empirically. Analytical investigation requires that the radio interference

**Table 5.4:** Calculated radio interference from hybrid dc/ac line

Configuration	Position (m)	-45	-30	-15	0	15	30	45
a b c p n	Rainy (dBA)	59.8	70.2	67.1	76.9	74.4	66.1	57.0
	Fair (dBA)	42.1	46.3	51.9	59.7	70.8	70.0	59.1
a b c n p	Rainy (dBA)	59.8	70.2	67.1	76.9	74.4	66.1	57.0
	Fair (dBA)	38.6	42.8	48.4	56.3	67.3	66.6	55.6

excitation function for the bundle used under varying weather conditions is known, and for dc lines of  $\pm 500$  kV and above there is, unfortunately, little knowledge in this area. Improved knowledge of the dc radio interference excitation function will require experiments on lines at these voltages, so an empirical method seems to be the best option at this stage.

Using expressions developed at BPA from data from operational and experimental lines [31], Cigre JWG-B2/B4/C1.17 [20] derived a formula for predicting the average fair weather radio interference from a bipolar line, including a correction term for measurements at frequencies other than 1 MHz, which allows CISPR limits to be applied instead of old ANSI limits.

$$RI_i = 60.5 + 86 \log \frac{E_i}{27.5} + 40 \log \frac{2r_i}{46.2} + 10 (1 - [\log(10f)]^2) + \frac{H}{300} + 40 \log \frac{19.9}{D_i} \quad (5.17)$$

The BPA expressions are also valid for ac lines [54], and by applying the same distance correction term as Cigre JWG-B2/B4/C1.17 [20], a formula for predicting the average rainy conditions radio interference from a three-phase ac line is generated.

$$RI_i = 48 + 120 \log \frac{E}{17.56} + 40 \log \frac{d}{35.1} + 10 (1 - [\log(10f)]^2) + \frac{H}{300} + 40 \log \frac{19.9}{D_i} \quad (5.18)$$

For all calculations, the maximum positive conductor surface gradient is used. In all cases, the highest value calculated from the three phase conductors and the positive pole conductor is taken as the radio interference, except where the two highest values are within 3 dB, in which case the average value increased by 1.5 dB is used.

$$RI_{tot} = \begin{cases} \max(RI_i) & \text{if } RI_i \text{ is at least 3dB above all others} \\ \frac{1}{2} (RI_i + RI_j) + 1.5 & \text{if } RI_i \text{ and } RI_j \text{ are within 3dB of each other} \end{cases} \quad (5.19)$$

From table 5.4 it can be seen that a fair weather limit of 72 dB [53] can be fulfilled a relatively short lateral distance away from the centre of the hybrid dc/ac line. Unlike audible noise, radio interference seems to be greater if the positive pole is placed closest to the ac phases, but this is acceptable, because it is much easier to comply with the radio interference limits. (Calculation results are in Appendix B.)

## 5.6 Space charge and ion currents

There are two distinct regions of the space charge field. Between the pole conductors, there is a bipolar field where positive and negative ions interact, and between the pole conductors and ground, there is a unipolar field where only positive or negative ions exists [15; 18]. The electric field at ground level and the dc currents injected into the phase conductors are of interest, so only the unipolar field region is analysed, although the same techniques are applicable to the bipolar field region. The phase conductors and shield-wires are treated as grounded, as done by Chartier et al. [15] and Maruvada and Drogi [18].

Experimental work [15] and calculations [18] have shown that the ac component of electric field for a hybrid dc/ac line, under typically encountered conditions, has only a small effect of the space charge. Under extremes, it is possible to produce substantial differences in ion behaviour due to the ac component of the electric field, but in realistic conditions the differences are within tolerances due to other unpredictable parameters such as electron mobility, wind and ultra-violet radiation levels.

Without software to solve the boundary-value problem, or experimental data for the suggested line design, the simple method suggested by Cigre JWG-B2/B4/C1.17 [20] is used to estimate the ground-level electric field. It is based on the "degree of corona saturation method" of Johnson and Zaffanella [19] with some simplification.

The degree of corona saturation method consists of three steps:

- The electrostatic electric field at ground level is calculated. This is the "corona-free" condition, which is a lower bound for ground-level electric field, ion density and ion current density. In fact, ion density and ion-current density are zero in the corona free condition.
- The ground-level electric field, ion density, and ion current density are determined for the "saturated-corona" condition from calculations or from measurements on a scale-model. This defines an an upper bound for the quantities.
- Actual quantities are estimated using an empirical "degree of corona saturation" to determine where the quantities lie between the upper and lower bounds.

The Cigre JWG-B2/B4/C1.17 [20] method simplifies the last step by defining an enhancement factor for the electric field which depends of the intensity of the corona. From field measurements, this enhancement factor is found to vary in the range of 1 to 3, and the method uses the value of 2 to do a preliminary assessment of the electric field which is used to determine the minimum conductor height. This method does not give a simple way of calculating the ion density and ion current; it gives an estimate of the electric field at ground level in the presence of corona only.

### 5.6.1 Corona-free condition

In the corona-free condition, all charge is retained on the conductors themselves and no charge is in space. This corresponds to the electrostatic condition calculated using Maxwell's method of potential coefficients described in section 3.1.4.

The dc electric field at ground level is calculated for the full system of phase conductors, pole conductors and shield-wires, as well as for a system consisting of the pole conductors only. The calculation results in figure 5.5 show that

- The dc electric field under the phase conductors for the full system is significantly lower than for the bipole only. Effectively, the pole conductors provide shielding from the dc electric field.
- The dc electric field under the pole conductors is slightly higher than for the bipole only, but the difference is of the order of 0.5%, which is not significant.

It is expected that similar behaviour will be observed for ion density and ion current density. That is, the ion density and ion current density under the phase conductors will be significantly reduced compared to the case of a bipole only, but under the pole conductors the levels will be almost the same as in the case of a bipole only. The levels under the pole conductors are expected to be the limiting factor, and a good estimate of these levels can be obtained from analysis of the bipole on its own. This aligns with Chartier et al. [15] and Maruvada and Drogi [18].

The maximum calculated value of  $E$  is 27.6 kV/cm just outside the positive pole of a bipole on its own. For the full system, the maximum value is 27.2 kV/cm, which shows the small error introduced by neglecting the phase conductors and shield-wires. (Calculation results are in Appendix B.)

The electric field under corona-free conditions  $E_e$  is determined graphically from figure 4-37 in Johnson and Zaffanella [19], reproduced in figure 5.6.

$$\begin{aligned}\frac{H}{d} &= \frac{h_a}{2R_i} \\ &= 16.6 \\ \frac{EH}{V} &= 0.4 \\ \therefore E_e &= 27.8 \text{ kV/cm}\end{aligned}$$

### 5.6.2 Saturated-corona condition

The saturated-corona condition is defined as the condition when all charge is in space, and the conductors themselves hold no charge at all. This cannot happen in reality, but it is definitely an upper bound for electric field, ion density, and ion current density.

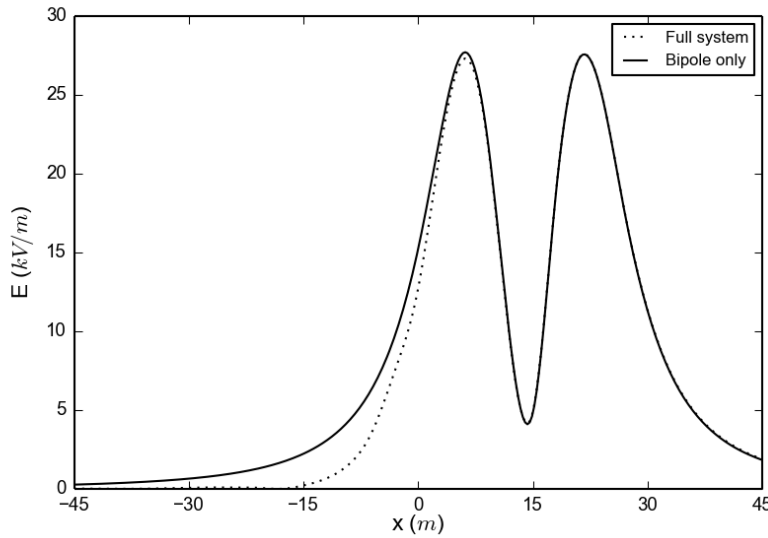


Figure 5.5: Lateral profiles of electric field

In principle, the saturated-corona quantities can be calculated by applying the boundary condition that the electric field is zero at the surface of the conductors, and solving the field equations:

$$\vec{E} = -\nabla V \quad (5.20)$$

$$\varepsilon \cdot \nabla V = \rho_i \quad (5.21)$$

$$\rho = \frac{J_i}{\mu E} \quad (5.22)$$

For all but the simplest geometries, this will require computerized numerical methods. In practice, it seems that measurements on scale models is a much easier way to determine the saturated-corona quantities. Based on an extensive experimental investigation, Johnson and Zaffanella [19] provides graphs and equations for comparing saturated-corona and corona-free conditions under HVDC bipoles.

Graphically from 5.6, the electric field under saturated-corona conditions is determined to be:

$$\frac{EH}{V} = 1.26$$

$$\therefore E_s = 87.4 \text{ V/m}$$

This is 2.9 times the value under corona-free conditions, which aligns with the observation is Cigre JWG-B2/B4/C1.17 [20] that the enhancement factor is normally between 1 and 3.

Alternatively, using equations for a bipolar line of horizontal configuration [19], the

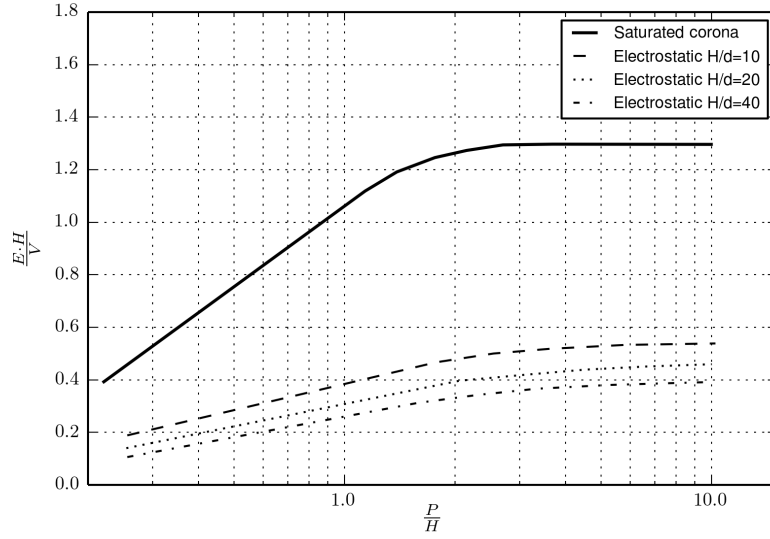


Figure 5.6: Corona-free and saturated-corona electric field (from [19])

electric field under saturated-corona conditions is calculated as:

$$\begin{aligned} E_s &= 1.31 \left(1 - e^{-1.7 \frac{P}{H}}\right) \frac{V}{H} \\ &= 87.6 \text{ V/m} \end{aligned} \quad (5.23)$$

The ion current density, also under saturated-corona conditions [19, eq. 4-54 and 4-55], is calculated separately for positive and negative ions. First for positive ions:

$$\begin{aligned} J_{+s} &= 1.65 \cdot 10^{-15} \left(1 - e^{-0.7 \frac{P}{H}}\right) \frac{V^2}{H^3} \\ &= 0.82 \cdot 10^{-6} \text{ A/m}^2 \end{aligned} \quad (5.24)$$

Similarly, for negative ions:

$$\begin{aligned} J_{-s} &= -2.15 \cdot 10^{-15} \left(1 - e^{0.7 \frac{P}{H}}\right) \frac{V^2}{H^3} \\ &= -1.1 \cdot 10^{-6} \text{ A/m}^2 \end{aligned} \quad (5.25)$$

The space charge density (in ions per cubic centimetre) under saturated-corona conditions does not depend on the polarity of the ions [19]. It is calculated as:

$$\begin{aligned} N_{is} &= 68.8 \frac{1 - e^{-0.7 \frac{P}{H}}}{1 - e^{-1.7 \frac{P}{H}}} \\ &= 5.1 \cdot 10^5 \text{ ions/cm}^3 \end{aligned} \quad (5.26)$$

Alternatively, from figure 5.7, the space charge density under saturated-corona

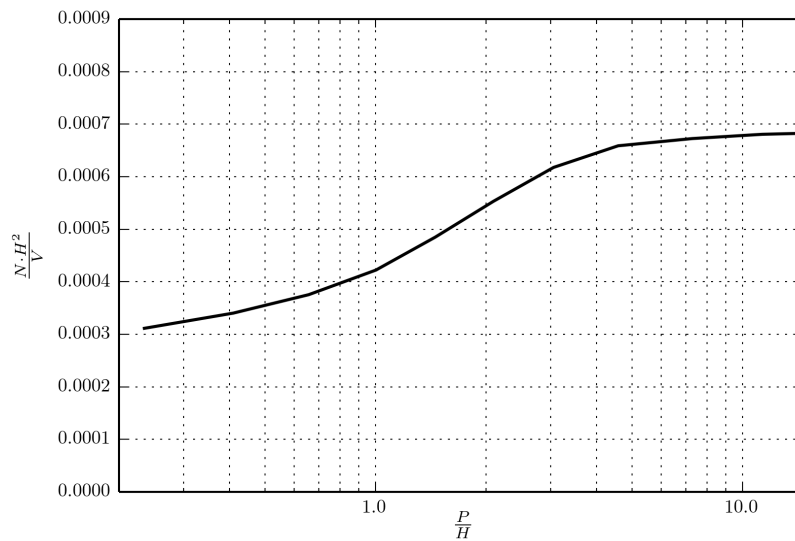


**Figure 5.7:** Saturated-corona space charge density (from [19, figure 4-39])

conditions is determined graphically as:

$$\begin{aligned} \frac{P}{H} &= 1.9 \\ \frac{NH^2}{V} &= 5.3 \cdot 10^4 \\ \therefore N_{is} &= 5.1 \cdot 10^5 \text{ ions/cm}^3 \end{aligned}$$

### 5.6.3 Degree of corona saturation

The degree of corona saturation indicates the relative position of a particular quantity in the range between the corona-free value and the saturated-corona value. For zero degree of corona saturation, the quantity is the corona-free value, and for unity degree of corona saturation, the quantity is the saturated-corona value [19].

The degree of corona saturation is weather- and season-dependent. The value is calculated for particular conditions from a formula and experimentally derived values [19]. All the corona-related phenomena investigated are worst for positive corona in fair weather, and the same is expected for space charge and ionic current. For this reason, "Summer Fair Weather" values are chosen to calculate the degree of corona saturation.

Dependence on altitude is not discussed by Johnson and Zaffanella [19], but it is stated that the reference gradient  $G_0$  in equation (5.27) is similar in concept to the corona inception gradient. It is assumed that the reference conductor surface gradient depends on the relative air density in the same way as the corona inception gradient, but it would be worthwhile to verify this experimentally. Thus, the season- and weather-related

parameters are:

$$K_c = 0.037$$

$$G_0 = \delta \cdot 9 = 7.2$$

The conductor surface gradient is calculated in section 5.6.1 as  $G = 27.6 \text{ kV/cm}$ , so the degree of corona saturation is calculated as:

$$\begin{aligned} S_c &= 1 - e^{-K(G-G_0)} \\ &= 0.53 \end{aligned} \quad (5.27)$$

#### 5.6.4 Space charge and ion current at ground level

Cigre JWG-B2/B4/C1.17 [20] suggests limits at the edge of the servitude of 25 kV/m for the electric field at ground level, and 100 nA/square metre for the ion current density. These values are conservative, based on perception experiments on human subjects, and can probably be considered annoyance-limits rather than safety-limits [20]. Britten [53] suggests limits based on insulation performance of 20 kV/m for the electric field at ground level, 300 nA/m<sup>2</sup> for the ion current density, and 150,000 ions/cm<sup>3</sup> for the space charge density.

First the maximum ground-level electric field, ion current density, and space charge density are calculated.

$$E = 27.6 + 0.53 (87.6 - 27.6)$$

$$= 59.0 \text{ kV/m}$$

$$J_+ = 0 + 0.53 (0.82 \cdot 10^{-6} - 0)$$

$$= 435 \text{ nA/m}^2$$

$$J_- = 0 + 0.53 (-1.1 \cdot 10^{-6} - 0)$$

$$= -567 \text{ nA/m}^2$$

$$N = 0 + 0.53 (5.1 \cdot 10^5 - 0)$$

$$= 4.0 \cdot 10^5 \text{ ions/cm}^3$$

The values are two to five times higher than the suggested limits, but they are the maximum values anywhere, and occur well-within the line servitude. Therefore, the values at the edge of the servitude should be investigated. For the dc line, the edge of the servitude is 15 m from the centre of the bipole. The ground-level electric field, ion current density, and space charge density at the edge of the servitude are calculated using equations 4-59 to 4-63 from Johnson and Zaffanella [19], and almost meet the Cigre

JWG-B2/B4/C1.17 [20] limits. First, the electric field at ground level in the presence of space charge:

$$E_e = 12.7$$

$$E_s = 1.46 \left(1 - e^{-2.5\frac{p}{H}}\right) \cdot e^{-0.7\frac{x-\frac{p}{2}}{H}} \cdot \frac{V}{H} \quad (5.28)$$

$$= 46.2$$

$$E = 12.7 + 0.53 (46.2 - 12.7) \quad (5.29)$$

$$= 30.4 \text{ kV/m} \quad (5.30)$$

The positive-ion current density at ground level:

$$J_{+e} = 0$$

$$J_{+s} = 1.54 \cdot 10^{-15} \left(1 - e^{-\frac{p}{H}}\right) \cdot e^{-1.75\frac{x-\frac{p}{2}}{H}} \cdot \frac{V^2}{H^3} \quad (5.31)$$

$$= 126 \cdot 10^{-9}$$

$$J_+ = 0.53 \cdot 126 \cdot 10^{-9}$$

$$= 57 \text{ nA/m}^2$$

The negative-ion current density at ground level:

$$J_{-e} = 0$$

$$J_{-s} = -2 \cdot 10^{-15} \left(1 - e^{-1.5\frac{p}{H}}\right) \cdot e^{-1.75\frac{x-\frac{p}{2}}{H}} \cdot \frac{V^2}{H^3} \quad (5.32)$$

$$= -181 \cdot 10^{-9}$$

$$J_- = 0.53 \cdot 181 \cdot 10^{-9}$$

$$= -96 \text{ nA/m}^2$$

To meet the Cigre JWG-B2/B4/C1.17 [20] limit on electric field at ground level, the height of the pole conductors must be increased to around 10.5 m. However, to satisfy the more onerous limit suggested by Britten [53] everywhere under the line, the height must be increased to at least 15 m, which is close to the midspan height of the ac shield-wires.

### 5.6.5 Ion currents injected into phase conductors

The magnitude of the dc current injected into the ac system via the phase conductors is of interest. These currents will cause a dc offset in the ac phase voltages, which if large enough, will cause saturation or power transformers. Neglecting hysteresis, the flux in a limb of the transformer core is proportional to the integral of the voltage across

**Table 5.5:** Direct current injected into phase conductors (from [18])

Weather conditions	Current (mA/100 km)		
	A	B	C
Rainy	0.29	1.36	11.8
Fair	0.70	3.50	28.0

the winding, so any significant dc component is certain to cause saturation in time. If the voltage is small, the effects of hysteresis and quasi-random variation of the phase voltages due to load and other changes will keep the transformer core out of saturation [5].

The simple technique used to investigate ion current does not provide a way to estimate the dc current injected into the phase conductors. This requires a full solution of the non-linear boundary value problem, which has been done by some authors in the literature. Maruvada and Drogi [18] calculates this current for a hybrid line of  $\pm 500$  kV dc/500 kV ac, and the results are shown in table 5.5. As expected, the phase closest to the dc line (phase C) has the largest current injected into it, and the phase furthest from the dc line (phase A) has the smallest.

Although the voltages and configuration are somewhat different to the study system, it is expected that similar values will be obtained for the  $\pm 500$  kV dc/400 kV ac hybrid configuration in the study system. Since the injected current at any point divides and travels in opposite directions, the total current flowing into the network at each end of the ac line will be of the order of 50 mA, which will not be problematic. The current in each phase is reduced to insignificance if the line is transposed, which is likely to be the case for 400 km.

## 5.7 Summary

The chapter analyses the performance of the study system, and attempts to identify opportunities for optimisation and improvement. Economic analysis of the transmission voltage and the conductor cross-section shows that the study system would be closer to optimal if the ac lines are rated for 800 MW and the dc lines are rated for 2000 MW. To limit ac currents induced in the dc lines under normal operating conditions, full transposition of the ac lines is required. Conductor surface gradients are calculated using hand calculations and the EPRI transmission line workstation software, and the results are similar. Using the calculated conductor surface gradients, levels of audible noise, radio interference, space charge and ion currents, electric and magnetic fields are calculated. These calculations showed that the height of the pole conductors needs to be substantially increased in order to meet field-effect limits.



## CHAPTER 6

## CONCLUSIONS

The study system is designed mainly on the basis of air insulation strength. It is not fully optimised, and analysis shows that it does not meet reasonable or generally-accepted limits on certain field-effect related parameters. Nevertheless, analysis of the study system identifies important design parameters other than air insulation strength, and provides some guidelines for developing of a better hybrid dc/ac line design. It also highlights factors which are of scientific interest, but which have only a small impact on the system performance and are, therefore, not of engineering interest (unless much higher voltages and power transfer levels than the study system, or extremely compact hybrid dc/ac lines are contemplated).

### 6.1 Key questions

In chapter 1, four key questions were posed, and all have been answered during the course of the analysis in preceding chapters.

*What ac current flows in the dc line (through coupling), and what effects could this have?*

In normal operation, an ac current of the order of 0.5% of the dc pole current flows in the dc line. This is large enough to cause asymmetric thyristor commutation, introduce non-characteristic harmonics, and cause converter transformer saturation. Under ac fault conditions, the ac current will be substantially larger. Transposition of the ac line, which would be normal for a line of 400 km long, substantially reduces the interfering current in normal operation. Under ac fault conditions, ac blocking filters or special thyristor firing controls will be needed.

*What dc current flows in the ac line (through ion flow), and what effects could this have?*

The ac and dc lines of similar height, the ion current flow is small and does not result in a dc current in the ac line which is of any concern. However, novel configurations for a hybrid dc/ac line with the dc line much higher than the ac line are worth investigating further, and the ion current will be higher in these configurations. It is not expected that this will be problematic, but it should be investigated in future work.

*How do the length and separation of the ac and dc lines affect these interactions?*

For ac and dc lines of similar height in a hybrid corridor, the separation dictated by

**Table 6.1:** Calculated servitude power density

	Width (m)	Power (MW)	Density (MW/m)
AC line	60	800 - 1000	13 - 17
Hybrid line	75	2800 - 4000	37 - 53
DC line	30	2000 - 3000	67 - 100

air insulation strength keeps interactions to a low level. From a design perspective, in these circumstances the ac phase conductor bundle and dc pole conductor bundle can almost be considered separately, because the mutual impacts are so small. However, analysis of dc electric and magnetic fields shows that dc lines should be substantially higher than ac lines. Novel configurations with the dc pole conductors almost above the ac phase conductors are suggested, which would have higher levels of interaction. Exploring these configuration is left for future work.

*How do these factors influence the technical feasibility of hybrid lines in specific applications?*

All of the analysis indicates that hybrid dc/ac transmission corridors are technically feasible and attractive. The servitude requirements are substantially less than for pure ac corridors, and all corona and field-effect limits can be met with a suitably designed hybrid dc/ac transmission corridor.

## 6.2 Servitude usage

Although the ac, dc, and hybrid dc/ac lines have not been optimised, the designed power transfer levels and the servitude widths required to meet reasonable design limits give a good indication of the servitude power density that can be achieved with each.

The servitude for the ac line is 60 m, which is required to obtain acceptable electric and magnetic fields at ground level at the edge of the servitude, and the ac line in the study system transmits 800 MW to 1,000 MW. The spacing of the ac and dc lines in the study system is 30 m centre-to-centre, and the electric field at ground level considering space charge on the dc line is acceptable at a distance of 15 m from the centre, so the total servitude width to transmit 2,800 MW to 4,000 MW with the hybrid dc/ac line is 75 m. The dc line on its own, transmits 2,000 MW to 3,000 MW and requires a servitude of 30 m. These are summarised in table 6.1, which shows the benefit of the hybrid dc/ac line.

## 6.3 AC ripple in pole currents

To prevent converter transformer saturation and generation of non-characteristic harmonics by the converters, the maximum ac ripple in the pole currents should be limited to 0.1% of the rated current of the converters. The spacing between pole conductors and

phase conductors has an impact on the ac ripple, but the largest effects are from the smoothing reactors and transposition of the ac line. During normal operation, these will generally be sufficient to limit the ac ripple in the pole current to an acceptable level, but for faults on or through the ac line this is unlikely to be the case. Since the ac faults should be of relatively short duration, it may be possible that the negative effects of the large ripple last for a short enough time that they do not cause problems with converter operation or saturation of converter transformers.

#### 6.4 Audible noise

The suggested limit in fair weather limit of 42 dBA [53] can be attained at a distance of approximately 45 m from the centre line, at altitude, using a four-conductor of ACSR Bittern, which has a diameter of 3.417 cm and an aluminium cross-section of 645 mm<sup>2</sup>. Bundles with larger numbers of smaller conductors also perform well. Recalculation of audible noise with a six-conductor bundle of ACSR Ruddy, having a diameter of 2.837 cm and aluminium cross-section of 456.1 mm<sup>2</sup>, shows that it is a good option.

The suggested limit for audible noise under rainy conditions is (50 ... 60) dBA [2] which is more challenging to attain. In a three-conductor bundle, acceptable performance cannot be attained with ACSR Tern, although in a four-conductor bundle, it performs well. A larger conductor such as ACSR Ruddy is needed in a three-conductor bundle. Smaller conductors such as ACSR Kingbird do not perform adequately in a four-conductor bundle. Even with very large conductors, two-conductor bundles have unacceptably high audible noise.

#### 6.5 Radio Interference

Without experimental data for the radio interference excitation function for dc lines, an empirical approach to calculating interference levels is taken. Based on calculations, the suggested fair weather limit of 72 dB [53] can be attained at a distance between 15 m and 30 m from both the ac and the dc lines. Based on this, it seems that compliance with radio interference limits is likely to be easier to achieve than compliance with audible noise limits. Stated simply, a line which is audio-quiet-enough, is likely to be radio-quiet-enough too.

#### 6.6 Space charge and ion currents

The ground level electric field profiles are very similar for the complete hybrid dc/ac line and a dc bipole only, and calculations of space charge related phenomena on a bipole are expected to closely model the hybrid dc/ac line. No empirical or numerical tools are readily available to analyse a hybrid dc/ac line in this regard.

From the perspective of avoiding human irritation, the ground level electric field and ion current density at the edge of the servitude need to be limited. The suggested electric field limit from Cigre JWG-B2/B4/C1.17 [20] imposes a minimum limit on the conductor height at midspan of around 12.5 m for a  $\pm 500$  kV bipole. The ion current density limit is comfortably met at the edge of the servitude. The calculated ion current density at the edge of the servitude is of the order of  $30 \text{ nA/m}^2$  against a suggested limit of  $100 \text{ nA/m}^2$ . This is so low that, from a practical point of view, ion current density does not constrain the design at all.

From the perspective of insulation strength under fire and other adverse environmental conditions, limits apply everywhere underneath the pole conductors. The electric field limit suggested by Britten [53] is quite onerous, and effectively imposes a minimum height of around 15 m for a  $\pm 500$  kV bipole. The ion current density limit, and the space charge density limit, are comfortably met everywhere at ground level. The maximum calculated ion current density is of the order of  $30 \text{ nA/m}^2$  against a suggested limit of  $300 \text{ nA/m}^2$ , and the calculated space charge density is of the order of  $70,000 \text{ ions/cm}^3$  against a limit of  $150,000 \text{ ions/cm}^3$ .

## 6.7 Analytical tools

The Maxwell Potential Coefficients are used extensively in this study. Other, more sophisticated, and more accurate methods for calculating conductor surface gradients exist, but the small accuracy improvements from using these other methods do not seem to justify the increased complexity of the calculations. Conductor surface gradient is only one factor in the investigation of field-effect related phenomena, and inaccuracies due to a host of physical parameters are probably as big or larger than the inaccuracy in the conductor surface gradients. Major benefits of the Maxwell Potential Coefficient method are simplicity, ease of programming in spreadsheets or other calculation software, and accessibility of interim calculation results. Thus, even for subsequent investigations, it is a very good option.

Phenomena related to electrostatic and magnetic coupling between the dc and ac lines are investigated using Maxwell Potential Coefficients only. Much of the investigation is quite simplistic, but more sophisticated investigation will need computer software such as EMTDC or ATP. Since ATP is easily-accessible, this would probably be the first choice. EMTDC has a significant advantage over ATP for simulating dc converters, but it is only available commercially. Both ATP and EMTDC can use overhead line models based on parameters calculated using Maxwell Potential Coefficients, so comparison of test-cases to hand-calculations is possible.

Audible noise is investigated using equations developed for stand-alone dc or ac lines, with contributions from individual lines combined. Other researchers found that this technique yields acceptably accurate results [15]. Different sets of equations exist for

the stand-alone lines, and some experimental work to select the best equations for use in Southern African conditions, and to verify again the acceptability of the technique used, would be valuable.

Radio interference is also investigated by separately calculating the disturbances for ac and dc, and combining them. Although other researchers found this technique acceptable [15], it is somewhat unsatisfying. Since radio interference is measured typically with quasi-peak meters, it seems reasonable that a dc offset which increases the peak of the ac waveform would increase the level of interference, but according to literature this is not the case. Experiments to verify or disprove this would be valuable, even though radio interference limits seem easier to meet than audible noise limits. Experimentally determining the radio interference excitation function for dc bipoles and monopoles would also be valuable, since this would allow pure analytic methods to be compared with the empirical techniques that are used.

Space charge and ion currents are investigated for dc only, because the influence of the ac seems small. The empirical Degree of Corona Saturation technique used is simple and effective [19], but it has been criticised by others [20; 22]. Computer software to apply alternative calculation methods suggested in the literature is not easily-accessible, and the algorithms are poorly explained in the literature. Nevertheless, a thorough search of literature and production of an easily-accessible, research-grade, computer program for investigating space charge and ion currents on hybrid dc/ac lines would be extremely valuable.

## 6.8 Possible design improvements

There are a host of possible improvements and optimisations of the study system, all of which could be analysed in more detail. The most obvious improvements are:

- **Power transfer ratings** can be selected so that 400 kV ac and 500 kV dc are closer to optimal. Suitable ratings would be 800 MW for the ac line and 2,000 MW for the dc line. This also gives a power transfer reduction of only 1,000 MW when a pole trips, which is probably more acceptable to system operators.
- **Conductor selection** can be revised so that both the ac and the dc lines use the same conductor. From audible noise and ampacity calculations, one suitable option would be ACSR Ruddy, in a three-conductor bundle for the ac line, and in a six-conductor bundle for the dc line.
- **Height of the dc line** should be increased to satisfy the limit on electric field at ground level, taking space charge into account. Enhancement of the electric field at ground level by the space charge makes this a defining design constraint for the dc line.

- **Spacing of the ac and dc lines** can be reduced if the ac and dc lines are at substantially different heights. Conductor-clashing is the defining design constraint when the phase and pole conductors are at almost the same height, but at substantially different heights, the pole-to-phase insulation strength will probably be the defining design constraint.
- **Novel geometries** should definitely be considered. Placing the poles on either side of the ac line, or even placing the poles above the outer phase conductors, could result in greater compaction of the hybrid dc/ac line.

### 6.9 Design criteria and field-effect limits

Based on the investigations and suggestions from Britten [53], some design limits for various field-effect related parameters are given in table 6.2. These limits can be used during design improvement and optimisation of the study system.

Table 6.2: Key design limits for hybrid 400 kV ac/500 kV dc line [53]

Parameter	Limit	Comment or rationale
Audible noise in fair weather	$\leq 42$ dBA	24 hour $L_{dn}$ at edge of servitude. This value is 7 dB higher than the night-time limit of 35 dBA from SANS0103.
Audible noise in rainy weather	$\leq 55$ dBA	24 hour $L_{dn}$ at edge of servitude.
Radio interference	$\leq 72$ dB ( $1\mu\text{V}/\text{m}$ ) at 0.5 MHz	$L_{50}$ limit at servitude boundary
Pole insulator specific creepage	$\geq 45$ mm/kV	Field experience
Pole to pole stress	$\leq 100$ kV/m	Air gap strength, allowing for swing out under wind.
Pole conductor surface gradient	$\leq \delta \cdot 25$ kV/cm	Field experience
Shield wire surface gradient	$\leq \delta \cdot 14$ kV/cm	Field experience
Electric field at ground level	$\leq 20$ kV/m	Considering space charge, allowing for fire
Magnetic field at ground level	$\leq 40$ mT	Not affected by space charge
Ion density at ground level	$\leq 150,000$ ions/cm <sup>3</sup>	Nelson River HVDC data and performance
Insulator specific creepage	$\geq 16$ mm/kV	Field experience, for lightly polluted areas
Electric field at ground level	$\leq 5$ kV/m	ICNIRP limit at edge of servitude, no limit within the servitude.
Magnetic field at ground level	$\leq 100\mu\text{T}$	ICNIRP limit at edge of servitude, no limit within the servitude.



## CHAPTER 7

## POSSIBILITIES FOR FURTHER INVESTIGATION

During the course of this study, several opportunities for further investigation have been identified. All are beyond the scope of the study, by virtue of either requiring longer time-frames, specialised software tools, or full-scale experimental work.

**7.1 Long-term space charge and ion current measurements**

Realising that there are large gaps in current knowledge of space charge fields and ion currents, it would be valuable to carry out long-term measurements at altitude on experimental dc and hybrid dc/ac lines to get accurate statistics of the electric field, space charge and ion currents. The extent to which ac fields affect the space charge and ion current, as well as the ion current flowing from dc to ac in a hybrid dc/ac line would be very important information arising from the measurements. Seasonal and weather-related variations would also be important. This could be extended to developing a computer program to calculate electric fields and ion currents in hybrid dc/ac lines, based on corona physics supported by measurement data.

**7.2 Experimental study to characterise the radio interference excitation function for dc lines**

In this study, empirical methods are used to study radio interference. Analytical methods are known to be applicable to both ac radio interference, and these methods might also be applicable to dc if there is good knowledge of the excitation function under dc conditions, for the conductor bundle used on the line under different seasonal and weather conditions. This data can only be obtained through studies on experimental lines.

**7.3 Converter operation in the presence of distortion**

Using Fourier series, mathematically investigate the behaviour of the converter in the presence of an induced ac current in the dc link. The induced current will have a phase

shift compared to the converter output, since the induced voltage will be in phase with the line current, which will not necessarily be in phase with the busbar voltage. Thus, the distorting waveform will alternately affect each of the ac phases. By integrating, the amount of distortion on each phase can be calculated, and converted to zero, positive and negative sequence currents. It is expected that the zero sequence current will be dependent on the phase shift. The zero sequence current is generally interpreted in protection schemes as indicating an earth-fault, so a high degree of coupling could result in converter transformers tripping. Mathematical analysis could be complemented with electromagnetic transient simulations using EMTDC or ATP.

#### **7.4 Line cost study**

The costing data used for economic analysis in chapter 5 by-an-large reflected market conditions that may no longer apply. Some of the data is old, and some originated outside of Southern Africa. Regression analysis of detailed cost estimates for hypothetical lines combined with pricing data from recent contracts in the region will provide up-to-date information, which would be valuable in planning of dc or hybrid dc/ac transmission lines.

## REFERENCES

- [1] D. Woodford. Secondary arc effects in ac/dc hybrid transmission. *IEEE Transactions on Power Delivery*, 8(2):704–711, April 1993.
- [2] U. Straumann and C.M. Franck. Discussion of converting a double-circuit ac-dc overhead line to an ac/dc hybrid line with regard to audible noise. In *The Electric Power System of the Future - Integrating Supergrids and Microgrids - Cigré 2011 Bologna Symposium*, 2011.
- [3] J. Lundkvist, I. Gutman, and L. Weimers. Feasibility study for converting 380 kV ac lines to hybrid ac/dc lines. In *EPRI High-Voltage Direct Current & Flexible AC Transmission Systems Conference*, November 2009.
- [4] A.C. Britten, D. Muftic, T. Pillay, F.F. Bologna, P. Naidoo, and N.M. Ijumba. Eskom's proposed strategic research into long-distance HVDC transmission. *Energize*, July 2005.
- [5] A. Dariani and H. Bakhshi. Assessment of HVDC transmission line transposition on induction issues due to ac/dc lines coupling in common transmission corridors. In *Modernizing the Grid to Better Serve Evolving Customer Need - 8th Cigré Canada Conference*, 2013.
- [6] K. Ramesh, T. Adhikari, S.C. Kapoor, and D.P. Gupta. Parallel operation of ac and dc lines running on the same tower. In *32nd Cigré Session*, 1988.
- [7] K. Tonmitr, N. Kamkaew, and A. Suksri. An investigation on the effects of hybrid ac and dc lines corona. In *2th International Conference on Electrical Engineering/Electronics, Computer, Telecommunications and Information Technology (ECTI-CON 2005)*, pages 161–164, 2005.
- [8] C. Petino, B. Fuchs, and A. Schnettler. Contact faults in hybrid ac/dc power systems. In *Innovation For Secure And Efficient Transmission Grids - Cigré Belgium Conference*, 2014.
- [9] Azim Lotfjou, Fu Yong, and Mohammed Shahidehpour. Hybrid ac/dc transmission expansion planning. *IEEE Transactions on Power Delivery*, 27(3):1620–1628, July 2012.

- [10] M. Kizilcay, A. Agdemir, and M. Lösing. Interaction of a HVDC system with 400 kV ac systems on the same tower. In *International Conference on Power Systems Transients (IPST2009)*, 2009.
- [11] Johan Ulleryd, Ming Ye, and Gérard Moreau. Fundamental frequency coupling between HVAC and HVDC lines in the Quebec-New England multiterminal system - comparison between field measurements and EMTDC simulations. In *International Conference on Power System Technology (POWERCON '98)*, pages 498–502, August 1998.
- [12] W. Bayer, K. Habur, D. Povh, D.A. Jacobson, J.M. Guedes, and D.A. Marshall. Long distance transmission with parallel ac/dc link from Cahora Bassa (Moçambique) to South Africa and Zimbabwe. In *36th Cigré Session*, 1996.
- [13] B. Sander, J. Lundquist, I. Gutman, C. Neumann, B. Rusek, and K.-H. Weck. Conversion of ac multi-circuit lines to ac-dc hybrid lines with respect to the environmental impact. In *45th Cigré Session*, 2014.
- [14] D.I. Lee and K.Y. Shin. A study for electric environment characteristics in 154kV ac / 80kV dc hybrid transmission line. In *44th Cigré Session*, 2012.
- [15] V.L. Chartier, S.H. Sarkinen, R.D. Stearns, and A.L. Burns. Investigation of corona and field effects of ac/dc hybrid transmission lines. *IEEE Transactions on Power Apparatus and Systems*, PAS-100(1):72–80, January 1981.
- [16] Rogério Verdolin. *Overvoltages and coupling effects on an ac-dc hybrid transmission system*. PhD thesis, Dept of Electrical and Computer Engineering, University of Manitoba, 1995.
- [17] R.V. Larsen, H.A. Walling, and C.J. Bridenbaugh. Parallel ac/dc transmission lines steady-state induction issues. *IEEE Transactions on Power Delivery*, 4(1):667–674, January 1989.
- [18] P. Sarma Maruvada and Serge Drogi. Field and ion interaction of hybrid ac/dc transmission lines. *IEEE Transactions on Power Delivery*, 2(3):1163–1172, July 1988.
- [19] G.B. Johnson and L.E. Zaffanella. HVDC fields and ions. In *HVDC Transmission Line Reference Book*. EPRI, 1993.
- [20] Cigre JWG-B2/B4/C1.17. Impacts of HVDC lines on the economics of HVDC projects. Technical report, Cigre, 2009.
- [21] Bonneville Power Administration. *Transmission line reference book HVDC to  $\pm 600$  kV*. EPRI, 1977.

- [22] P. Sarma Maruvada. *Corona in transmission systems - Theory, design and performance*. Crown Publications, 2011.
- [23] U. Straumann and C.M. Franck. Finite element simulation of ion current from corona HVDC overhead lines. In *International Symposium on High Voltage Engineering (ISH)*, 2011.
- [24] Aurecon. GECOL 220 kV transmission lines and substation project, (accessed 2015-12-09). <http://www.aurecongroup.com/en/projects/energy/gecol-220-kv-transmission-lines-substation.aspx>.
- [25] John D. Kraus. *Electromagnetics*. McGraw-Hill, 3 edition, 1984.
- [26] P. Kundar. *Power system stability and control*. Mc Graw Hill, 1994.
- [27] H.P. St Clair. Practical concepts in capability and performance of transmission lines. In *AIEE Pacific General Meeting, Vancouver, B.C., September 1-4 1953*, 1953.
- [28] Dzevad Muftic and Arthur Burger. Basic electrical design. In *The planning, design & construction of overhead power lines*, chapter 11, pages 224–232. Eskom, 2005.
- [29] Antony Britten and Arthur Burger. Corona. In *The Planning, Design & Construction of Overhead Power Lines*, chapter 6, pages 122–152. Eskom, 2005.
- [30] A.C. Britten, V.L. Chartier, and L. Zaffanella. Audible noise. In *EPRI AC Transmission Line Reference Book - 200 kV and Above, Third Edition*. Electric Power Research Institute, 2005.
- [31] Vernon Chartier. Empirical expressions for calculating high voltage transmission corona phenomena. In *BPA Engineering Seminar*, 1983.
- [32] Win van Driel. Radio quiet zones and the square kilometre array. In *XXXth URSI General Assembly and Scientific Symposium*, 2011.
- [33] ICNIRP. Guidelines for limiting exposure to time-varying electric, magnetic, and electromagnetic field (up to 300 GHz). *Health Physics*, 74(4):494–522, 1998.
- [34] L. de Andrade and T. Ponce de Leao. A brief history of direct current in electrical power systems. In *Third IEEE Conference on History of Electro-technology*, 2012.
- [35] Wikipedia. Cahora bassa (HVDC), (accessed 2015-12-09). [https://en.wikipedia.org/wiki/Cahora\\_Bassa\\_\(HVDC\)](https://en.wikipedia.org/wiki/Cahora_Bassa_(HVDC)).
- [36] Nelson Ijumba and Gary Sibilant. High voltage direct current HVDC transmission. In *The planning, design & construction of overhead power lines*, chapter 4, pages 68–89. Eskom, 2005.

- [37] ABB Power Systems. Hallsjon: The first HVDC Light transmission, (accessed 2015-07-18). <http://new.abb.com/systems/hvdc/references/hallsjon-the-first-hvdc-light-transmission>.
- [38] ABB Power Systems. Gotland HVDC light, (accessed 2015-07-18). <http://new.abb.com/systems/hvdc/references/gotland-hvdc-light>.
- [39] Andrew Williamson and Kjell Eriksson. HVDC schemes and application. In *HVDC Power Transmission - Basic Principles, Planning and Converter Technology (Part 1)*, chapter 4, pages 92–126. Eskom, 2012.
- [40] M Rashwan and A Williamson. Technological trends in HVDC. In *HVDC Power Transmission - Basic Principles, Planning and Converter Technology (Part 1)*, chapter 22, pages 780 – 795. Eskom, 2012.
- [41] Karl Barker. *HVDC for beginners and beyond*. Areva T&D UK Ltd, 2009.
- [42] R.E. Steven. *Electrical machines and power electronics*. Van Nostrand Reinhold, 1983.
- [43] Jindal Africa. Mmamabula coalfield, (accessed 2015-02-28). <http://www.jindalafrika.com/botswana/Mmamabula-Coalfield>.
- [44] Gauteng Provincial Government. Gauteng pillars of radical transformation, (accessed 2015-04-03). <http://www.gautengonline.gov.za/Documents/10pillars.pdf>.
- [45] Frik Venter. Principles of operation of converters. In *HVDC Power Transmission - Basic Principles, Planning and Converter Technology (Part 1)*, chapter 3, pages 64–87. Eskom, 2012.
- [46] B. Hutzler, E. Garbagnati, E. Lemke, and A. Pignini. Strength under switching overvoltages in reference ambient conditions. In *Guidelines for the evaluation of the dielectric strength of external insulation (TB072)*. Cigre, 1992.
- [47] VTF Electrofarfor Ltd. Minimum guaranteed characteristics of toughened glass suspension type insulators (standard profile), (accessed 2015-11-08). [http://electrofarfor.com/catalog/5\\_2/u.html](http://electrofarfor.com/catalog/5_2/u.html).
- [48] A. L. Nelson, K. W. Folley, and M. Coral. *Differential Equations*. D.C. Heath & Co., Boston, 1952.
- [49] Murray Spiegel, Seymour Lipschutz, and John Liu. *Schaum's Outline of Mathematical Handbook of Formulas and Tables, 3ed*. McGraw-Hill Professional, 3 edition, 2008.
- [50] H.W. Dommel. *Electromagnetic Transients Program: Reference Manual: (EMTP Theory Book)*. Bonneville Power Administration, 1986.

- [51] A. Pignini, L. Thione, and F. Rizk. Dielectric strength under ac and dc voltages. In *Guidelines for the evaluation of the dielectric strength of external insulation (TB072)*. Cigre, 1992.
- [52] Richard C. Dorf. *Modern control systems*. Adison-Wesley, 1986.
- [53] A.C. Britten. Listing of key design limits and minimum performance targets for overhead hvdc lines. To be included in unpublished "HVDC Overhead Line Technology", Eskom Power Series, Volume 9, Part 2., 2014.
- [54] Robert Olsen and Vernon Chartier. Electromagnetic interference. In *EPRI AC Transmission Line Reference Book - 200 kV and Above, Third Edition*. Electric Power Research Institute, 2005.



APPENDIX A

RESULTS FROM EPRI TL WORKSTATION 3.0

-----  
Results of AC/DCLINE program CORONA (EPRI/HVTRC 7-93) for:  
-----

SURFACE GRADIENTS at AVERAGE LINE HEIGHT  
AUDIBLE NOISE

Configuration file name:  
C:\TLW30\ACDCLINE\DATA\ACCASE01  
Date: 12/18/2015 Time: 12:22

CASE01 Hybrid case: 400 kVAC and +/- 500 kVDC, with shield wires

\*\*\*\*\*  
\* BUNDLE INFORMATION \*

BNDL	CIRC	VOLTAGE	ANGLE	LOAD	ANGLE	#	X	Y	SAG	PH
#	#	(kV)	(DEG)	(A)	(DEG)	COND	(feet)	(feet)	(feet)	
1	1	400.0	0.	1443.	0.	3	-81.7	38.7	.0	A
2	1	400.0	240.	1443.	240.	3	-49.2	38.7	.0	B
3	1	400.0	120.	1443.	120.	3	-16.7	38.7	.0	C
6	2	500.0	0.	3000.	0.	4	26.3	35.8	.0	+
7	2	-500.0	0.	-3000.	0.	4	72.2	35.8	.0	-
4	1	.0	0.	0.	0.	1	-75.8	60.0	.0	GND
5	1	.0	0.	0.	0.	1	-22.6	60.0	.0	GND
8	2	.0	0.	0.	0.	1	49.2	75.8	.0	GND

\*\*\*\*\*  
\* MINIMUM GROUND CLEARANCE = 35.76 feet \*  
\* POWER SYSTEM FREQUENCY = 50. Hz \*  
\* SOIL RESISTIVITY = 300. ohm meter \*  
\*\*\*\*\*

\*\*\*\*\*  
\* SUBCONDUCTOR INFORMATION - REGULAR BUNDLES \*  
\*\*\*\*\*

BNDL	CONDUCTOR	DIAMETER	SPACING	DC RESIST	AC RESIST	AC REACT
#	NAME	(inch)	(inch)	(ohm/mile)	(ohm/mile)	(ohm/mile)
1	TERN	1.060	17.720	.1170	.1190	.4060
2	TERN	1.060	17.720	.1170	.1190	.4060
3	TERN	1.060	17.720	.1170	.1190	.4060
6	BITTERN	1.350	17.720	.0730	.0760	.3780
7	BITTERN	1.350	17.720	.0730	.0760	.3780
4	3/8EHS	.520	.000	4.4890	4.4890	1.4400
5	3/8EHS	.520	.000	4.4890	4.4890	1.4400
8	3/8EHS	.520	.000	4.4890	4.4890	1.4400

\*\*\*\*\*

\*\*\*\*\*  
 \* \*  
 \* MAXIMUM SURFACE GRADIENT (kV/cm) \*  
 \* \*  
 \*\*\*\*\*

BNDL #	Type	DC	ACrms	PEAK(+)	PEAK(-)
1	AC	-.15	14.52	20.37	-20.68
2	AC	-.52	15.34	21.17	-22.20
3	AC	-2.53	14.69	18.24	-23.30
6	DC	21.52	.76	22.59	20.45
7	DC	-21.12	.12	-20.95	-21.29
4	Ground Wire	-.89	7.77	10.10	-11.89
5	Ground Wire	-5.27	7.18	4.89	-15.43
8	Ground Wire	1.13	1.45	3.18	-.91

\*\*\*\*\*  
 \* \*  
 \* AUDIBLE NOISE \*  
 \* GENERATED ACOUSTIC POWER \*  
 \* (dB above 1W/m) \*  
 \* \*  
 \*\*\*\*\*

BNDL #	Type	Summer Fair	L5 RAIN	L50 RAIN
1	AC	-75.93	-55.32	-63.05
2	AC	-73.35	-53.82	-60.84
3	AC	-71.31	-54.32	-59.67
6	DC	-54.85	-60.85	-60.85
7	DC	*****	*****	*****
4	Ground Wire	*****	-98.42	*****
5	Ground Wire	*****	-82.78	*****
8	Ground Wire	*****	*****	*****

\*\*\*\*\*  
 \* \*  
 \* AUDIBLE NOISE \*  
 \* \*  
 \* Microphone is .00 feet above ground \*  
 \* Altitude 5905.5 feet \*  
 \* \*  
 \*\*\*\*\*

<----- HVTRC CALCULATION METHOD ----->

LATERAL	L50	L5	L50		
DISTANCE	FAIR	RAIN	RAIN	Leq(24)	Ldn

(feet)	(meters)	(dB(A))	(dB(A))	(dB(A))	(dB(A))	(dB(A))
-196.9	-60.00	40.0	47.3	41.2	41.5	48.0
-177.2	-54.00	40.5	48.0	41.9	42.1	48.6
-157.5	-48.00	41.1	48.8	42.6	42.7	49.3
-137.8	-42.00	41.7	49.7	43.4	43.5	50.0
-118.1	-35.99	42.3	50.7	44.4	44.3	50.9
-98.4	-29.99	43.1	51.7	45.4	45.2	51.7
-93.5	-28.50	43.3	51.9	45.6	45.4	52.0
-88.6	-27.00	43.5	52.2	45.8	45.6	52.2
-83.7	-25.50	43.7	52.4	46.0	45.8	52.4
-78.8	-24.00	43.9	52.5	46.2	46.0	52.6
-73.8	-22.50	44.1	52.7	46.4	46.2	52.8
-68.9	-21.00	44.3	52.8	46.6	46.4	52.9
-64.0	-19.50	44.5	52.9	46.7	46.5	53.1
-59.1	-18.00	44.8	53.0	46.9	46.7	53.3
-54.2	-16.50	45.0	53.1	47.0	46.9	53.4
-49.2	-15.01	45.2	53.1	47.1	47.0	53.6
-44.3	-13.51	45.5	53.1	47.2	47.2	53.7
-39.4	-12.01	45.7	53.1	47.2	47.3	53.9
-34.5	-10.51	46.0	53.1	47.3	47.5	54.0
-29.5	-9.01	46.3	53.0	47.3	47.6	54.1
-24.6	-7.51	46.6	53.0	47.3	47.8	54.3
-19.7	-6.01	46.9	52.9	47.3	47.9	54.4
-14.8	-4.51	47.1	52.7	47.3	48.1	54.6
-9.9	-3.01	47.4	52.6	47.3	48.2	54.7
-4.9	-1.51	47.7	52.4	47.2	48.4	54.9
.0	-.01	48.0	52.2	47.1	48.5	55.0
4.9	1.49	48.3	52.0	47.0	48.7	55.1
9.8	2.99	48.5	51.8	47.0	48.8	55.3
14.7	4.49	48.7	51.6	46.9	48.9	55.4
19.7	5.99	48.9	51.4	46.8	49.0	55.4
24.6	7.49	49.0	51.2	46.6	49.0	55.4
29.5	8.99	48.9	51.0	46.5	49.0	55.4
34.4	10.49	48.8	50.7	46.3	48.8	55.2
39.3	11.99	48.7	50.5	46.1	48.6	55.0
44.3	13.49	48.4	50.2	45.8	48.4	54.8
49.2	14.99	48.2	50.0	45.6	48.1	54.5
54.1	16.49	47.9	49.8	45.3	47.9	54.3
59.0	17.99	47.5	49.5	45.0	47.6	54.0
63.9	19.49	47.2	49.3	44.8	47.3	53.7
68.9	20.99	46.9	49.1	44.5	47.0	53.4
73.8	22.49	46.6	48.9	44.2	46.7	53.1
78.7	23.98	46.3	48.6	44.0	46.4	52.8
83.6	25.48	46.0	48.4	43.8	46.1	52.5
88.5	26.98	45.7	48.2	43.5	45.8	52.2
93.4	28.48	45.4	48.0	43.3	45.6	52.0
98.4	29.98	45.2	47.9	43.1	45.3	51.7
118.1	36.00	44.2	47.2	42.3	44.4	50.8
137.8	42.00	43.3	46.5	41.6	43.6	50.0
157.5	48.01	42.6	45.9	40.9	42.9	49.3

177.2	54.01	41.9	45.4	40.4	42.2	48.6
196.9	60.01	41.3	44.9	39.8	41.6	48.1

```

*****
*
*           AUDIBLE NOISE           *
*      (other methods)              *
*
*   Altitude   5905.5 feet         *
*
*****

```

LATERAL DISTANCE		<----- BPA METHOD ----->				<- CRIEPI -->		EdF	ENEL	IREQ
(feet)	(meters)	FAIR WEATHER	L5 RAIN	L50 RAIN	Ldn	AVERAGE FAIR	L5 RAIN	L5 RAIN	L5 RAIN	L5 RAIN
		dB(A)	dB(A)	dB(A)	dB(A)	dB(A)	dB(A)	dB(A)	dB(A)	dB(A)
-196.9	-60.00	35.9	43.2	39.7	44.4	.0	.0	.0	.0	.0
-177.2	-54.00	36.3	43.9	40.4	45.0	.0	.0	.0	.0	.0
-157.5	-48.00	36.8	44.6	41.1	45.6	.0	.0	.0	.0	.0
-137.8	-42.00	37.4	45.6	42.1	46.4	.0	.0	.0	.0	.0
-118.1	-35.99	38.0	46.6	43.1	47.3	.0	.0	.0	.0	.0
-98.4	-29.99	38.7	47.7	44.2	48.2	.0	.0	.0	.0	.0
-93.5	-28.50	38.8	48.0	44.5	48.4	.0	.0	.0	.0	.0
-88.6	-27.00	39.0	48.2	44.7	48.7	.0	.0	.0	.0	.0
-83.7	-25.50	39.2	48.4	44.9	48.9	.0	.0	.0	.0	.0
-78.8	-24.00	39.4	48.6	45.1	49.0	.0	.0	.0	.0	.0
-73.8	-22.50	39.7	48.7	45.2	49.2	.0	.0	.0	.0	.0
-68.9	-21.00	39.9	48.8	45.3	49.4	.0	.0	.0	.0	.0
-64.0	-19.50	40.1	48.9	45.4	49.5	.0	.0	.0	.0	.0
-59.1	-18.00	40.3	49.0	45.5	49.6	.0	.0	.0	.0	.0
-54.2	-16.50	40.6	49.0	45.5	49.7	.0	.0	.0	.0	.0
-49.2	-15.01	40.8	49.0	45.5	49.8	.0	.0	.0	.0	.0
-44.3	-13.51	41.1	48.9	45.4	49.9	.0	.0	.0	.0	.0
-39.4	-12.01	41.4	48.8	45.3	50.0	.0	.0	.0	.0	.0
-34.5	-10.51	41.7	48.7	45.2	50.1	.0	.0	.0	.0	.0
-29.5	-9.01	42.0	48.6	45.1	50.1	.0	.0	.0	.0	.0
-24.6	-7.51	42.3	48.4	44.9	50.2	.0	.0	.0	.0	.0
-19.7	-6.01	42.6	48.2	44.7	50.3	.0	.0	.0	.0	.0
-14.8	-4.51	42.9	48.1	44.6	50.4	.0	.0	.0	.0	.0
-9.9	-3.01	43.3	47.9	44.4	50.6	.0	.0	.0	.0	.0
-4.9	-1.51	43.6	47.8	44.3	50.7	.0	.0	.0	.0	.0
.0	-.01	43.9	47.6	44.1	50.9	.0	.0	.0	.0	.0
4.9	1.49	44.3	47.5	44.0	51.1	.0	.0	.0	.0	.0
9.8	2.99	44.5	47.4	43.9	51.2	.0	.0	.0	.0	.0
14.7	4.49	44.8	47.3	43.8	51.4	.0	.0	.0	.0	.0
19.7	5.99	44.9	47.1	43.6	51.5	.0	.0	.0	.0	.0
24.6	7.49	45.0	47.0	43.5	51.5	.0	.0	.0	.0	.0
29.5	8.99	45.0	46.8	43.3	51.4	.0	.0	.0	.0	.0
34.4	10.49	44.9	46.6	43.1	51.3	.0	.0	.0	.0	.0
39.3	11.99	44.7	46.4	42.9	51.1	.0	.0	.0	.0	.0

44.3	13.49	44.4	46.2	42.7	50.9	.0	.0	.0	.0	.0
49.2	14.99	44.2	45.9	42.4	50.6	.0	.0	.0	.0	.0
54.1	16.49	43.8	45.7	42.2	50.3	.0	.0	.0	.0	.0
59.0	17.99	43.5	45.5	42.0	50.0	.0	.0	.0	.0	.0
63.9	19.49	43.2	45.2	41.7	49.6	.0	.0	.0	.0	.0
68.9	20.99	42.8	45.0	41.5	49.3	.0	.0	.0	.0	.0
73.8	22.49	42.5	44.7	41.2	49.0	.0	.0	.0	.0	.0
78.7	23.98	42.2	44.5	41.0	48.7	.0	.0	.0	.0	.0
83.6	25.48	41.9	44.3	40.8	48.4	.0	.0	.0	.0	.0
88.5	26.98	41.6	44.1	40.6	48.2	.0	.0	.0	.0	.0
93.4	28.48	41.3	43.9	40.4	47.9	.0	.0	.0	.0	.0
98.4	29.98	41.0	43.7	40.2	47.7	.0	.0	.0	.0	.0
118.1	36.00	40.0	43.0	39.5	46.7	.0	.0	.0	.0	.0
137.8	42.00	39.1	42.4	38.9	46.0	.0	.0	.0	.0	.0
157.5	48.01	38.4	41.9	38.4	45.3	.0	.0	.0	.0	.0
177.2	54.01	37.7	41.4	37.9	44.7	.0	.0	.0	.0	.0
196.9	60.01	37.2	40.9	37.4	44.2	.0	.0	.0	.0	.0

Audible noise prediction methods do not apply to all line geometries, voltages, or weather conditions. If a prediction method does not apply, the appropriate output data column will be zeros.

-----  
Results of AC/DCLINE program RADIO (EPRI/HVTRC 7-93) for:  
-----

RADIO NOISE

Configuration file name:  
C:\TLW30\ACDCLINE\DATA\ACCASE01  
Date: 12/18/2015 Time: 12:22

MODE NO.	ATTN(dB/mi)	ATTN(neper/ft)
1	.5147E-01	.1123E-05
2	.1875E+00	.4090E-05
3	.8096E+00	.1766E-04
4	.3251E+01	.7091E-04
5	.8803E+01	.1920E-03

\*\*\*\*\*  
\* \*  
\* MAXIMUM SURFACE GRADIENT (kV/cm) \*  
\* \*  
\*\*\*\*\*

BNDL #	Type	DC	ACrms	PEAK(+)	PEAK(-)
1	AC	-.15	14.52	20.37	-20.68
2	AC	-.52	15.34	21.17	-22.20
3	AC	-2.53	14.69	18.24	-23.30
6	DC	21.52	.76	22.59	20.45

7	DC	-21.12	.12	-20.95	-21.29
4	Ground Wire	-.89	7.77	10.10	-11.89
5	Ground Wire	-5.27	7.18	4.89	-15.43
8	Ground Wire	1.13	1.45	3.18	-.91

```

*****
*
*          RADIO NOISE          *
*    GENERATION FUNCTION      *
* (dB above 1uA/sqrt(m))    *
*
*****

```

BNDL #	Type	Average Stable Foul	L1 Rain	L50 Rain
----	----	-----	-----	-----
1	AC	28.41	35.10	24.33
2	AC	31.28	36.61	26.56
3	AC	29.03	30.38	17.40
6	DC	.00	18.70	18.70
7	DC	.00	*****	*****

NOTE: The sequence of the "\*" symbols in the Table indicates that the Radio Noise Generation Function associated with the negative polarity DC conductors is negligible.

```

*****
*
*    RADIO NOISE PROFILES    *
*      at 500.00 kHz        *
*
*    ANSI, loop antenna     *
*    ALTITUDE 5905.5 ft     *
*****

```

Lateral Distance	Average Stable Foul	Heavy Rain	Wet Conductor
(feet) (meters)	Weather Noise (1,2)	Noise (3)	Noise (3)
-----	(dB)	(dB)	(dB)
-196.9 -60.00	55.3	61.3	50.8
-177.2 -54.00	58.8	64.8	54.3
-157.5 -48.00	62.9	68.8	58.3
-137.8 -42.00	67.5	73.4	62.9
-118.1 -35.99	72.4	78.3	67.8
-98.4 -29.99	76.2	82.0	71.6
-93.5 -28.50	76.4	82.3	71.8
-88.6 -27.00	76.1	82.1	71.6
-83.7 -25.50	75.2	81.2	70.7
-78.8 -24.00	73.8	79.8	69.1
-73.8 -22.50	73.0	78.7	68.0
-68.9 -21.00	74.6	79.7	69.2
-64.0 -19.50	77.2	82.2	71.8

-59.1	-18.00	79.2	84.3	74.0
-54.2	-16.50	80.4	85.5	75.3
-49.2	-15.01	80.7	85.9	75.7
-44.3	-13.51	80.1	85.4	75.3
-39.4	-12.01	78.7	84.1	73.9
-34.5	-10.51	76.9	82.1	71.8
-29.5	-9.01	76.0	80.2	69.8
-24.6	-7.51	76.8	80.1	69.3
-19.7	-6.01	78.1	81.2	70.4
-14.8	-4.51	78.9	82.2	71.3
-9.9	-3.01	78.9	82.3	71.5
-4.9	-1.51	78.0	81.7	71.0
.0	-.01	76.4	80.3	69.8
4.9	1.49	73.9	78.3	68.2
9.8	2.99	71.1	76.1	67.1
14.7	4.49	69.7	74.8	67.1
19.7	5.99	71.0	75.4	67.9
24.6	7.49	72.6	76.4	68.6
29.5	8.99	73.4	76.9	68.8
34.4	10.49	73.4	76.7	68.4
39.3	11.99	72.5	75.8	67.2
44.3	13.49	71.0	74.2	65.4
49.2	14.99	68.7	72.0	62.7
54.1	16.49	65.9	69.2	59.5
59.0	17.99	63.0	66.7	57.0
63.9	19.49	62.0	66.2	57.8
68.9	20.99	63.1	67.3	59.8
73.8	22.49	64.3	68.4	61.1
78.7	23.98	64.9	68.9	61.6
83.6	25.48	64.8	68.8	61.5
88.5	26.98	64.3	68.2	61.0
93.4	28.48	63.4	67.3	60.1
98.4	29.98	62.3	66.2	59.0
118.1	36.00	57.1	60.9	53.7
137.8	42.00	52.0	55.7	48.5
157.5	48.01	47.6	51.4	44.1
177.2	54.01	44.1	47.8	40.4
196.9	60.01	41.2	44.9	37.3

(1) The "Average Stable Foul Weather" noise is calculated using an empirical expression for the radio noise excitation function that was derived (see REF. [A]) to best fit the long term radio noise measurements of existing lines (in the 345 kV to 765 kV range). This generation function is used also in the program RNOISE, which is applicable to AC transmission lines. If AC lines are not present, the "Average Stable Foul Weather" column contains zeros.

(2) The "Average Fair Weather" radio noise values can be obtained by subtracting 21.6 dB from the "Average Stable Foul Weather" radio noise data.

(3) The "Heavy Rain" and the "Wet Conductor" radio noise levels, are defined in the EPRI's Transmission Line Reference Book - 345 kV and Above. The equations for the excitation functions for AC conductors are derived from the Reference Book and are applicable for large ranges of surface gradients (from 10 to 25 kV/cm), subconductor diameters (2 to 8 cm) and number of subconductors (1 to 12). The equations for the excitation functions for DC and HYBRID line conductors are derived from the EPRI RP 2472-6. Heavy rain was defined as rain with intensity of the order of 8 - 12 mm/hr. In the Northeastern climate, the "Heavy Rain" noise is exceeded only 1% of the time during periods of rain. "Wet Conductor" noise corresponds to the condition of the conductor saturated with water drops and with little noise caused by the impingement of rain droplets. Experimental data from which the equations for the "Wet Conductor" noise were derived, indicate that the "Wet Conductor" noise is exceeded 50% of the time during natural rain periods. "Wet Conductor" noise also corresponds to the maximum noise that can be produced during fog.

REFERENCES:

[A] R.G. Olsen, S.D. Schennum and V.L. Chartier, "Comparison of Several Methods for Calculating Power Line Electromagnetic Interference Levels and Calibration with Long Term Data", EPRI report, Project RP-2025, 1991.

=====

-----  
 Results of AC/DCLINE program EFION (EPRI/HVTRC 7-93) for:  
 -----

SURFACE GRADIENTS at ACTUAL LINE HEIGHT  
 ELECTRIC FIELD & IONS WITHOUT SHIELDING OBJECTS

Configuration file name:  
 C:\TLW30\ACDCLINE\DATA\ACCASE01  
 Date: 12/18/2015 Time: 12:22

\*\*\*\*\*  
 \* \*  
 \* MAXIMUM SURFACE GRADIENT (kV/cm) \*  
 \* \*  
 \*\*\*\*\*

BNDL #	Type	DC	ACrms	PEAK(+)	PEAK(-)
1	AC	-.15	14.52	20.37	-20.68
2	AC	-.52	15.34	21.17	-22.20
3	AC	-2.53	14.69	18.24	-23.30
6	DC	21.52	.76	22.59	20.45
7	DC	-21.12	.12	-20.95	-21.29
4	Ground Wire	-.89	7.77	10.10	-11.89



-24.6	-7.51	4.456	.129	4.442	.671	4.409
-19.7	-6.01	4.916	.085	4.909	.489	4.866
-14.8	-4.51	5.173	.055	5.172	.298	5.125
-9.9	-3.01	5.160	.036	5.159	.206	5.118
-4.9	-1.51	4.894	.023	4.888	.270	4.858
.0	-.01	4.439	.015	4.426	.351	4.408
4.9	1.49	3.876	.009	3.856	.393	3.850
9.8	2.99	3.277	.006	3.253	.396	3.255
14.7	4.49	2.695	.003	2.670	.370	2.677
19.7	5.99	2.168	.002	2.144	.325	2.155
24.6	7.49	1.717	.000	1.695	.271	1.707
29.5	8.99	1.349	.001	1.332	.215	1.344
34.4	10.49	1.063	.002	1.050	.165	1.060
39.3	11.99	.845	.002	.835	.126	.843
44.3	13.49	.679	.003	.672	.096	.678
49.2	14.99	.552	.003	.546	.075	.550
54.1	16.49	.450	.003	.446	.061	.449
59.0	17.99	.368	.003	.364	.050	.367
63.9	19.49	.300	.003	.298	.040	.299
68.9	20.99	.246	.003	.244	.032	.245
73.8	22.49	.203	.004	.202	.024	.203
78.7	23.98	.172	.004	.171	.018	.172
83.6	25.48	.149	.004	.149	.013	.149
88.5	26.98	.133	.003	.133	.009	.133
93.4	28.48	.122	.003	.121	.007	.122
98.4	29.98	.113	.002	.113	.005	.113
118.1	36.00	.088	.001	.088	.004	.088
137.8	42.00	.068	.000	.068	.003	.068
157.5	48.01	.053	.001	.053	.002	.053
177.2	54.01	.041	.001	.041	.002	.041
196.9	60.01	.033	.002	.033	.001	.033

```

*****
*
*           ELECTROSTATIC AND SATURATED           *
* DC FIELD, CURRENT, AND ION DENSITY PROFILES *
*
*           wind speed = 0                         *
*           longitudinal distance: 500.00 feet     *
*
*****

```

LATERAL		<-- DC ELECTRIC FIELD -->		CURRENT	ION
DISTANCE		ELECTROSTATIC	SATURATED	DENSITY	DENSITY
(feet)	(meters)	(kV/m)	(kV/m)	(nA/m2)	(1/cm3)
-196.9	-60.00	.04	1.46	.0	1192.
-177.2	-54.00	.05	1.57	.0	1345.
-157.5	-48.00	.06	1.63	.0	1493.
-137.8	-42.00	.08	1.76	.1	1742.

-118.1	-35.99	.10	1.84	.1	1973.
-98.4	-29.99	.13	2.20	.1	2152.
-93.5	-28.50	.14	2.57	.2	3734.
-88.6	-27.00	.16	4.45	.6	7560.
-83.7	-25.50	.18	4.63	.8	9101.
-78.8	-24.00	.22	4.89	.9	10470.
-73.8	-22.50	.26	5.30	1.2	12116.
-68.9	-21.00	.32	5.83	1.5	14086.
-64.0	-19.50	.40	6.38	1.9	16158.
-59.1	-18.00	.50	7.03	2.4	18500.
-54.2	-16.50	.63	8.06	3.2	21861.
-49.2	-15.01	.80	9.11	4.2	25285.
-44.3	-13.51	1.03	10.32	5.6	29254.
-39.4	-12.01	1.32	11.98	7.6	34690.
-34.5	-10.51	1.69	13.67	10.2	40484.
-29.5	-9.01	2.18	15.63	13.6	47242.
-24.6	-7.51	2.81	18.29	18.9	56134.
-19.7	-6.01	3.61	21.15	25.5	65585.
-14.8	-4.51	4.61	24.44	34.3	76371.
-9.9	-3.01	5.83	28.51	47.2	90002.
-4.9	-1.51	7.26	32.90	63.9	105501.
.0	-.01	8.85	37.46	84.8	123043.
4.9	1.49	10.53	41.94	109.8	142293.
9.8	2.99	12.14	46.02	137.3	162209.
14.7	4.49	13.45	49.26	164.1	180981.
19.7	5.99	14.16	51.26	185.3	196467.
24.6	7.49	14.00	51.39	194.7	205929.
29.5	8.99	12.80	48.51	183.1	205142.
34.4	10.49	10.55	42.71	154.1	196044.
39.3	11.99	7.45	33.07	107.7	177006.
44.3	13.49	3.77	19.74	55.3	152135.
49.2	14.99	-.21	-1.66	-3.9	-97948.
54.1	16.49	-4.20	-21.15	-77.8	-153199.
59.0	17.99	-7.92	-34.02	-144.7	-177206.
63.9	19.49	-11.08	-43.48	-204.4	-195851.
68.9	20.99	-13.41	-49.28	-242.3	-204820.
73.8	22.49	-14.74	-52.31	-257.9	-205413.
78.7	23.98	-15.05	-52.55	-247.2	-195978.
83.6	25.48	-14.51	-51.02	-220.6	-180185.
88.5	26.98	-13.40	-47.86	-182.8	-159171.
93.4	28.48	-11.99	-44.11	-145.6	-137531.
98.4	29.98	-10.51	-40.21	-113.1	-117176.
118.1	36.00	-5.73	-26.53	-37.6	-59091.
137.8	42.00	-3.20	-18.01	-13.7	-31757.
157.5	48.01	-1.92	-12.93	-5.8	-18729.
177.2	54.01	-1.23	-9.70	-2.8	-11874.
196.9	60.01	-.83	-7.44	-1.4	-7869.

\*\*\*\*\*  
\* \* \* \* \*  
\* DC FIELD AND ION DENSITY PROFILES AT GROUND LEVEL \*

```

*
*
*           wind speed = 0
*           longitudinal distance: 500.00 feet
*
*****

```

		<----- SUMMER FAIR ----->				<----- RAIN ----->			
LATERAL		FIELD	FIELD	IONS	IONS	FIELD	FIELD	IONS	IONS
DISTANCE		50%	95%	50%	95%	50%	95%	50%	95%
(feet)	(meters)	(kV/m)	(kV/m)	(1/cc)	(1/cc)	(kV/m)	(kV/m)	(1/cc)	(1/cc)
-196.9	-60.00	.4	.9	1113.	1171.	.9	1.1	1172.	1182.
-177.2	-54.00	.5	1.0	1239.	1316.	1.0	1.2	1318.	1331.
-157.5	-48.00	.5	1.0	1351.	1454.	1.0	1.3	1456.	1474.
-137.8	-42.00	.5	1.1	1553.	1689.	1.1	1.4	1692.	1716.
-118.1	-35.99	.6	1.1	1726.	1903.	1.2	1.4	1907.	1939.
-98.4	-29.99	.7	1.4	1864.	2070.	1.4	1.7	2074.	2112.
-93.5	-28.50	.8	1.6	3261.	3600.	1.6	2.0	3608.	3670.
-88.6	-27.00	1.3	2.7	6906.	7380.	2.8	3.4	7391.	7474.
-83.7	-25.50	1.4	2.8	8235.	8861.	2.9	3.5	8875.	8986.
-78.8	-24.00	1.5	3.0	9368.	10163.	3.1	3.8	10181.	10322.
-73.8	-22.50	1.7	3.3	10715.	11722.	3.3	4.1	11745.	11926.
-68.9	-21.00	1.8	3.6	12298.	13578.	3.7	4.5	13607.	13841.
-64.0	-19.50	2.0	4.0	13876.	15503.	4.1	4.9	15540.	15841.
-59.1	-18.00	2.3	4.4	15589.	17653.	4.5	5.4	17701.	18089.
-54.2	-16.50	2.7	5.1	18133.	20764.	5.2	6.3	20826.	21327.
-49.2	-15.01	3.1	5.8	20531.	23865.	5.9	7.1	23944.	24592.
-44.3	-13.51	3.6	6.6	23190.	27412.	6.7	8.1	27514.	28352.
-39.4	-12.01	4.3	7.7	26905.	32289.	7.8	9.4	32422.	33510.
-34.5	-10.51	5.0	8.8	30529.	37354.	9.0	10.8	37525.	38940.
-29.5	-9.01	5.9	10.2	34553.	43168.	10.4	12.4	43389.	45222.
-24.6	-7.51	7.1	12.0	39972.	50850.	12.3	14.5	51135.	53502.
-19.7	-6.01	8.4	14.1	45249.	58794.	14.3	16.9	59157.	62185.
-14.8	-4.51	10.1	16.4	51020.	67723.	16.7	19.6	68180.	72019.
-9.9	-3.01	12.1	19.4	58513.	79066.	19.7	23.0	79639.	84473.
-4.9	-1.51	14.3	22.6	66753.	91805.	22.9	26.7	92516.	98544.
.0	-.01	16.7	25.9	75861.	106086.	26.3	30.5	106958.	114389.
4.9	1.49	19.2	29.3	85682.	121638.	29.7	34.3	122692.	131708.
9.8	2.99	21.5	32.4	95749.	137653.	32.8	37.8	138898.	149581.
14.7	4.49	23.3	34.8	105338.	152784.	35.3	40.6	154207.	166443.
19.7	5.99	24.4	36.3	113777.	165545.	36.8	42.3	167103.	180510.
24.6	7.49	24.3	36.3	119950.	173894.	36.9	42.3	175511.	189414.
29.5	8.99	22.6	34.1	121100.	174091.	34.6	39.9	175665.	189173.
34.4	10.49	19.4	29.7	118808.	167978.	30.2	34.9	169414.	181678.
39.3	11.99	14.5	22.7	111123.	153601.	23.1	26.9	154813.	165099.
44.3	13.49	8.2	13.3	101303.	134756.	13.5	15.9	135674.	143383.
49.2	14.99	-.5	-.9	64655.	85378.	-1.1	-1.3	90280.	93903.
54.1	16.49	-7.6	-12.1	85309.	124802.	-14.4	-16.9	135423.	143638.
59.0	17.99	-13.1	-20.1	91684.	139896.	-23.6	-27.5	153577.	164381.
63.9	19.49	-17.5	-26.2	96895.	151588.	-30.6	-35.3	167616.	180438.
68.9	20.99	-20.6	-30.1	97972.	156134.	-35.0	-40.3	173593.	187698.

73.8	22.49	-22.2	-32.2	96478.	155282.	-37.4	-42.9	173163.	187688.
78.7	23.98	-22.5	-32.5	91250.	147558.	-37.6	-43.1	164784.	178813.
83.6	25.48	-21.8	-31.5	84204.	135896.	-36.5	-41.9	151669.	164501.
88.5	26.98	-20.3	-29.5	75009.	120511.	-34.1	-39.2	134314.	145515.
93.4	28.48	-18.4	-27.0	65822.	104866.	-31.3	-36.1	116582.	126045.
98.4	29.98	-16.4	-24.4	57229.	90170.	-28.4	-32.8	99913.	107737.
118.1	36.00	-9.9	-15.4	31671.	47366.	-18.3	-21.3	51707.	55101.
137.8	42.00	-6.2	-10.1	18555.	26388.	-12.1	-14.3	28421.	29973.
157.5	48.01	-4.1	-7.0	11753.	16012.	-8.5	-10.2	17059.	17844.
177.2	54.01	-2.9	-5.2	7878.	10370.	-6.3	-7.6	10957.	11391.
196.9	60.01	-2.2	-3.9	5433.	6975.	-4.8	-5.8	7327.	7584.

-----  
Results of AC/DCLINE program MAGFLD (EPRI/HVTRC 7-93) for:  
-----

MAGNETIC FIELD CALCULATIONS

Configuration file name:  
C:\TLW30\ACDCLINE\DATA\ACCASE01  
Date: 12/18/2015 Time: 12:22

-----  
AC CURRENTS IN EACH BUNDLE:  
-----

BNDL #	----- AC CURRENTS (Amperes) -----			BUNDLE POSITION	
	REAL	IMAGINARY	TOTAL	X-COORD	Y-COORD
1	1443.00	.00	1443.00	-81.69	38.71
2	-721.50	-1249.67	1443.00	-49.21	38.71
3	-721.50	1249.67	1443.00	-16.73	38.71
6	.00	.00	.00	26.25	35.76
7	.00	.00	.00	72.18	35.76
4	-27.97	-16.29	32.37	-75.79	60.04
5	24.55	18.63	30.82	-22.64	60.04
8	15.52	6.71	16.91	49.21	75.79

\*\*\*\*\*  
\* \* \* \* \*  
\* MAGNETIC FIELD PROFILE \*  
\* at 3.28 feet above ground \*  
\* \* \* \* \*  
\* longitudinal distance: 500.00 feet \*  
\* \* \* \* \*  
\*\*\*\*\*

<----- AC MAGNETIC FIELD -----> <-- DC MAGNETIC FIELD -->

LATERAL DISTANCE		MAJOR AXIS	MINOR/ MAJOR	VERTICAL COMP	HORIZONTAL COMP	TOTAL	VERTICAL COMP	HORIZONTAL COMP
(feet)	(meters)	(mG)	(RATIO)	(mG)	(mG)	(mG)	(mG)	(mG)
-196.9	-60.00	24.14	.022	21.28	11.40	14.80	14.28	-3.87
-177.2	-54.00	31.94	.030	26.85	17.33	17.46	16.74	-4.96
-157.5	-48.00	44.12	.043	34.15	28.00	20.89	19.86	-6.48
-137.8	-42.00	64.25	.064	42.25	48.57	25.45	23.92	-8.70
-118.1	-35.99	99.17	.100	43.64	89.60	31.66	29.28	-12.05
-98.4	-29.99	156.38	.166	25.95	156.37	40.42	36.52	-17.33
-93.5	-28.50	173.00	.190	42.26	170.94	43.15	38.70	-19.10
-88.6	-27.00	189.22	.218	71.57	179.96	46.19	41.08	-21.12
-83.7	-25.50	203.76	.251	107.25	180.66	49.55	43.65	-23.44
-78.8	-24.00	215.53	.290	144.01	172.10	53.28	46.45	-26.10
-73.8	-22.50	223.88	.334	176.87	156.29	57.45	49.49	-29.18
-68.9	-21.00	228.70	.383	202.03	138.39	62.11	52.78	-32.74
-64.0	-19.50	230.50	.434	217.96	125.00	67.34	56.34	-36.88
-59.1	-18.00	230.23	.482	225.70	119.93	73.25	60.19	-41.74
-54.2	-16.50	229.25	.518	228.24	120.65	79.94	64.33	-47.45
-49.2	-15.01	228.92	.531	228.91	121.55	87.55	68.74	-54.21
-44.3	-13.51	229.81	.516	229.12	119.98	96.25	73.41	-62.25
-39.4	-12.01	231.23	.480	227.30	118.78	106.24	78.26	-71.86
-34.5	-10.51	231.77	.432	220.06	123.77	117.77	83.16	-83.39
-29.5	-9.01	230.11	.382	204.40	137.49	131.13	87.90	-97.31
-24.6	-7.51	225.32	.335	179.33	155.90	146.68	92.11	-114.15
-19.7	-6.01	216.93	.293	146.44	172.20	164.84	95.22	-134.56
-14.8	-4.51	205.07	.257	109.58	181.15	186.08	96.29	-159.23
-9.9	-3.01	190.42	.226	73.83	180.71	210.92	93.92	-188.86
-4.9	-1.51	174.07	.200	44.51	171.83	239.87	86.01	-223.92
.0	-.01	157.21	.178	28.01	157.20	273.31	69.62	-264.29
4.9	1.49	140.83	.159	28.24	139.79	311.27	40.98	-308.56
9.8	2.99	125.58	.144	35.06	121.94	353.19	-4.08	-353.16
14.7	4.49	111.80	.131	40.75	105.14	397.53	-68.71	-391.55
19.7	5.99	99.58	.121	44.06	90.11	441.69	-152.83	-414.41
24.6	7.49	88.86	.112	45.35	77.06	482.35	-250.88	-411.96
29.5	8.99	79.52	.104	45.22	65.94	516.38	-351.92	-377.89
34.4	10.49	71.40	.098	44.15	56.55	541.96	-442.84	-312.43
39.3	11.99	64.34	.093	42.51	48.66	558.95	-513.02	-221.89
44.3	13.49	58.19	.088	40.55	42.04	568.38	-556.57	-115.24
49.2	14.99	52.81	.084	38.45	36.48	571.39	-571.39	-1.06
54.1	16.49	48.11	.081	36.31	31.79	568.49	-557.10	113.20
59.0	17.99	43.97	.077	34.21	27.84	559.19	-514.07	220.06
63.9	19.49	40.32	.074	32.18	24.48	542.35	-444.33	310.98
68.9	20.99	37.09	.072	30.25	21.63	516.92	-353.71	376.96
73.8	22.49	34.22	.069	28.43	19.19	483.04	-252.75	411.64
78.7	23.98	31.66	.066	26.73	17.09	442.48	-154.52	414.62
83.6	25.48	29.37	.064	25.15	15.28	398.35	-70.08	392.14
88.5	26.98	27.31	.061	23.68	13.72	353.98	-5.08	353.95
93.4	28.48	25.46	.059	22.32	12.35	312.01	40.31	309.39
98.4	29.98	23.79	.057	21.05	11.17	273.96	69.22	265.07
118.1	36.00	18.49	.048	16.85	7.67	164.92	95.23	134.65

137.8	42.00	14.78	.042	13.74	5.50	106.26	78.27	71.88
157.5	48.01	12.08	.036	11.39	4.07	73.25	60.19	41.74
177.2	54.01	10.06	.032	9.58	3.10	53.28	46.45	26.10
196.9	60.01	8.50	.029	8.16	2.42	40.40	36.50	17.31

## APPENDIX B

## HAND CALCULATION RESULTS

Section 5.2

Calculation of ac current induced in a parallel dc  
<http://en.smith.info/>

Conductor numbers are allocated as follows:

- 1,2,3 - ac line phase conductors A, B, C
- 4,5 - dc line pole conductors +, -
- 6,7,8 - shieldwires

Relative air density is:

$$\text{RAD}=0.8$$

The centre-centre separation of the two line is 2.d [m]:

$$d:=15$$

Attachment and midspan heights, and lateral positions of the conductors are:

$$h_a := \begin{pmatrix} 19.2 \\ 19.2 \\ 19.2 \\ 18.4 \\ 18.4 \\ 24.2 \\ 24.2 \\ 29 \end{pmatrix} \quad h_m := \begin{pmatrix} 8.1 \\ 8.1 \\ 8.1 \\ 7.2 \\ 7.2 \\ 15.3 \\ 15.3 \\ 20.1 \end{pmatrix} \quad X_{ac} := \begin{pmatrix} -9.9 \\ 0 \\ 9.9 \\ -8.1 \\ 8.1 \end{pmatrix} \quad X_{dc} := \begin{pmatrix} -7 \\ 7 \\ 0 \end{pmatrix}$$

The line geometry consists of bundle coordinates (X [m]; Y [m]):

$$X := \begin{pmatrix} -d+X_{ac1} \\ -d+X_{ac2} \\ -d+X_{ac3} \\ d+X_{dc1} \\ d+X_{dc2} \\ -d+X_{ac4} \\ -d+X_{ac5} \\ d+X_{dc3} \end{pmatrix} = \begin{pmatrix} -24.9 \\ -15 \\ -5.1 \\ 8 \\ 22 \\ -23.1 \\ -6.9 \\ 15 \end{pmatrix} \quad Y := \frac{h_a + 2 \cdot h_m}{3} = \begin{pmatrix} 11.8 \\ 11.8 \\ 11.8 \\ 10.9333 \\ 10.9333 \\ 18.2667 \\ 18.2667 \\ 23.0667 \end{pmatrix}$$

Diameters of shield wires [cm], individual ac phase conductors [cm] and individual dc pole conductors [cm] are:

$$d_{ac} := 2.703 \quad d_{dc} := 3.417 \quad d_{sw} := 1.325$$

Bundle diameters [cm] are:

$$s_{ac} := 45$$

$$n_{ac} := 3$$

$$s_{dc} := 45$$

$$n_{dc} := 4$$

$$PCD_{ac} := \frac{s_{ac}}{\sin\left(\frac{\pi}{n_{ac}}\right)} = 51.9615 \quad PCD_{dc} := \frac{s_{dc}}{\sin\left(\frac{\pi}{n_{dc}}\right)} = 63.6396$$

Bundle configurations are (n; conductor radius [cm]; bundle radius [cm]; voltage [kV]):

$$\begin{array}{l}
 \begin{pmatrix} 4 \\ 4 \\ 4 \\ 4 \\ 4 \\ 1 \\ 1 \\ 1 \end{pmatrix} \\
 n :=
 \end{array}
 \begin{array}{l}
 \begin{pmatrix} \frac{d_{ac}}{2} \\ \frac{d_{ac}}{2} \\ \frac{d_{ac}}{2} \\ \frac{d_{dc}}{2} \\ \frac{d_{dc}}{2} \\ \frac{d_{sw}}{2} \\ \frac{d_{sw}}{2} \\ \frac{d_{sw}}{2} \end{pmatrix} \\
 r_{cond} :=
 \end{array}
 \begin{array}{l}
 \begin{pmatrix} 1.3515 \\ 1.3515 \\ 1.3515 \\ 1.7085 \\ 1.7085 \\ 0.6625 \\ 0.6625 \\ 0.6625 \end{pmatrix} \\
 = \\
 \begin{pmatrix} PCD_{ac} \\ PCD_{ac} \\ PCD_{ac} \\ PCD_{dc} \\ PCD_{dc} \\ 0 \\ 0 \\ 0 \end{pmatrix} \\
 r_{bundle} :=
 \end{array}
 \begin{array}{l}
 \begin{pmatrix} 25.9808 \\ 25.9808 \\ 25.9808 \\ 31.8198 \\ 31.8198 \\ 0 \\ 0 \\ 0 \end{pmatrix}
 \end{array}$$

The effective radii [cm] for each bundle are calculated from the bundle configurations (using effective conductor diameters for inductance calculations):

$$\text{for } p \in 1 \dots 8$$

$$r_{\text{eff } p} := \text{if} \left( n_p = 1 \right)$$

$$\quad \text{eval} \left( r_{\text{cond } p} \cdot \exp \left( -\frac{1}{4} \right) \right)$$

$$\quad \text{else}$$

$$\quad \left( \text{eval} \left( \sqrt[ n_p ]{ n_p \cdot r_{\text{cond } p} \cdot \exp \left( -\frac{1}{4} \right) \cdot \left( r_{\text{bundle } p} \right)^{ n_p - 1 } } \right) \right)$$

$$r_{\text{eff}} = \begin{pmatrix} 16.4841 \\ 16.4841 \\ 16.4841 \\ 20.3493 \\ 20.3493 \\ 0.516 \\ 0.516 \\ 0.516 \end{pmatrix}$$

Geometric mean radius [cm] for each bundle is calculated from the bundle configurations:

$$\text{for } p \in 1 \dots 8$$

$$\text{GMR } p := \text{if} \left( n_p = 1 \right)$$

$$\quad \text{eval} \left( r_{\text{cond } p} \right)$$

$$\quad \text{else}$$

$$\quad \text{eval} \left( r_{\text{bundle } p} \cdot \left( \frac{ n_p \cdot r_{\text{cond } p} }{ r_{\text{bundle } p} } \right)^{ \left( \frac{1}{n_p} \right) } \right)$$

$$\text{GMR} = \begin{pmatrix} 17.5472 \\ 17.5472 \\ 17.5472 \\ 21.6617 \\ 21.6617 \\ 0.6625 \\ 0.6625 \\ 0.6625 \end{pmatrix}$$

The equivalent image depth [m] due to earth resistivity  $\rho$  [ $\Omega \cdot \text{m}$ ] is calculated at the power frequency  $f$  [Hz]:

$$\rho := 300$$

$$\mu_0 := 4 \cdot \pi \cdot 10^{-7}$$

$$f := 50$$

$$\delta := \sqrt{ \frac{ \rho }{ 2 \cdot \pi \cdot \mu_0 \cdot f } } = 871.7275$$

$\Phi$ -matrix is calculated from the line geometry:

```

for p ∈ 1..8
  for q ∈ 1..8
    if (p=q)
      
$$\Phi_{pq} := \text{eval} \left( \frac{\mu_0}{2 \cdot \pi} \cdot \ln \left( \frac{(y_p + \delta)}{0.01 \cdot r_{\text{eff} p}} \right) \right)$$

      (converting radius and spacing to same units)
    
```

else

$$\Phi_{pq} := \text{eval} \left( \frac{\mu_0}{2 \cdot \pi} \cdot \ln \left( \frac{\sqrt{(y_p + \delta)^2 + (x_p - x_q)^2}}{\sqrt{((y_p - y_q)^2 + (x_p - x_q)^2)}} \right) \right)$$

$$\frac{\Phi}{10^{-6}} = \begin{pmatrix} 1.7173 & 0.8983 & 0.7597 & 0.6582 & 0.5874 & 0.976 & 0.7666 & 0.612 \\ 0.8983 & 1.7173 & 0.8983 & 0.7296 & 0.6347 & 0.8891 & 0.8891 & 0.6635 \\ 0.7597 & 0.8983 & 1.7173 & 0.8418 & 0.6969 & 0.7666 & 0.976 & 0.7294 \\ 0.658 & 0.7294 & 0.8417 & 1.675 & 0.8288 & 0.6639 & 0.7947 & 0.8287 \\ 0.5872 & 0.6345 & 0.6967 & 0.8288 & 1.675 & 0.5925 & 0.6777 & 0.8287 \\ 0.9774 & 0.8906 & 0.7681 & 0.6655 & 0.5941 & 2.4116 & 0.8013 & 0.6288 \\ 0.7681 & 0.8906 & 0.9774 & 0.7963 & 0.6793 & 0.8013 & 2.4116 & 0.7363 \\ 0.6146 & 0.666 & 0.7319 & 0.8314 & 0.8314 & 0.6299 & 0.7374 & 2.4127 \end{pmatrix}$$

The  $\Phi$ -matrix is partitioned into 5x5, 5x3, 3x5 and 3x3 matrices

```

for p ∈ 1..5
  for q ∈ 1..5
     $\Phi_{cc} := \Phi_{pq}$ 
  
```

$$\Phi_{cc} = \begin{pmatrix} 1.7173 \cdot 10^{-6} & 8.9829 \cdot 10^{-7} & 7.597 \cdot 10^{-7} & 6.5816 \cdot 10^{-7} & 5.8743 \cdot 10^{-7} \\ 8.9829 \cdot 10^{-7} & 1.7173 \cdot 10^{-6} & 8.9829 \cdot 10^{-7} & 7.2961 \cdot 10^{-7} & 6.3472 \cdot 10^{-7} \\ 7.597 \cdot 10^{-7} & 8.9829 \cdot 10^{-7} & 1.7173 \cdot 10^{-6} & 8.4185 \cdot 10^{-7} & 6.9687 \cdot 10^{-7} \\ 6.5796 \cdot 10^{-7} & 7.2942 \cdot 10^{-7} & 8.4165 \cdot 10^{-7} & 1.675 \cdot 10^{-6} & 8.288 \cdot 10^{-7} \\ 5.8723 \cdot 10^{-7} & 6.3453 \cdot 10^{-7} & 6.9667 \cdot 10^{-7} & 8.288 \cdot 10^{-7} & 1.675 \cdot 10^{-6} \end{pmatrix}$$

for p ∈ 1..5

for q ∈ 1..3

```

 $\Phi_{cs} := \Phi_{p5+q}$ 
 $\Phi_{cs} := \Phi_{pq}$ 

```

$$\Phi_{cs} = \begin{pmatrix} 9.7599 \cdot 10^{-7} & 7.6661 \cdot 10^{-7} & 6.1204 \cdot 10^{-7} \\ 8.8911 \cdot 10^{-7} & 8.8911 \cdot 10^{-7} & 6.6347 \cdot 10^{-7} \\ 7.6661 \cdot 10^{-7} & 9.7599 \cdot 10^{-7} & 7.2937 \cdot 10^{-7} \\ 6.6386 \cdot 10^{-7} & 7.9465 \cdot 10^{-7} & 8.2867 \cdot 10^{-7} \\ 5.9246 \cdot 10^{-7} & 6.7769 \cdot 10^{-7} & 8.2867 \cdot 10^{-7} \end{pmatrix}$$

$$\begin{aligned}
& \text{for } p \in 1 \dots 3 \\
& \text{for } q \in 1 \dots 5 \\
& \Phi_{sc} := \Phi_{5+p,q} \\
& \Phi_{sc} = \begin{pmatrix} 9.7745 \cdot 10^{-7} & 8.9057 \cdot 10^{-7} & 7.6807 \cdot 10^{-7} & 6.6551 \cdot 10^{-7} & 5.9411 \cdot 10^{-7} \\ 7.6807 \cdot 10^{-7} & 8.9057 \cdot 10^{-7} & 9.7745 \cdot 10^{-7} & 7.9631 \cdot 10^{-7} & 6.7934 \cdot 10^{-7} \\ 6.1457 \cdot 10^{-7} & 6.66 \cdot 10^{-7} & 7.319 \cdot 10^{-7} & 8.314 \cdot 10^{-7} & 8.314 \cdot 10^{-7} \end{pmatrix} \\
& \text{for } p \in 1 \dots 3 \\
& \text{for } q \in 1 \dots 3 \\
& \Phi_{ss} := \Phi_{5+p,5+q} \\
& \Phi_{ss} = \begin{pmatrix} 2.4116 \cdot 10^{-6} & 8.0127 \cdot 10^{-7} & 6.2881 \cdot 10^{-7} \\ 8.0127 \cdot 10^{-7} & 2.4116 \cdot 10^{-6} & 7.3631 \cdot 10^{-7} \\ 6.2988 \cdot 10^{-7} & 7.3739 \cdot 10^{-7} & 2.4127 \cdot 10^{-6} \end{pmatrix}
\end{aligned}$$

An equivalent 5x5 matrix  $\Phi'$  is generated through Kron reduction

$$\begin{aligned}
& L' := \Phi_{cc} - (\Phi_{cs} \cdot \text{invert}(\Phi_{ss})) \cdot \Phi_{sc} \\
& L' = \begin{pmatrix} 1.201 \cdot 10^{-6} & 3.8156 \cdot 10^{-7} & 2.5843 \cdot 10^{-7} & 2.0963 \cdot 10^{-7} & 1.8214 \cdot 10^{-7} \\ 3.8152 \cdot 10^{-7} & 1.1857 \cdot 10^{-6} & 3.6758 \cdot 10^{-7} & 2.555 \cdot 10^{-7} & 2.0713 \cdot 10^{-7} \\ 2.5836 \cdot 10^{-7} & 3.6756 \cdot 10^{-7} & 1.1716 \cdot 10^{-6} & 3.5114 \cdot 10^{-7} & 2.533 \cdot 10^{-7} \\ 2.0953 \cdot 10^{-7} & 2.5544 \cdot 10^{-7} & 3.5112 \cdot 10^{-7} & 1.2126 \cdot 10^{-6} & 4.009 \cdot 10^{-7} \\ 1.821 \cdot 10^{-7} & 2.0714 \cdot 10^{-7} & 2.5334 \cdot 10^{-7} & 4.0098 \cdot 10^{-7} & 1.2747 \cdot 10^{-6} \end{pmatrix}
\end{aligned}$$

The  $\Phi'$  matrix is used to generate the  $L'$  capacitance matrix [H/m]:

$$\frac{L'}{10^{-6}} = \begin{pmatrix} 1.201 & 0.3816 & 0.2584 & 0.2096 & 0.1821 \\ 0.3815 & 1.1857 & 0.3676 & 0.2555 & 0.2071 \\ 0.2584 & 0.3676 & 1.1716 & 0.3511 & 0.2533 \\ 0.2095 & 0.2554 & 0.3511 & 1.2126 & 0.4009 \\ 0.1821 & 0.2071 & 0.2533 & 0.401 & 1.2747 \end{pmatrix}$$

For untransposed ac and dc lines

$$X' := i \cdot 2 \cdot \pi \cdot f \cdot L' = \begin{pmatrix} 0.0004 \cdot i & 0.0001 \cdot i & 8.1187 \cdot 10^{-5} \cdot i & 6.5858 \cdot 10^{-5} \cdot i & 5.722 \cdot 10^{-5} \cdot i \\ 0.0001 \cdot i & 0.0004 \cdot i & 0.0001 \cdot i & 8.0267 \cdot 10^{-5} \cdot i & 6.5071 \cdot 10^{-5} \cdot i \\ 8.1167 \cdot 10^{-5} \cdot i & 0.0001 \cdot i & 0.0004 \cdot i & 0.0001 \cdot i & 7.9575 \cdot 10^{-5} \cdot i \\ 6.5826 \cdot 10^{-5} \cdot i & 8.025 \cdot 10^{-5} \cdot i & 0.0001 \cdot i & 0.0004 \cdot i & 0.0001 \cdot i \end{pmatrix}$$

$$\left[ \begin{array}{ccc} 5.7208 \cdot 10^{-3} \cdot i & 6.5075 \cdot 10^{-3} \cdot i & 7.9588 \cdot 10^{-3} \cdot i \\ 0.0001 \cdot i & 0.0001 \cdot i & 0.0004 \cdot i \end{array} \right]$$

For presentation purposes, the reactance per 400 km is calculated

$$X' \cdot 4 \cdot 10^5 = \begin{pmatrix} 150.9201 \cdot i & 47.9479 \cdot i & 32.475 \cdot i & 26.3432 \cdot i & 22.8879 \cdot i \\ 47.9429 \cdot i & 149.0044 \cdot i & 46.1915 \cdot i & 32.107 \cdot i & 26.0282 \cdot i \\ 32.4669 \cdot i & 46.1886 \cdot i & 147.2277 \cdot i & 44.126 \cdot i & 31.8301 \cdot i \\ 26.3303 \cdot i & 32.1 \cdot i & 44.1224 \cdot i & 152.3806 \cdot i & 50.3784 \cdot i \\ 22.8833 \cdot i & 26.0298 \cdot i & 31.8352 \cdot i & 50.3887 \cdot i & 160.1852 \cdot i \end{pmatrix}$$

The ac line currents for 1000 MW are:

$$I = \frac{1000 \cdot 10^6}{\sqrt{3} \cdot 400 \cdot 10^3} \cdot \begin{pmatrix} \exp(i \cdot 0) \\ \exp\left(i \cdot \frac{2 \cdot \pi}{3}\right) \\ \exp\left(i \cdot \frac{4 \cdot \pi}{3}\right) \\ 0 \\ 0 \end{pmatrix} = \begin{pmatrix} 1443.3757 \\ -721.6878 + 1250 \cdot i \\ -721.6878 - 1250 \cdot i \\ 0 \\ 0 \end{pmatrix}$$

The corresponding voltages are:

$$V = X' \cdot I \cdot 400 \cdot 10^3 = \begin{pmatrix} -19341.2188 + 1.5979 \cdot 10^5 \cdot i \\ -1.2852 \cdot 10^5 - 71670.9325 \cdot i \\ 1.263 \cdot 10^5 - 92724.2531 \cdot i \\ 15027.9733 - 17004.3386 \cdot i \\ 7256.7857 - 8731.2731 \cdot i \end{pmatrix}$$

The common- and differential mode longitudinally induced voltages on the dc line due to the currents flowing in the ac line are:

$$C := \begin{pmatrix} .5 & .5 \\ 1 & -1 \end{pmatrix} \quad D := \begin{pmatrix} 1 & .5 \\ 1 & -.5 \end{pmatrix} \quad C \cdot D = \begin{pmatrix} 1 & 0 \\ 0 & 1 \end{pmatrix}$$

$$V_{pp} := \begin{pmatrix} V_4 \\ V_5 \end{pmatrix} = \begin{pmatrix} 15027.9733-17004.3386i \\ 7256.7857-8731.2731i \end{pmatrix}$$

$$V_{cm} := C \cdot V_{pp} = \begin{pmatrix} 11142.3795-12867.8058i \\ 7771.1875-8273.0656i \end{pmatrix}$$

From the differential mode voltage and the differential mode reactance calculated previously, the differential mode current disturbing the converters is calculated:

$$I_1 := \frac{V_{cm2}}{2 \cdot \pi \cdot 50 \cdot \left( 0.846 \cdot 10^{-6} \cdot 400 \cdot 10^3 + 4 \cdot 500 \cdot 10^{-3} \right)} = 10.5784 - 11.2615 \cdot i$$

$$|I_1| = 15.4507$$

$$CC := \begin{pmatrix} .5 & .5 \\ 1 & -1 \end{pmatrix}$$

$$\text{invert}(CC) = \begin{pmatrix} 1 & 0.5 \\ 1 & -0.5 \end{pmatrix}$$

Section 5.3  
 Effect of separation between ac and dc  
<http://en.smith.info/>

Conductor numbers are allocated as follows:  
 1,2,3 - ac line phase conductors A, B, C  
 4,5 - dc line pole conductors +, -  
 6,7,8 - shieldwires

$$\epsilon_0 := 8.85 \cdot 10^{-12}$$

Relative air density is:

$$\text{RAD} := 0.8$$

The pole and phase spacings are

$$\begin{array}{l}
 P_{dc} := 7 \\
 P_{ac} := 9.9 \\
 h_a := \begin{pmatrix} 19.2 \\ 19.2 \\ 19.2 \\ 18.4 \\ 18.4 \\ 24.2 \\ 24.2 \\ 29 \end{pmatrix} \\
 h_m := \begin{pmatrix} 8.1 \\ 8.1 \\ 8.1 \\ 7.2 \\ 7.2 \\ 15.3 \\ 15.3 \\ 20.1 \end{pmatrix}
 \end{array}$$

$$\begin{array}{l}
 X_{ac} := \begin{pmatrix} -P_{ac} \\ 0 \\ P_{ac} \\ -8.1 \\ 8.1 \end{pmatrix} \\
 X_{dc} := \begin{pmatrix} -P_{dc} \\ P_{dc} \\ 0 \end{pmatrix}
 \end{array}$$

The pole-conductor spacing is

$$x := 11.9$$

The centre-centre separation of the two line is 2.d [m]:

$$d := \frac{P_{ac} + x + P_{dc} + 1.2}{2} = 15$$

The line geometry consists of bundle coordinates (X [m], Y [m]):

$$\begin{aligned}
 \begin{pmatrix} -d+X_{ac1} \\ -d+X_{ac2} \\ -d+X_{ac3} \\ d+X_{dc1} \\ d+X_{dc2} \\ -d+X_{ac4} \\ -d+X_{ac5} \\ d+X_{dc3} \end{pmatrix} &= \begin{pmatrix} -24.9 \\ -15 \\ -5.1 \\ 8 \\ 22 \\ -23.1 \\ -6.9 \\ 15 \end{pmatrix} \\
 Y &:= \frac{h_a + 2 \cdot h_m}{3} = \begin{pmatrix} 11.8 \\ 11.8 \\ 11.8 \\ 10.9333 \\ 10.9333 \\ 18.2667 \\ 18.2667 \\ 23.0667 \end{pmatrix}
 \end{aligned}$$

Diameters of shield wires [cm], individual ac phase conductors [cm] and individual dc pole conductors [cm] are:

$$d_{ac} := 2.702 \quad d_{dc} := 3.417 \quad d_{sw} := 1.325$$

Bundle diameters [cm] are:

$$s_{ac} := 45 \quad s_{dc} := 45$$

$$n_{ac} := 3 \quad n_{dc} := 4$$

$$PCD_{ac} := \frac{s_{ac}}{\sin\left(\frac{\pi}{n_{ac}}\right)} = 51.9615 \quad PCD_{dc} := \frac{s_{dc}}{\sin\left(\frac{\pi}{n_{dc}}\right)} = 63.6396$$



P-matrix is calculated from the line geometry:

```
for p ∈ 1 .. 8
  for q ∈ 1 .. 8
    if (p = q)
```

$$P_{pp} := \text{eval} \left( \frac{1}{2 \cdot \pi \cdot \epsilon_0} \cdot \ln \left( \frac{2 \cdot Y_p \cdot 100}{\text{GMR}_p} \right) \right) \quad (\text{converting GMR and } y \text{ to same units})$$

else

$$P_{pq} := \text{eval} \left( \frac{1}{2 \cdot \pi \cdot \epsilon_0} \cdot \ln \left( \frac{\sqrt{\left( (Y_p + Y_q)^2 + (X_p - X_q)^2 \right)}}{\sqrt{\left( (Y_p - Y_q)^2 + (X_p - X_q)^2 \right)}} \right) \right)$$

$$P = \begin{pmatrix} 92.2264 & 17.0801 & 7.9492 & 3.5035 & 1.8945 & 26.9976 & 10.8892 & 4.4118 \\ 17.0801 & 92.2264 & 17.0801 & 6.1156 & 2.8749 & 19.7827 & 19.7827 & 6.4992 \\ 7.9492 & 17.0801 & 92.2264 & 12.4518 & 4.7817 & 10.8892 & 26.9976 & 10.0288 \\ 3.5035 & 6.1156 & 12.4518 & 82.9871 & 11.1079 & 5.1971 & 12.2299 & 16.3202 \\ 1.8945 & 2.8749 & 4.7817 & 11.1079 & 82.9871 & 2.9133 & 5.7649 & 16.3202 \\ 26.9976 & 19.7827 & 10.8892 & 5.1971 & 2.9133 & 154.9311 & 16.2386 & 6.8533 \\ 10.8892 & 19.7827 & 26.9976 & 12.2299 & 5.7649 & 16.2386 & 154.9311 & 13.2258 \\ 4.4118 & 6.4992 & 10.0288 & 16.3202 & 16.3202 & 6.8533 & 13.2258 & 159.1269 \end{pmatrix}$$

The inverted P-matrix will be used to calculate the Q-matrix and the maximum and average surface voltage gradients [kv/cm] from the impressed voltages [kV]:

```
P_inv := eval(invert(P))
```

$$P_{inv} = \begin{pmatrix} 11.747 & -1.636 & -0.367 & -0.128 & -0.065 & -1.766 & -0.346 & -0.111 \\ -1.636 & 11.901 & -1.592 & -0.314 & -0.104 & -1 & -0.979 & -0.173 \\ -0.367 & -1.592 & 11.924 & -1.284 & -0.252 & -0.332 & -1.672 & -0.366 \\ -0.128 & -0.314 & -1.284 & 12.749 & -1.374 & -0.143 & -0.581 & -1.015 \\ -0.065 & -0.104 & -0.252 & -1.374 & 12.486 & -0.078 & -0.192 & -1.098 \\ -1.766 & -1 & -0.332 & -0.143 & -0.078 & 6.967 & -0.395 & -0.134 \\ -0.346 & -0.979 & -1.672 & -0.581 & -0.192 & -0.395 & 7.018 & -0.332 \\ -0.111 & -0.173 & -0.366 & -1.015 & -1.098 & -0.134 & -0.332 & 6.568 \end{pmatrix}$$

Each element in the Q-matrix will have an ac component and a dc component. The ac component is determined by multiplying columns 1 to 3 of the P-matrix by the ac voltages. Since the frequencies are equal, each of these will resolve to a single sinusoidal voltage defined by an amplitude and phase.

Extract the columns 1 to 3 from the inverted P-matrix

```
for p ∈ 1..8
for q ∈ 1..3
Pac p q := Pinv p q
```

Convert the ac voltages into a sum of sine and cosine functions (with no phase shift), since orthogonal functions can be added termwise, which facilitates matrix multiplication

$$V_{ac} := \begin{pmatrix} \frac{400 \cdot \sqrt{2}}{\sqrt{3}} \cdot \cos\left(\frac{2 \cdot \pi}{3}\right) & \frac{400 \cdot \sqrt{2}}{\sqrt{3}} \cdot \sin\left(\frac{2 \cdot \pi}{3}\right) \\ \frac{400 \cdot \sqrt{2}}{\sqrt{3}} \cdot \cos(0) & \frac{400 \cdot \sqrt{2}}{\sqrt{3}} \cdot \sin(0) \\ \frac{400 \cdot \sqrt{2}}{\sqrt{3}} \cdot \cos\left(-\frac{2 \cdot \pi}{3}\right) & \frac{400 \cdot \sqrt{2}}{\sqrt{3}} \cdot \sin\left(-\frac{2 \cdot \pi}{3}\right) \end{pmatrix} = \begin{pmatrix} -163.2993 & 282.8427 \\ 326.5986 & 0 \\ -163.2993 & -282.8427 \end{pmatrix}$$

The sine and cosine coefficients for the ac component of the Q-matrix will be:

```
A := Pac · Vac
```

These can be converted into an amplitude and phase shift, and the amplitude is of interest in this case.

```
for p ∈ 1..8
Qac p := √(Ap 1² + Ap 2²)
```

$$\frac{Q_{ac}}{10^{-9}} = \begin{pmatrix} 4.1791 \\ 4.414 \\ 4.2285 \\ 0.3511 \\ 0.0558 \\ 0.4059 \\ 0.3752 \\ 0.0752 \end{pmatrix}$$

Similarly, the dc component is determined by multiplying columns 4 to 8 of the P-matrix by the dc voltages.

Extract the columns 4 to 8 from the inverted P-matrix

```
for p ∈ 1 .. 8
  for q ∈ 4 .. 8
    P_dc_p(q-3) := P_inv_p q
```

$$V_{dc} := \begin{pmatrix} -500 \\ 500 \\ 0 \\ 0 \\ 0 \end{pmatrix}$$

$$Q_{dc} := P_{dc} \cdot V_{dc}$$

$$\frac{Q_{dc}}{10^{-9}} = \begin{pmatrix} 0.0315 \\ 0.105 \\ 0.516 \\ -7.0615 \\ 6.93 \\ 0.0325 \\ 0.1945 \\ -0.0415 \end{pmatrix}$$

The minimum and maximum values of for the Q-matrix are calculated from the amplitude of the ac component and the dc component

```

for p ∈ 1..8
  if Q_dc < 0
    Q_max_p := eval(Q_dc - Q_ac_p)
  else
    Q_max_p := eval(Q_dc + Q_ac_p)
  end if
end for

for p ∈ 1..8
  if Q_dc < 0
    Q_min_p := eval(Q_dc + Q_ac_p)
  else
    Q_min_p := eval(Q_dc - Q_ac_p)
  end if
end for

```

$$\begin{matrix}
 Q_{\max} = \begin{pmatrix} 4.2106 \cdot 10^{-9} \\ 4.519 \cdot 10^{-9} \\ 4.7445 \cdot 10^{-9} \\ -7.4126 \cdot 10^{-9} \\ 6.9858 \cdot 10^{-9} \\ 4.3841 \cdot 10^{-10} \\ 5.6968 \cdot 10^{-10} \\ -1.1673 \cdot 10^{-10} \end{pmatrix} & Q_{\min} = \begin{pmatrix} -4.1476 \cdot 10^{-9} \\ -4.309 \cdot 10^{-9} \\ -3.7125 \cdot 10^{-9} \\ -6.7104 \cdot 10^{-9} \\ 6.8742 \cdot 10^{-9} \\ -3.7341 \cdot 10^{-10} \\ -1.8068 \cdot 10^{-10} \\ 3.373 \cdot 10^{-11} \end{pmatrix}
 \end{matrix}$$

For assessing performance, the maximum value of the Q-matrix is used

$$\text{E}_{\text{ave}_p} := \frac{Q_{\max_p}}{2 \cdot \pi \cdot \epsilon_0 \cdot n_p \cdot r_{\text{cond}_p}}$$

```

for p in 1..8
  if n == 1
    E_max_p := E_ave_p
  else

```

$$E_{\max_p} := E_{\text{ave}_p} \cdot \left( 1 + (n_p - 1) \cdot \frac{r_{\text{cond}_p}}{r_{\text{bundle}_p}} \right)$$

$$E_{\text{ave}} = \begin{pmatrix} 18.6828 \\ 20.0513 \\ 21.0518 \\ -19.5063 \\ 18.3831 \\ 11.9007 \\ 15.4639 \\ -3.1686 \end{pmatrix}$$

$$E_{\max} = \begin{pmatrix} 20.6258 \\ 22.1366 \\ 23.2412 \\ -22.6483 \\ 21.3442 \\ 11.9007 \\ 15.4639 \\ -3.1686 \end{pmatrix}$$

### Section 5.3

Calculation of conductor surface voltage gradients  
<http://en.smath.info/>

Conductor numbers are allocated as follows:

- 1, 2, 3 - ac line phase conductors A, B, C
- 4, 5 - dc line pole conductors +, -
- 6, 7, 8 - shieldwires

$$\epsilon_0 := 8.85 \cdot 10^{-12}$$

Relative air density is:

$$\text{RAD} := 0.8$$

The centre-centre separation of the two line is 2.d [m]:

$$d := 15$$

Attachment and midspan heights, and lateral positions of the conductors are:

$$\begin{array}{l}
 \begin{pmatrix} 19.2 \\ 19.2 \\ 19.2 \\ 18.4 \\ 18.4 \\ 24.2 \\ 24.2 \\ 29 \end{pmatrix} \quad \begin{pmatrix} 8.1 \\ 8.1 \\ 8.1 \\ 7.2 \\ 7.2 \\ 15.3 \\ 15.3 \\ 20.1 \end{pmatrix} \quad \begin{pmatrix} -9.9 \\ 0 \\ 9.9 \\ -8.1 \\ 8.1 \end{pmatrix} \quad \begin{pmatrix} -7 \\ 7 \\ 0 \end{pmatrix} \\
 h_a := \quad h_m := \quad X_{ac} := \quad X_{dc} :=
 \end{array}$$

The line geometry consists of bundle coordinates (X [m]; Y [m]):

$$\begin{array}{l}
 \begin{pmatrix} -d + X_{ac1} \\ -d + X_{ac2} \\ -d + X_{ac3} \\ d + X_{dc1} \\ d + X_{dc2} \\ -d + X_{ac4} \\ -d + X_{ac5} \\ d + X_{dc3} \end{pmatrix} = \begin{pmatrix} -24.9 \\ -15 \\ -5.1 \\ 8 \\ 22 \\ -23.1 \\ -6.9 \\ 15 \end{pmatrix} \\
 Y := \frac{h_a + 2 \cdot h_m}{3} = \begin{pmatrix} 11.8 \\ 11.8 \\ 11.8 \\ 10.9333 \\ 10.9333 \\ 18.2667 \\ 18.2667 \\ 23.0667 \end{pmatrix}
 \end{array}$$

Diameters of shield wires [cm], individual ac phase conductors [cm] and individual dc pole conductors [cm] are:

$$d_{ac} := 2.702 \quad d_{dc} := 3.417 \quad d_{sw} := 1.325$$

Bundle diameters [cm] are:

$$s_{ac} := 45 \quad s_{dc} := 45$$

$$n_{ac} := 3$$

$$n_{dc} := 4$$

$$PCD_{ac} := \frac{s_{ac}}{\sin\left(\frac{\pi}{n_{ac}}\right)} = 51.9615 \quad PCD_{dc} := \frac{s_{dc}}{\sin\left(\frac{\pi}{n_{dc}}\right)} = 63.6396$$

Bundle configurations are (n; conductor radius [cm]; bundle radius [cm]; voltage [kV]):

$$n := \begin{pmatrix} n_{ac} \\ n_{ac} \\ n_{ac} \\ n_{dc} \\ n_{dc} \\ 1 \\ 1 \\ 1 \end{pmatrix} \quad r_{cond} := \begin{pmatrix} \frac{d_{ac}}{2} \\ \frac{d_{ac}}{2} \\ \frac{d_{ac}}{2} \\ \frac{d_{dc}}{2} \\ \frac{d_{dc}}{2} \\ \frac{d_{dc}}{2} \\ \frac{d_{sw}}{2} \\ \frac{d_{sw}}{2} \\ \frac{d_{sw}}{2} \end{pmatrix} = \begin{pmatrix} 1.351 \\ 1.351 \\ 1.351 \\ 1.7085 \\ 1.7085 \\ 0.6625 \\ 0.6625 \\ 0.6625 \end{pmatrix}$$

$$r_{bundle} := \begin{pmatrix} \frac{PCD_{ac}}{2} \\ PCD_{ac} \\ \frac{PCD_{ac}}{2} \\ \frac{PCD_{ac}}{2} \\ PCD_{dc} \\ \frac{PCD_{dc}}{2} \\ PCD_{dc} \\ \frac{PCD_{dc}}{2} \\ 0 \\ 0 \\ 0 \end{pmatrix} = \begin{pmatrix} 25.9808 \\ 25.9808 \\ 25.9808 \\ 31.8198 \\ 31.8198 \\ 0 \\ 0 \\ 0 \end{pmatrix}$$

Geometric mean radius [cm] for each bundle is calculated from the bundle configurations:

$$\text{for } p \in 1 \dots 8$$

$$\text{GMR}_p := \text{if} \left( n_p = 1 \right)$$

$$\quad \text{eval} \left( r_{\text{cond}_p} \right)$$

$$\quad \text{else}$$

$$\quad \text{eval} \left[ r_{\text{bundle}_p} \cdot \left( \frac{n_p \cdot r_{\text{cond}_p}}{r_{\text{bundle}_p}} \right) \left( \frac{1}{n_p} \right) \right]$$

$$\text{GMR} = \begin{pmatrix} 13.986 \\ 13.986 \\ 13.986 \\ 21.6617 \\ 21.6617 \\ 0.6625 \\ 0.6625 \\ 0.6625 \end{pmatrix}$$

P-matrix is calculated from the line geometry:

$$\text{for } p \in 1 \dots 8$$

$$\quad \text{for } q \in 1 \dots 8$$

$$\quad \quad \text{if} (p = q)$$

$$\quad \quad \quad P_{p,q} := \text{eval} \left[ \frac{1}{2 \cdot \pi \cdot \epsilon_0} \cdot \ln \left( \frac{2 \cdot Y_p \cdot 100}{\text{GMR}_p} \right) \right] \quad (\text{converting GMR and } y \text{ to same units})$$

$$\quad \quad \quad \text{else}$$

$$\quad \quad \quad P_{p,q} := \text{eval} \left[ \frac{1}{2 \cdot \pi \cdot \epsilon_0} \cdot \ln \left( \frac{\sqrt{\left( (y_p + y_q)^2 + (x_p - x_q)^2 \right)}}{\sqrt{\left( (y_p - y_q)^2 + (x_p - x_q)^2 \right)}} \right) \right]$$

$$\frac{P}{10} = \begin{pmatrix} 92.2264 & 17.0801 & 7.9492 & 3.5035 & 1.8945 & 26.9976 & 10.8892 & 4.4118 \\ 17.0801 & 92.2264 & 17.0801 & 6.1156 & 2.8749 & 19.7827 & 19.7827 & 6.4992 \\ 7.9492 & 17.0801 & 92.2264 & 12.4518 & 4.7817 & 10.8892 & 26.9976 & 10.0288 \\ 3.5035 & 6.1156 & 12.4518 & 82.987 & 11.1079 & 5.1971 & 12.2299 & 16.3202 \\ 1.8945 & 2.8749 & 4.7817 & 11.1079 & 82.987 & 2.9133 & 5.7649 & 16.3202 \\ 26.9976 & 19.7827 & 10.8892 & 5.1971 & 2.9133 & 154.9311 & 16.2386 & 6.8533 \\ 10.8892 & 19.7827 & 26.9976 & 12.2299 & 5.7649 & 16.2386 & 154.9311 & 13.2258 \\ 4.4118 & 6.4992 & 10.0288 & 16.3202 & 16.3202 & 6.8533 & 13.2258 & 159.1269 \end{pmatrix}$$

The inverted P-matrix will be used to calculate the Q-matrix and the maximum and average surface voltage gradients [kv/cm] from the impressed voltages [kV]:

```
P_inv:=eval(invert(P))
```

$$\frac{P_{inv}}{10^{-12}} = \begin{pmatrix} 11.747 & -1.636 & -0.367 & -0.128 & -0.065 & -1.766 & -0.346 & -0.111 \\ -1.636 & 11.901 & -1.592 & -0.314 & -0.104 & -1 & -0.979 & -0.173 \\ -0.367 & -1.592 & 11.924 & -1.284 & -0.252 & -0.332 & -1.672 & -0.366 \\ -0.128 & -0.314 & -1.284 & 12.749 & -1.374 & -0.143 & -0.581 & -1.015 \\ -0.065 & -0.104 & -0.252 & -1.374 & 12.486 & -0.078 & -0.192 & -1.098 \\ -1.766 & -1 & -0.332 & -0.143 & -0.078 & 6.967 & -0.395 & -0.134 \\ -0.346 & -0.979 & -1.672 & -0.581 & -0.192 & -0.395 & 7.018 & -0.332 \\ -0.111 & -0.173 & -0.366 & -1.015 & -1.098 & -0.134 & -0.332 & 6.568 \end{pmatrix}$$

Each element in the Q-matrix will have an ac component and a dc component. The ac component is determined by multiplying columns 1 to 3 of the P-matrix by the ac voltages. Since the frequencies are equal, each of these will resolve to a single sinusoidal voltage defined by an amplitude and phase.

Extract the columns 1 to 3 from the inverted P-matrix

```
for p in 1..3
for q in 1..3
P_ac_p_q:=P_inv_p_q
```

Convert the ac voltages into a sum of sine and cosine functions (with no phase shift), since orthogonal functions can be added termwise, which facilitates matrix multiplication

$$V_{ac} := 1000 \cdot \frac{400}{\sqrt{3}} \cdot \begin{pmatrix} \cos\left(\frac{2\cdot\pi}{3}\right) & \sin\left(\frac{2\cdot\pi}{3}\right) \\ \cos(0) & \sin(0) \\ \cos\left(\frac{-2\cdot\pi}{3}\right) & \sin\left(\frac{-2\cdot\pi}{3}\right) \end{pmatrix} \begin{pmatrix} -1.1547\cdot 10^5 & 2\cdot 10^5 \\ 2.3094\cdot 10^5 & 0 \\ -1.1547\cdot 10^5 & -2\cdot 10^5 \end{pmatrix}$$

The sine and cosine coefficients for the ac component of the Q-matrix will be:

$$A := P_{ac} \cdot V_{ac}$$

These can be converted into an amplitude and phase shift, and the amplitude is of interest in this case.

for  $p \in 1 \dots 8$

$$Q_{ac,p} := \sqrt{(A_{p1})^2 + (A_{p2})^2}$$

$$\frac{Q_{ac}}{10^{-6}} = \begin{pmatrix} 2.9551 \\ 3.1212 \\ 2.99 \\ 0.2483 \\ 0.0395 \\ 0.287 \\ 0.2653 \\ 0.0532 \end{pmatrix}$$

$$\frac{A}{10^{-6}} = \begin{pmatrix} -1.6919 & 2.4228 \\ 3.1212 & -0.0088 \\ -1.7021 & -2.4582 \\ 0.0905 & 0.2312 \\ 0.0126 & 0.0374 \\ 0.0113 & -0.2868 \\ 0.0069 & 0.2652 \\ 0.0151 & 0.051 \end{pmatrix}$$

Similarly, the dc component is determined by multiplying columns 6 to 7 of the P-matrix by the dc voltages.

Extract the columns 6 to 7 from the inverted P-matrix

for  $p \in 1 \dots 8$

for  $q \in 4 \dots 5$

$$P_{dc,p} := P_{inv,p,q}$$

$$V_{dc} := 1000 \cdot \begin{pmatrix} 500 \\ -500 \end{pmatrix}$$

$$P_{dc} = \begin{pmatrix} -1.28 \cdot 10^{-13} & -6.5 \cdot 10^{-14} \\ -3.14 \cdot 10^{-13} & -1.04 \cdot 10^{-13} \\ -1.284 \cdot 10^{-12} & -2.52 \cdot 10^{-13} \\ 1.2749 \cdot 10^{-11} & -1.374 \cdot 10^{-12} \\ -1.374 \cdot 10^{-12} & 1.2486 \cdot 10^{-11} \\ -1.43 \cdot 10^{-13} & -7.8 \cdot 10^{-14} \\ -5.81 \cdot 10^{-13} & -1.92 \cdot 10^{-13} \\ -1.015 \cdot 10^{-12} & -1.098 \cdot 10^{-12} \end{pmatrix}$$

$$Q_{dc} := P_{dc} \cdot V_{dc}$$

$$\begin{pmatrix} -0.0315 \\ -0.105 \\ -0.516 \end{pmatrix}$$

$$\frac{Q_{dc}}{10^{-6}} = \begin{pmatrix} 7.0615 \\ -6.93 \\ -0.0325 \\ -0.1945 \\ 0.0415 \end{pmatrix}$$

The minimum and maximum values of for the Q-matrix are calculated from the amplitude of the ac component and the dc component

for  $p \in 1 \dots 8$

if  $Q_{dc,p} < 0$

$Q_{max,p} := \text{eval} \left( Q_{dc,p} - \sqrt{2} \cdot Q_{ac,p} \right)$

else

$Q_{max,p} := \text{eval} \left( Q_{dc,p} + \sqrt{2} \cdot Q_{ac,p} \right)$

for  $p \in 1 \dots 8$

if  $Q_{dc,p} < 0$

$Q_{min,p} := \text{eval} \left( Q_{dc,p} + \sqrt{2} \cdot Q_{ac,p} \right)$

else

$Q_{min,p} := \text{eval} \left( Q_{dc,p} - \sqrt{2} \cdot Q_{ac,p} \right)$

$Q_{max} = \begin{pmatrix} -4.2106 \cdot 10^{-6} \\ -4.519 \cdot 10^{-6} \\ -4.7445 \cdot 10^{-6} \\ 7.4126 \cdot 10^{-6} \\ -6.9858 \cdot 10^{-6} \\ -4.3841 \cdot 10^{-7} \\ -5.6968 \cdot 10^{-7} \\ 1.1673 \cdot 10^{-7} \end{pmatrix}$

$Q_{min} = \begin{pmatrix} 4.1476 \cdot 10^{-6} \\ 4.309 \cdot 10^{-6} \\ 3.7125 \cdot 10^{-6} \\ 6.7104 \cdot 10^{-6} \\ -6.8742 \cdot 10^{-6} \\ 3.7341 \cdot 10^{-7} \\ 1.8068 \cdot 10^{-7} \\ -3.373 \cdot 10^{-8} \end{pmatrix}$

For assessing performance, the maximum value of the Q-matrix is used

$$\begin{aligned}
 &\text{for } p \in 1 \dots 8 \\
 &E_{\text{ave } p} := \frac{Q_{\text{max } p}}{2 \cdot \pi \cdot \varepsilon_0 \cdot \binom{n}{p} \cdot r_{\text{cond } p}} \\
 &\text{for } p \in 1 \dots 8 \\
 &\text{if } n_p = 1 \\
 &E_{\text{max } p} := E_{\text{ave } p} \\
 &\text{else} \\
 &E_{\text{max } p} := E_{\text{ave } p} \cdot \left( 1 + \binom{n-p-1}{r_{\text{bundle } p}} \cdot \frac{r_{\text{cond } p}}{r_{\text{bundle } p}} \right) \\
 &E_{\text{ave}} = \begin{pmatrix} -18682.8302 \\ -20051.2943 \\ -21051.8037 \\ 19506.2894 \\ -18383.0864 \\ -11900.7259 \\ -15463.9333 \\ 3168.6574 \end{pmatrix} \quad E_{\text{max}} = \begin{pmatrix} -20625.8451 \\ -22136.6295 \\ -23241.1919 \\ 22648.3415 \\ -21344.2142 \\ -11900.7259 \\ -15463.9333 \\ 3168.6574 \end{pmatrix}
 \end{aligned}$$

The ac components are also calculated separately for use in subsequent audible noise assessments

$$\text{for } p \in 1 \dots 8 \quad E_{\text{ave } p} := \frac{Q_{\text{ac } p}}{2 \cdot \pi \cdot \varepsilon_0 \cdot \binom{n}{p} \cdot r_{\text{cond } p}}$$

```

for p ∈ 1..8
  if n_p = 1
    E_max_p := E_ave_p
  else
    E_max_p := E_ave_p · (1 + (n_p - 1) · (r_cond_p / r_bundle_p))
  end if
end for

E_ave = (
  13111.9244
  13848.9675
  13266.9175
  653.3778
  103.8414
  7791.2639
  7201.3289
  1444.0089
)
E_max = (
  14475.5649
  15289.2606
  14646.6773
  758.6232
  120.568
  7791.2639
  7201.3289
  1444.0089
)

```

The dc components are also calculated separately for use in subsequent audible noise assessments

```

for p ∈ 1..8
  E_ave_p := (Q_dc_p / (2 · π · ε_0 · n_p · r_cond_p))
  if n_p = 1
    E_max_p := E_ave_p
  else
    E_max_p := E_ave_p · (1 + (n_p - 1) · (r_cond_p / r_bundle_p))
  end if
end for

r_cond = (
  1.351
  1.351
  1.351
  1.7085
  1.7085
  0.6625
  0.6625
  0.6625
)

```

$$E_{\text{ave}} = \begin{pmatrix} -139.769 \\ -465.8966 \\ -2289.5491 \\ 18582.2736 \\ -18236.2325 \\ -882.2148 \\ -5279.7163 \\ 1126.5204 \end{pmatrix}$$

$$E_{\text{max}} = \begin{pmatrix} -154.305 \\ -514.3499 \\ -2527.6623 \\ 21575.4862 \\ -21173.7052 \\ -882.2148 \\ -5279.7163 \\ 1126.5204 \end{pmatrix}$$

Section 5.4  
 Calculation of audible noise for hybrid line  
<http://en.smath.info/>

The observer position is on the ground, at various distances from the centre-line of either the ac or the dc line

$$X_{\text{obs}} := 0 \qquad Y_{\text{obs}} := 1$$

Define a function for the audible noise from an ac line

$$P_{\text{ac}}(n, d, E, D, R) := \text{if } n < 3 \quad 55 \cdot \log_{10}(d) + 120 \cdot \log_{10}(E) + \frac{1800}{300} - 115.4 - 11.4 \cdot \log_{10}(R)$$

$$\text{else} \quad 26.4 \cdot \log_{10}(n) + 55 \cdot \log_{10}(d) + 120 \cdot \log_{10}(E) + \frac{1800}{300} - 128.4 - 11.4 \cdot \log_{10}(R)$$

From the line configuration, the relative positions of the phase conductors, and the radial distance to the observer position is calculated

$$X_{\text{ac}} := \begin{pmatrix} -15-9.9 \\ 15 \\ 15-9.9 \end{pmatrix} = \begin{pmatrix} -24.9 \\ 15 \\ 5.1 \end{pmatrix} \qquad Y_{\text{ac}} := \begin{pmatrix} 11.8 \\ 11.8 \\ 11.8 \end{pmatrix}$$

$$R_{\text{a}} := \sqrt{\left( X_{\text{ac}1} - X_{\text{obs}} \right)^2 + \left( Y_{\text{ac}1} - Y_{\text{obs}} \right)^2} = 27.1413$$

$$R_{\text{b}} := \sqrt{\left( X_{\text{ac}2} - X_{\text{obs}} \right)^2 + \left( Y_{\text{ac}2} - Y_{\text{obs}} \right)^2} = 18.4835$$

$$R_{\text{c}} := \sqrt{\left( X_{\text{ac}3} - X_{\text{obs}} \right)^2 + \left( Y_{\text{ac}3} - Y_{\text{obs}} \right)^2} = 11.9436$$

From the surface voltage gradients on the phase conductors and the bundle parameters, calculate the sound power from each phase conductor

$$E_a := 14.5 \quad E_b := 15.3 \quad E_c := 14.7$$

$$n_{ac} := 4 \quad d_{ac} := 2.703 \quad s_{ac} := 45$$

$$D_{ac} := \frac{s_{ac}}{\sin\left(\frac{\pi}{n_{ac}}\right)} = 63.6396$$

$$d_a := P_{ac}(n_{ac}, d_{ac}, E_a, D_{ac}, R_a) = 40.2667$$

$$d_b := P_{ac}(n_{ac}, d_{ac}, E_b, D_{ac}, R_b) = 44.9675$$

$$d_c := P_{ac}(n_{ac}, d_{ac}, E_c, D_{ac}, R_c) = 45.0446$$

Combine the effect of the conductors, and apply corrections to calculate the audible noise levels in rainy conditions and fair weather

Audible noise in rainy conditions

$$\text{Rain}_{ac} := 10 \cdot \log_{10}\left(10 + 10 \frac{d_a}{10} + 10 \frac{d_b}{10} + 10 \frac{d_c}{10}\right) + 3.5 = 52.1906 \quad \text{This is L5-ac-rain}$$

Audible noise in fair weather

$$\text{Fair}_{ac} := \text{Rain}_{ac} - 28.5 = 23.6906$$

This is L50-ac-fair

Define a function for the audible noise from a dc line

$$P_{dc}(n, d, E, D, R) := \text{if } n < 3 \quad \begin{aligned} & 40 \cdot \log_{10}(d) + 86 \cdot \log_{10}(E) + \frac{1800}{300} - 93.4 - 11.4 \cdot \log_{10}(R) \\ & \text{else} \\ & 25.6 \cdot \log_{10}(n) + 40 \cdot \log_{10}(d) + 86 \cdot \log_{10}(E) + \frac{1800}{300} - 100.62 - 11.4 \cdot \log_{10}(R) \end{aligned}$$

From the line configuration, the relative positions of the pole conductors, and the radial distance to the observer position is calculated

$$X_{dc} := \begin{pmatrix} 15-7 \\ 15+7 \end{pmatrix} = \begin{pmatrix} 8 \\ 22 \end{pmatrix} \quad Y_{dc} := \begin{pmatrix} 10.9 \\ 10.9 \end{pmatrix}$$

$$R_p := \sqrt{\left( X_{dc_1} - X_{obs} \right)^2 + \left( Y_{dc_1} - Y_{obs} \right)^2} = 12.7283$$

$$R_n := \sqrt{\left( X_{dc_2} - X_{obs} \right)^2 + \left( Y_{dc_2} - Y_{obs} \right)^2} = 24.1249$$

From the surface voltage gradients on the positive pole and the bundle parameters, calculate the sound power for the dc line under fair weather and rainy conditions

$$E_p := 21.2 \quad E_n := -21.6$$

$$n_{dc} := 4 \quad d_{dc} := 3.417 \quad s_{dc} := 45$$

$$D_{dc} := \frac{s_{dc}}{\sin\left(\frac{\pi}{n_{dc}}\right)} = 63.6396$$

Audible noise in rain condition

$$\text{Rain}_{dc} := P_{dc} \left( n_{dc} d_{dc}' E_p' E_{dc}' R_p \right) - 6 = 37.609$$

This is L50-rain-dc

Audible noise in fair weather

$$\text{Fair}_{dc} := P_{dc} \left( n_{dc} d_{dc}' E_p' D_{dc}' R_p \right) + 3.5 = 47.109$$

This is L5-fair-dc

Combine ac and dc to estimate the audible noise from the hybrid ac/dc line in rainy conditions and fair weather

$$\text{Rain} = 10 \cdot \log_{10} \left( 10 \frac{\text{Rain}_{ac}}{10} + 10 \frac{\text{Rain}_{dc}}{10} \right) = 52.3392$$

$$\text{Fair} = 10 \cdot \log_{10} \left( 10 \frac{\text{Fair}_{ac}}{10} + 10 \frac{\text{Fair}_{dc}}{10} \right) = 47.1288$$

Section 5.5  
 Calculation of audible noise for hybrid line  
<http://en.smath.info/>

The observer position is on the ground, at various distances from the centre-line of either the ac or the dc line

$$X_{\text{obs}} := 45 \quad Y_{\text{obs}} := 0$$

Define functions for the radio interference from ac and dc conductor bundles

$$RI_{\text{ac}}(E, d, f, H, R) := 48 + 120 \cdot \log_{10} \left( \frac{E}{17.56} \right) + 40 \cdot \log_{10} \left( \frac{d}{3.51} \right) + 10 \cdot \left( 1 - (\log_{10}(10 \cdot f))^2 \right) + \frac{H}{300} + 40 \cdot \log_{10} \left( \frac{19.9}{R} \right)$$

$$RI_{\text{dc}}(E, d, f, H, R) := 60.5 + 86 \cdot \log_{10} \left( \frac{E}{27.5} \right) + 40 \cdot \log_{10} \left( \frac{d}{4.62} \right) + 10 \cdot \left( 1 - (\log_{10}(10 \cdot f))^2 \right) + \frac{H}{300} + 40 \cdot \log_{10} \left( \frac{19.9}{R} \right)$$

From the line configuration, the relative positions of the phase conductors, and the radial distance to the observer position is calculated

$$X_{\text{ac}} := \begin{pmatrix} -15 - 9.9 \\ 15 \\ 15 - 9.9 \end{pmatrix} = \begin{pmatrix} -24.9 \\ 15 \\ 5.1 \end{pmatrix} \quad Y_{\text{ac}} := \begin{pmatrix} 11.8 \\ 11.8 \\ 11.8 \end{pmatrix}$$

$$R_{\text{a}} := \sqrt{\left( X_{\text{ac}1} - X_{\text{obs}} \right)^2 + \left( Y_{\text{ac}1} - Y_{\text{obs}} \right)^2} = 70.889$$

$$R_{\text{b}} := \sqrt{\left( X_{\text{ac}2} - X_{\text{obs}} \right)^2 + \left( Y_{\text{ac}2} - Y_{\text{obs}} \right)^2} = 32.2372$$

$$R_{\text{c}} := \sqrt{\left( X_{\text{ac}3} - X_{\text{obs}} \right)^2 + \left( Y_{\text{ac}3} - Y_{\text{obs}} \right)^2} = 41.6083$$

From the surface voltage gradients on the phase conductors and the bundle parameters, calculate the radio interference from each phase conductor

$$E_a := 20.5 \quad E_b := 21.6 \quad E_c := 23.3 \quad f := 0.5$$

$$n := 3 \quad d := 2.703 \quad s := 45 \quad D := \frac{s}{\sin\left(\frac{\pi}{n}\right)} = 51.9615$$

$$RI_1 := RI_{ac}(E_a, d, f, 1800, R_a) = (40.5745)$$

$$RI_2 := RI_{ac}(E_b, d, f, 1800, R_b) = \begin{pmatrix} 40.5745 \\ 56.9873 \end{pmatrix}$$

$$RI_3 := RI_{ac}(E_c, d, f, 1800, R_c) = \begin{pmatrix} 40.5745 \\ 56.9873 \\ 56.5027 \end{pmatrix}$$

From the line configuration, the relative positions of the pole conductors, and the radial distance to the observer position is calculated

$$X_{dc} := \begin{pmatrix} 15+7 \\ 15-7 \end{pmatrix} = \begin{pmatrix} 22 \\ 8 \end{pmatrix} \quad Y_{dc} := \begin{pmatrix} 10.9 \\ 10.9 \end{pmatrix}$$

$$R_p := \sqrt{\left(X_{dc} - X_{obs}\right)^2 + \left(Y_{dc} - Y_{obs}\right)^2} = 25.4521$$

From the surface voltage gradients on the positive pole and the bundle parameters, calculate the sound power for the dc line under fair weather and rainy conditions

$$E_p := 25.8$$

Radio interference in fair conditions

$$RI_p := RI_{dc}(E_p, d, f, 1800, R_p) = 55.6444$$

$$Fair_{dc} := RI_p = 55.6444$$

$$Rain_{dc} := RI_p - 3 = 52.6444$$

Fair<sub>ac</sub> := max(RI) - 25 = 31.9873

Rain<sub>ac</sub> := max(RI) = 56.9873

Rain := Rain<sub>ac</sub> = 56.9873

Fair := Fair<sub>dc</sub> = 55.6444

Section 5.6  
 Comparison of full system to bipole only  
<http://en.smash.info/>

Conductor numbers are allocated as follows:

- 1,2,3 - ac line phase conductors A, B, C
- 4,5 - dc line pole conductors +, -
- 6,7,8 - shieldwires

$$\epsilon_0 := 8.85 \cdot 10^{-12}$$

Relative air density is:

$$\text{RAD} := 0.8$$

The centre-centre separation of the two line is 2.d [m]:

$$d := 15$$

Attachment and midspan heights, and lateral positions of the conductors are:

$$h_a := \begin{pmatrix} 19.2 \\ 19.2 \\ 19.2 \\ 18.4 \\ 18.4 \\ 24.2 \\ 24.2 \\ 29 \end{pmatrix} \quad \begin{pmatrix} 8.1 \\ 8.1 \\ 8.1 \\ 7.2 \\ 7.2 \\ 15.3 \\ 15.3 \\ 20.1 \end{pmatrix} \quad X_{ac} := \begin{pmatrix} -9.9 \\ 0 \\ 9.9 \\ -8.1 \\ 8.1 \end{pmatrix} \quad X_{dc} := \begin{pmatrix} -7 \\ 7 \\ 0 \end{pmatrix}$$

The line geometry consists of bundle coordinates (X [m]; Y [m]):

$$X := \begin{pmatrix} -d + X_{ac1} \\ -d + X_{ac2} \\ -d + X_{ac3} \\ d + X_{dc1} \\ d + X_{dc2} \\ -d + X_{ac4} \\ -d + X_{ac5} \\ d + X_{dc3} \end{pmatrix} = \begin{pmatrix} -24.9 \\ -15 \\ -5.1 \\ 8 \\ 22 \\ -23.1 \\ -6.9 \\ 15 \end{pmatrix} \quad Y := \frac{h_a + 2 \cdot h_m}{3} = \begin{pmatrix} 11.8 \\ 11.8 \\ 11.8 \\ 10.9333 \\ 10.9333 \\ 18.2667 \\ 18.2667 \\ 23.0667 \end{pmatrix}$$

Diameters of shield wires [cm], individual ac phase conductors [cm] and individual dc pole conductors [cm] are:

$$d_{ac} := 2.702 \quad d_{dc} := 3.417 \quad d_{sw} := 1.325$$

Bundle diameters [cm] are:

$$s_{ac} := 45 \quad s_{dc} := 45$$

$$n_{ac} := 3$$

$$n_{dc} := 4$$

$$PCD_{ac} := \frac{s_{ac}}{\sin\left(\frac{\pi}{n_{ac}}\right)} = 51.9615 \quad PCD_{dc} := \frac{s_{dc}}{\sin\left(\frac{\pi}{n_{dc}}\right)} = 63.6396$$

Bundle configurations are (n; conductor radius [cm]; bundle radius [cm]; voltage [kV]):

$$n := \begin{pmatrix} n_{ac} \\ n_{ac} \\ n_{ac} \\ n_{dc} \\ n_{dc} \\ 1 \\ 1 \\ 1 \end{pmatrix} \quad r_{cond} := \begin{pmatrix} \frac{d_{ac}}{2} \\ \frac{d_{ac}}{2} \\ \frac{d_{ac}}{2} \\ \frac{d_{dc}}{2} \\ \frac{d_{dc}}{2} \\ \frac{d_{sw}}{2} \\ \frac{d_{sw}}{2} \\ \frac{d_{sw}}{2} \end{pmatrix} = \begin{pmatrix} 1.351 \\ 1.351 \\ 1.351 \\ 1.7085 \\ 1.7085 \\ 0.6625 \\ 0.6625 \\ 0.6625 \end{pmatrix}$$

$$r_{bundle} := \begin{pmatrix} \frac{PCD_{ac}}{2} \\ \frac{PCD_{ac}}{2} \\ \frac{PCD_{ac}}{2} \\ \frac{PCD_{dc}}{2} \\ \frac{PCD_{dc}}{2} \\ 0 \\ 0 \\ 0 \end{pmatrix} = \begin{pmatrix} 25.9808 \\ 25.9808 \\ 25.9808 \\ 31.8198 \\ 31.8198 \\ 0 \\ 0 \\ 0 \end{pmatrix}$$

Geometric mean radius [cm] for each bundle is calculated from the bundle configurations:

$$\begin{aligned}
 &\text{for } p \in 1 \dots 8 \\
 &\quad \text{GMR}_p := \text{if} \left( n_p = 1 \right) \\
 &\quad \quad \text{eval} \left( r_{\text{cond}_p} \right) \\
 &\quad \text{else} \\
 &\quad \quad \text{eval} \left[ r_{\text{bundle}_p} \cdot \left( \frac{n_p \cdot r_{\text{cond}_p}}{r_{\text{bundle}_p}} \right) \left( \frac{1}{n_p} \right) \right]
 \end{aligned}$$

$$\text{GMR} = \begin{pmatrix} 13.986 \\ 13.986 \\ 13.986 \\ 21.6617 \\ 21.6617 \\ 0.6625 \\ 0.6625 \\ 0.6625 \end{pmatrix}$$

P-matrix is calculated from the line geometry:

for  $p \in 1 \dots 8$   
 for  $q \in 1 \dots 8$   
 if ( $p = q$ )

$$P_{p,q} := \text{eval} \left[ \frac{1}{2 \cdot \pi \cdot \epsilon_0} \cdot \ln \left( \frac{2 \cdot Y_p \cdot 100}{\text{GMR}_p} \right) \right] \quad (\text{converting GMR and } y \text{ to same units})$$

else

$$P_{p,q} := \text{eval} \left[ \frac{1}{2 \cdot \pi \cdot \epsilon_0} \cdot \ln \left( \frac{\sqrt{\left( (y_p + y_q)^2 + (x_p - x_q)^2 \right)}}{\sqrt{\left( (y_p - y_q)^2 + (x_p - x_q)^2 \right)}} \right) \right]$$

$$\frac{P}{10} = \begin{pmatrix} 92.2264 & 17.0801 & 7.9492 & 3.5035 & 1.8945 & 26.9976 & 10.8892 & 4.4118 \\ 17.0801 & 92.2264 & 17.0801 & 6.1156 & 2.8749 & 19.7827 & 19.7827 & 6.4992 \\ 7.9492 & 17.0801 & 92.2264 & 12.4518 & 4.7817 & 10.8892 & 26.9976 & 10.0288 \\ 3.5035 & 6.1156 & 12.4518 & 82.987 & 11.1079 & 5.1971 & 12.2299 & 16.3202 \\ 1.8945 & 2.8749 & 4.7817 & 11.1079 & 82.987 & 2.9133 & 5.7649 & 16.3202 \\ 26.9976 & 19.7827 & 10.8892 & 5.1971 & 2.9133 & 154.9311 & 16.2386 & 6.8533 \\ 10.8892 & 19.7827 & 26.9976 & 12.2299 & 5.7649 & 16.2386 & 154.9311 & 13.2258 \\ 4.4118 & 6.4992 & 10.0288 & 16.3202 & 16.3202 & 6.8533 & 13.2258 & 159.1269 \end{pmatrix}$$

The inverted P-matrix will be used to calculate the Q-matrix and the maximum and average surface voltage gradients [kv/cm] from the impressed voltages [kV]:

$$P_{inv} := \text{eval}(\text{invert}(P))$$

$$\frac{P_{inv}}{10^{-12}} = \begin{pmatrix} 11.747 & -1.636 & -0.367 & -0.128 & -0.065 & -1.766 & -0.346 & -0.111 \\ -1.636 & 11.901 & -1.592 & -0.314 & -0.104 & -1 & -0.979 & -0.173 \\ -0.367 & -1.592 & 11.924 & -1.284 & -0.252 & -0.332 & -1.672 & -0.366 \\ -0.128 & -0.314 & -1.284 & 12.749 & -1.374 & -0.143 & -0.581 & -1.015 \\ -0.065 & -0.104 & -0.252 & -1.374 & 12.486 & -0.078 & -0.192 & -1.098 \\ -1.766 & -1 & -0.332 & -0.143 & -0.078 & 6.967 & -0.395 & -0.134 \\ -0.346 & -0.979 & -1.672 & -0.581 & -0.192 & -0.395 & 7.018 & -0.332 \\ -0.111 & -0.173 & -0.366 & -1.015 & -1.098 & -0.134 & -0.332 & 6.568 \end{pmatrix}$$

The dc voltages only are used, since the ac phase conductors are taken to be grounded

$$V := 10^3 \cdot \begin{pmatrix} 0 \\ 0 \\ 0 \\ 500 \\ -500 \\ 0 \\ 0 \\ 0 \end{pmatrix}$$

$$Q := P_{inv} \cdot V = \begin{pmatrix} -3.15 \cdot 10^{-8} \\ -1.05 \cdot 10^{-7} \\ -5.16 \cdot 10^{-7} \\ 7.0615 \cdot 10^{-6} \\ -6.93 \cdot 10^{-6} \\ -3.25 \cdot 10^{-8} \\ -1.945 \cdot 10^{-7} \\ 4.15 \cdot 10^{-8} \end{pmatrix}$$

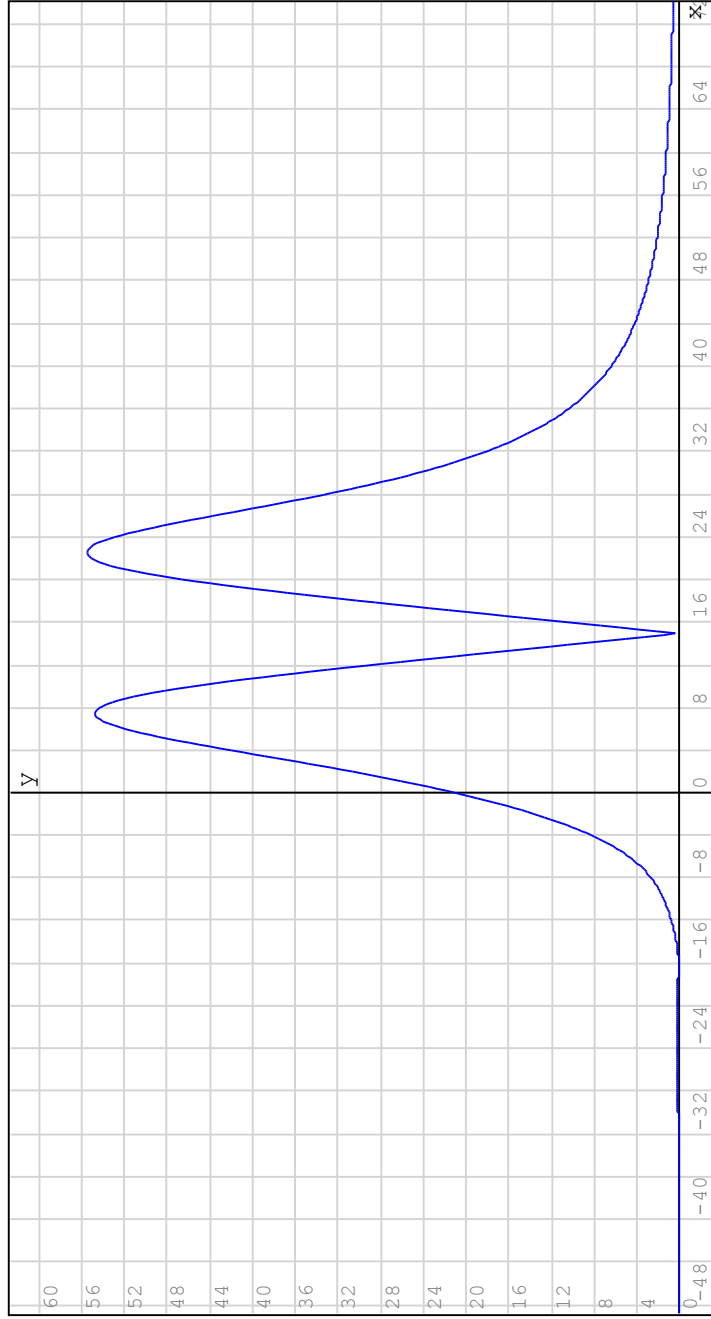
$$h := 0$$

$$H := h_m = \begin{pmatrix} 8.1 \\ 8.1 \\ 8.1 \\ 7.2 \\ 7.2 \\ 15.3 \\ 15.3 \\ 20.1 \end{pmatrix}$$

$$S(s) := \begin{pmatrix} \frac{s-X_1}{(s-X_1)^2 + (H_1-h)^2} + i \cdot \frac{s-X_1}{(s-X_1)^2 + (H_1+h)^2} & \frac{h-H_1}{(s-X_1)^2 + (H_1-h)^2} & \frac{h+H_1}{(s-X_1)^2 + (H_1+h)^2} \\ \frac{s-X_2}{(s-X_2)^2 + (H_2-h)^2} + i \cdot \frac{s-X_2}{(s-X_2)^2 + (H_2+h)^2} & \frac{h-H_2}{(s-X_2)^2 + (H_2-h)^2} & \frac{h+H_2}{(s-X_2)^2 + (H_2+h)^2} \\ \frac{s-X_3}{(s-X_3)^2 + (H_3-h)^2} + i \cdot \frac{s-X_3}{(s-X_3)^2 + (H_3+h)^2} & \frac{h-H_3}{(s-X_3)^2 + (H_3-h)^2} & \frac{h+H_3}{(s-X_3)^2 + (H_3+h)^2} \\ \frac{s-X_4}{(s-X_4)^2 + (H_4-h)^2} + i \cdot \frac{s-X_4}{(s-X_4)^2 + (H_4+h)^2} & \frac{h-H_4}{(s-X_4)^2 + (H_4-h)^2} & \frac{h+H_4}{(s-X_4)^2 + (H_4+h)^2} \\ \frac{s-X_5}{(s-X_5)^2 + (H_5-h)^2} + i \cdot \frac{s-X_5}{(s-X_5)^2 + (H_5+h)^2} & \frac{h-H_5}{(s-X_5)^2 + (H_5-h)^2} & \frac{h+H_5}{(s-X_5)^2 + (H_5+h)^2} \\ \frac{s-X_6}{(s-X_6)^2 + (H_6-h)^2} + i \cdot \frac{s-X_6}{(s-X_6)^2 + (H_6+h)^2} & \frac{h-H_6}{(s-X_6)^2 + (H_6-h)^2} & \frac{h+H_6}{(s-X_6)^2 + (H_6+h)^2} \\ \frac{s-X_7}{(s-X_7)^2 + (H_7-h)^2} + i \cdot \frac{s-X_7}{(s-X_7)^2 + (H_7+h)^2} & \frac{h-H_7}{(s-X_7)^2 + (H_7-h)^2} & \frac{h+H_7}{(s-X_7)^2 + (H_7+h)^2} \end{pmatrix}$$

$$E(s) = \frac{1}{1000} \cdot \text{eval} \left( \left\| \frac{Q \cdot s(s)}{2 \cdot \pi \cdot \epsilon_0} \right\| \right)$$

$$E(0) = 10.3221$$



$$2 \cdot E(x)$$

np:= 31

for p in 1 .. np

$$EE_p := E \left( -45 + \frac{p \cdot 90}{np} \right)$$

0.0195
0.0152
0.0059
0.0112
0.0385
0.0719
0.093
0.0904
0.0728
0.0021
0.2174
0.6621
1.5797
3.6399
7.5422
EE=
13.7096
21.8312
27.2888
22.3109
9.4415
4.8916
18.6843
27.2735
25.0849
17.6051
11.3682
7.3963
4.9819
3.4866
2.5272
1.8884

Considering only the bipole

$$P' := \begin{pmatrix} P_{44} & P_{45} \\ P_{54} & P_{55} \end{pmatrix} = \begin{pmatrix} 8.2987 \cdot 10^{10} & 1.1108 \cdot 10^{10} \\ 1.1108 \cdot 10^{10} & 8.2987 \cdot 10^{10} \end{pmatrix}$$

$$C' := \text{invert}(P') = \begin{pmatrix} 1.227 \cdot 10^{-11} & -1.6423 \cdot 10^{-12} \\ -1.6423 \cdot 10^{-12} & 1.227 \cdot 10^{-11} \end{pmatrix}$$

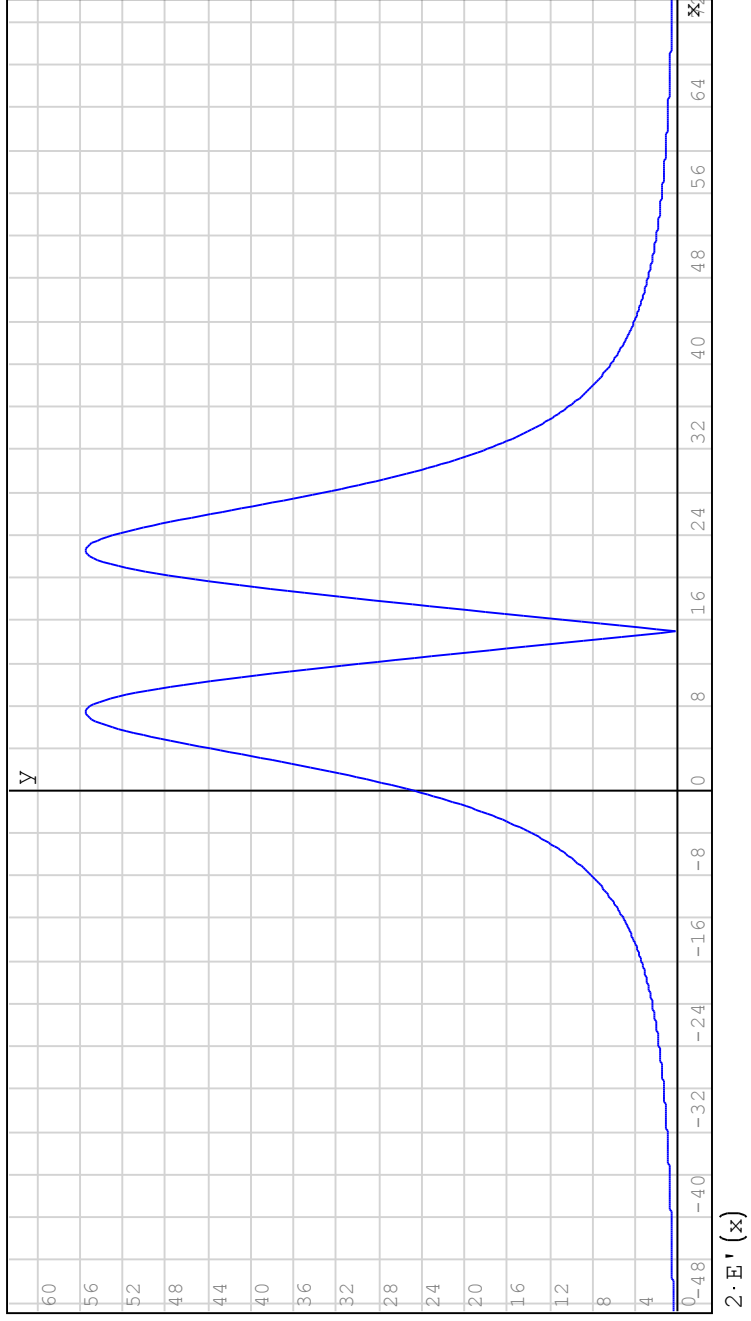
(■)

$$Q' := C' \cdot \begin{pmatrix} 500 \\ -500 \end{pmatrix} \cdot 10^3 = \begin{pmatrix} 6.9561 \cdot 10^{-6} \\ -6.9561 \cdot 10^{-6} \end{pmatrix}$$

$$S'(s) := \begin{pmatrix} \frac{s - X_4}{(s - X_4)^2 + (H_4 - h)^2} + i \cdot \frac{s - X_4}{(s - X_4)^2 + (H_4 + h)^2} & \frac{h - H_4}{(s - X_4)^2 + (H_4 - h)^2} - \frac{h + H_4}{(s - X_4)^2 + (H_4 + h)^2} \\ \frac{s - X_5}{(s - X_5)^2 + (H_5 - h)^2} + i \cdot \frac{s - X_5}{(s - X_5)^2 + (H_5 + h)^2} & \frac{h - H_5}{(s - X_5)^2 + (H_5 - h)^2} - \frac{h + H_5}{(s - X_5)^2 + (H_5 + h)^2} \end{pmatrix}$$

$$E'(s) := \frac{1}{1000} \cdot \text{eval} \left\| \left\| \frac{Q'^T \cdot S'(s)}{2 \cdot \pi \cdot \varepsilon_0} \right\| \right\|$$

$$E'(0) = 12.1888$$



```

for p in 1...np
    EE' p := E' ( - 45 +  $\frac{p \cdot 90}{np}$  )

```

$$EE' = \begin{pmatrix} 0.2702 \\ 0.3159 \\ 0.3725 \\ 0.4433 \\ 0.5333 \\ 0.6493 \\ 0.8013 \\ 1.0044 \\ 1.2818 \\ 1.67 \\ 2.2293 \\ 3.0613 \\ 4.3443 \\ 6.3961 \\ 9.7669 \\ 15.218 \\ 22.6996 \\ 27.6914 \\ 22.4942 \\ 9.5672 \\ 4.7973 \\ 18.6334 \\ 27.2578 \\ 25.0684 \\ 17.5689 \\ 11.3169 \\ 7.3378 \\ 4.9214 \\ 3.4268 \\ 2.4695 \\ 1.8335 \end{pmatrix}$$

$$EE = \begin{pmatrix} 0.0195 \\ 0.0152 \\ 0.0059 \\ 0.0112 \\ 0.0385 \\ 0.0719 \\ 0.093 \\ 0.0904 \\ 0.0728 \\ 0.0021 \\ 0.2174 \\ 0.6621 \\ 1.5797 \\ 3.6399 \\ 7.5422 \\ 13.7096 \\ 21.8312 \\ 27.2888 \\ 22.3109 \\ 9.4415 \\ 4.8916 \\ 18.6843 \\ 27.2735 \\ 25.0849 \\ 17.6051 \\ 11.3682 \\ 7.3963 \\ 4.9819 \\ 3.4866 \\ 2.5272 \\ 1.8884 \end{pmatrix}$$

$$EE - EE' = \begin{pmatrix} -0.2507 \\ -0.3008 \\ -0.3666 \\ -0.4321 \\ -0.4948 \\ -0.5774 \\ -0.7083 \\ -0.914 \\ -1.209 \\ -1.668 \\ -2.0119 \\ -2.3992 \\ -2.7646 \\ -2.7562 \\ -2.2247 \\ -1.5084 \\ -0.8685 \\ -0.4025 \\ -0.1833 \\ -0.1257 \\ 0.0944 \\ 0.0509 \\ 0.0157 \\ 0.0165 \\ 0.0361 \\ 0.0513 \\ 0.0585 \\ 0.0606 \\ 0.0598 \\ 0.0577 \\ 0.0549 \end{pmatrix}$$

Section 5.6  
 Space charge and ions  
<http://en.smath.info/>

Electron charge

$$q = 1.6 \cdot 10^{-19}$$

Study system parameters

$$P := 14 \quad H := 7.2 \quad V := 500000$$

$$d := 0.434 \quad X := 15$$

$$\frac{P}{H} = 1.9444$$

$$X - \frac{P}{2} = 1.1111$$

Corona-free

$$E_e := \frac{2 \cdot V \cdot H}{\ln\left(4 \cdot \frac{H}{d}\right) - \frac{1}{2} \cdot \ln\left(\frac{4 \cdot H^2 + P^2}{P^2}\right)} \cdot \left[ \frac{1}{H^2 + \left(X - \frac{P}{2}\right)^2} - \frac{1}{H^2 + \left(X + \frac{P}{2}\right)^2} \right] = 12706.0363$$

$$E_{em} := \frac{2 \cdot V \cdot H}{\ln\left(4 \cdot \frac{H}{d}\right) - \frac{1}{2} \cdot \ln\left(\frac{4 \cdot H^2 + P^2}{P^2}\right)} \cdot \left[ \frac{1}{H^2 + \left(9.4 - \frac{P}{2}\right)^2} - \frac{1}{H^2 + \left(9.4 + \frac{P}{2}\right)^2} \right] = 26747.52$$

Saturated-corona

$$E_{sm} := 1.31 \cdot \left[ 1 - \exp\left(-1.7 \cdot \frac{P}{H}\right) \right] \cdot \frac{V}{H} = 87635.4676$$

$$E_s := 1.46 \cdot \left( 1 - \exp\left(-2.5 \cdot \frac{P}{H}\right) \right) \cdot \exp\left(-0.7 \cdot \frac{V}{H}\right) \cdot \left( \frac{X - \frac{P}{2}}{H} \right) \cdot \frac{V}{H} = 46220.052$$

$$J_{ps} := 1.54 \cdot 10^{-15} \cdot \left( 1 - \exp\left(-\frac{P}{H}\right) \right) \cdot \exp\left(-1.75 \cdot \frac{V}{H}\right) \cdot \left( \frac{X - \frac{P}{2}}{H} \right) \cdot \frac{V^2}{H^3} = 1.2646 \cdot 10^{-7}$$

$$J_{psm} := 1.65 \cdot 10^{-15} \cdot \left( 1 - \exp\left(-0.7 \cdot \frac{P}{H}\right) \right) \cdot \frac{V^2}{H^3} = 8.2183 \cdot 10^{-7}$$

$$J_{ns} := (-2) \cdot 10^{-15} \cdot \left( 1 - \exp\left(-\frac{1.5 \cdot P}{H}\right) \right) \cdot \exp\left(-1.75 \cdot \frac{V}{H}\right) \cdot \left( \frac{X - \frac{P}{2}}{H} \right) \cdot \frac{V^2}{H^3} = -1.8128 \cdot 10^{-7}$$

$$J_{nsm} := -2.15 \cdot 10^{-15} \cdot \left( 1 - \exp\left(-0.7 \cdot \frac{P}{H}\right) \right) \cdot \frac{V^2}{H^3} = -1.0709 \cdot 10^{-6}$$

$$\mu_p := 1.15 \cdot 10^{-4}$$

$$\mu_n := -1.5 \cdot 10^{-4}$$

$$\rho_n := \frac{J_{ns}}{\mu_n \cdot E_s} = 2.6147 \cdot 10^{-8}$$

$$\rho_p := \frac{J_{ps}}{\mu_p \cdot E_s} = 2.3791 \cdot 10^{-8}$$

$$\rho_{\max} := 1.1 \cdot 10^{-11} \cdot \frac{\left( 1 - \exp\left(-0.7 \cdot \frac{P}{H}\right) \right) \cdot \frac{V}{H}}{\left( 1 - \exp\left(-1.7 \cdot \frac{P}{H}\right) \right) \cdot \frac{V^2}{H^2}} = 8.1899 \cdot 10^{-8}$$

$$n_s := 68.8 \cdot \frac{\left(1 - \exp\left(-0.7 \cdot \frac{P}{H}\right)\right)^2}{\left(1 - \exp\left(-1.7 \cdot \frac{P}{H}\right)\right)^2} \cdot \frac{V}{H} = 5.1224 \cdot 10^5$$

$$10^6 \cdot n_s \cdot q = 8.1959 \cdot 10^{-8}$$

$$10^6 \cdot n_s \cdot q \cdot \mu \cdot E_s = 4.3564 \cdot 10^{-7}$$

$$10^6 \cdot n_s \cdot q \cdot \mu \cdot E_s = -5.6822 \cdot 10^{-7}$$

$$K := 0.037$$

$$G_0 := 9 \cdot 0.8 = 7.2 \quad G := 21.6$$

$$S := 1 - \exp(-K \cdot (G - G_0)) = 0.413$$

$$Q(Q_e, Q_s, S) := Q_e + s \cdot (Q_s - Q_e)$$

Cigre limits (edge of servitude at ground level)

$$Q(E_e, E_s, S) = 26548.6928$$

$$Q(0, J_{ps}, S) = 5.2233 \cdot 10^{-8}$$

$$Q(0, J_{ns}, S) = -7.4876 \cdot 10^{-8}$$

$$Q(0, n_s, S) = 2.1158 \cdot 10^5$$

$$n_p := \frac{Q(0, J_{ps}, S)}{\mu_p \cdot Q(E_e, E_s, S) \cdot q \cdot 10^6} = 1.0693 \cdot 10^5$$

$$n_n := \frac{Q(0, J_{ns}, S)}{\mu_n \cdot Q(E_e, E_s, S) \cdot q \cdot 10^6} = 1.1751 \cdot 10^5$$

Britten Limits (maximum at ground level)

$$Q(E_{em}, E_{sm}, S) = 51896.7278$$

$$Q(0, J_{psm}, S) = 3.3945 \cdot 10^{-7}$$

$$Q(0, J_{nsm}, S) = -4.4231 \cdot 10^{-7}$$

$$n_{pm} := \frac{Q(0, J_{psm}, S)}{\mu_p \cdot Q(E_{em}, E_{sm}, S) \cdot q \cdot 10^6} = 3.5548 \cdot 10^5$$

$$n_n := \frac{Q(0, J_{nsm}, S)}{\mu_n \cdot Q(E_{em}, E_{sm}, S) \cdot q \cdot 10^6} = 3.5512 \cdot 10^5$$